THE DEFORMATION BEHAVIOR OF WET LIGNOCELLULOSIC FIBERS

A Dissertation
Presented to
The Academic Faculty

By

Robert M Lowe

In Partial Fulfillment
Of the Requirements for the Degree
Doctor of Philosophy in the
School of Chemical and Biomolecular Engineering

Georgia Institute of Technology

May 2007

THE DEFORMATION BEHAVIOR OF WET LIGNOCELLULOSIC FIBERS

Approved by:

Dr. Arthur Ragauskas, Co-Advisor
School of Chemistry and Biochemistry
Georgia Institute of Technology

Dr. Yulin Deng, Co-Advisor
School of Chemical and Biomolecular Engineering
Georgia Institute of Technology

Dr. John Muzzy
School of Chemical and Biomolecular Engineering
Georgia Institute of Technology

Dr. Jeffery Hsieh
School of Chemical and Biomolecular Engineering
Georgia Institute of Technology

Dr. Derek Page
Pulp and Paper Research Institute of Canada

Date Approved:
December 19, 2006

“Et ignotas animum dimittit in artes”

- Ovid, *Metamorphoses*

ACKNOWLEDGEMENTS

There are many people who have helped me through my graduate education. First, I would like to thank my advisor, Dr. Art Ragauskas, for giving me the academic freedom to explore the areas of paper and fiber physics that I found interesting. Also, as members of my defense committee, Dr. Yulin Deng, Dr. Jeff Hsieh, and Dr. John Muzzy have each been an invaluable source of advice and support for my research. I would especially like to thank Dr. Derek Page for taking the time to serve on my committee and keeping my science sound. His advice and guidance made much of this research possible.

Next, I would like to thank my colleagues. John Waterhouse has been an invaluable resource for this research program and exploring the potential implications of its results. Naveen Cheluka at the Indian Institute of Technology Roorkee along with Elisabeth Duker and Tom Lindstrom at STFI are gratefully acknowledged for their assistance. Tim Patterson, Lauri Lehtonen, and Dan Dyer have all provided experimental insight and reviewed my work for which I am truly grateful. My fellow students have been a source of advisement, entertainment, and commiseration: Andy, Cam, Laura, Fran, Brett, Chris, Kim, Aaron, Tudor, Dong Cheng, thank you for keeping things fun. I would particularly like to thank Cameron Thomson

and Andy DeMaio for collaborating on several aspects of my research. Both have taken me down research paths that were rewarding and unexpected. Lenong Allison, Yunqiao Pu, Tuwanda Strowbridge, Connie Adams, and Marian Pena have all made my work at IPST possible. And of course, nothing would have been the same without Major White watching out for the students. Most importantly, I would like to thank Bryan Raybon. Without his help, I would not have been able to finish this research program.

Finally, none of this would have been possible without the support of my family. They provided the encouragement to continue my education and gave me the determination to see it through.

To those above, many thanks.

TABLE OF CONTENTS

LIST OF TABLES

LIST OF FIGURES

LIST OF EQUATIONS

NOMENCLATURE

A	=	Fiber cross-sectional area
Aa	=	Acceptor fiber imaged with the acceptor filter
Ad	=	Donor fiber imaged with the acceptor filter
Afa	=	FRETN correction component
Ax	=	Fiber crossing imaged with the acceptor filter
CMC	=	Carboxymethylcellulose
CSF	=	Canadian Standard Freeness
D	=	Chlorine dioxide bleaching stage
d	=	deflection or stepheight
Da	=	Acceptor fiber imaged with the donor filter
DCCH	=	Coumarin dye
Dd	=	Donor fiber imaged with the donor filter
Dfd	=	FRETN correction component
DS	=	Degree of substitution
Dx	=	Fiber crossing imaged with the donor filter
E	=	Elastic modulus
E	=	Extraction bleaching stage
ECF	=	Elemental chlorine free
F	=	Freespan
Fa	=	Acceptor fiber imaged with the FRET filter

Fd	=	Donor fiber imaged with the FRET filter
FRET	=	Fluorescence resonance energy transfer
FRET1	=	FRETN correction component
FRETN	=	Normalized FRET signal
f_s	=	Fiber shape factor
FTSC	=	Fluorescein dye
Fx	=	Fiber crossing imaged with the FRET filter
G	=	Shear modulus
H	=	Local height of an interference fringe
HW	=	Hardwood
$h\nu$	=	light energy
I	=	Moment of inertia
ML	=	Middle lamella
M_W	=	Molecular weight
n	=	interference fringe order
NRET	=	Non-radiative energy transfer
O	=	Oxygen beaching stage
P	=	Peroxide bleaching stage
P	=	Pressure
Q	=	Chelation bleaching stage
q	=	Distributed load
r_{DA}	=	Average donor-acceptor distance

Revs	=	Refining revolutions
S	=	Steadman's loaded span or stepheight
S1	=	Outer part of the secondary cell wall layer
S2	=	Middle part of the secondary cell wall layer
S3	=	Inner part of the secondary cell wall layer
S_{MS}	=	Average local fiber stiffness
SW	=	Softwood
WRV	=	Water retention value
Z	=	Ozone bleaching stage
ZDT	=	Z-direction tensile strength
λ	=	Light wavelength

SUMMARY

As some companies in the paper industry struggle to shift from commodity grades to value added products, technical challenges and opportunities have grown tremendously. These new products require more stringent manufacturing specifications and improved performance relative to those of lignocellulosic fibers currently being produced. Hence, topochemical and mechanical modifications of pulp fibers have moved to the forefront of many corporate strategies. Researchers are beginning to develop new tools to help better understand the fundamental mechanisms of fiber modifications and how to most efficiently apply them. Two novel approaches are presented.

First, a new method to observe single fiber crossings is developed. It was found that refining reduces the stepheight in the fiber crossing for both hardwood and softwood kraft pulps by increasing the tendency of the fibers to collapse, deform, and assume a lens like shape. The effect of pulp type, bleaching, drying, wet pressing, and fiber charge were also investigated. Graphs of stepheight versus freespan were linear through the origin suggesting that the freespan (flexibility) of the crossing fiber is largely unimportant to the formation of fiber crossings. Quite surprisingly, the ratio of stepheight to freespan remained relatively constant no matter

the treatment. Only bleaching and the addition of surface charge via CMC had any independent impact on freespan. The data do not fit bending or shear mechanisms that have been developed in the literature suggesting that another mechanism may be responsible for the deformation behavior of single fiber crossings.

Also, a method employing fluorescence microscopy and fluorescence resonance energy transfer is used to image the areas of a fiber-fiber interface while they were bonded. Analysis of the FRET signal from fiber crossings indicate that wet pressing increased the FRET occurring between the two dyed fiber surfaces. The results are consistent with the increased amount of interdiffusion expected with higher levels of wet pressing.

Two novel techniques are used to investigate fundamental aspects of fiber deformation behavior and fiber-fiber bond formation. As these methods are further refined and utilized they will provide new avenues for researchers to explore and expand the property space of fibers and paper sheets.

CHAPTER 1: INTRODUCTION

Some companies in the paper industry are currently suffering from an identity crisis. With flat production rates and the commoditization of many paper products, companies have to decide whether they will be low cost product providers or try to compete in nontraditional or value added markets. No matter which route is taken, the successful players will be those that create innovative ways to provide an expanded property set which can be utilized to produce products that are cheaper, more cost effective, or new products altogether.

To create these expanded property sets, researchers must find ways to impact the fiber deformation behavior that controls fiber and paper properties. For the past decade, the salient approach has been to modify the fiber ultrastructure and topochemistry. Unfortunately, most of the traditional tools available to paper researchers do not aid in developing a fundamental understanding of the new properties that are imparted.

This thesis presents what is currently known about the ultrastructure and topochemistry of lignocellulosic fibers and how they can be modified. The tools traditionally used to investigate how these modifications impact the

deformation and bonding behavior are also reviewed. Finally, two new techniques are introduced that examine wet fiber deformation behavior and the formation of fiber-fiber bonds.

Highly engineered fiber products will require new tools to probe their fundamental behavior. As researchers build novel properties into fibers, companies will develop new technology platforms that will foster an ever growing property portfolio. An efficient implementation of these new characteristics will only occur with an understanding of how modified fiber ultrastructure and topochemistry control the properties of paper and fiber products.

CHAPTER 2: LITERATURE REVIEW

2.1 Pulp Fiber Characteristics

Knowledge of pulp fiber topochemistry and morphology is essential for any discussion on the chemical and physical interactions of lignocellulosics. Wood fibers are complex composite structures composed mainly of cellulose, lignin and hemicelluloses (Rowell, Pettersen, Han et al. 2005) which are heterogeneously distributed within the cell wall (Saka 2001). The polymeric constituents and their organization have a tremendous influence over the fiber deformation behavior. Hence, the composition and structure of the wood cell wall are discussed below.

2.1.1 Cell Wall Components

The wood cell wall is essentially composed of three basic building blocks: cellulose, hemicellulose, and lignin. Comprising approximately 40-50% of the cell wall, cellulose is the largest constituent of a wood fiber. It is a linear homopolymer chain of D-glucose units linked by β-1,4-glycosidic bonds. The glucose monomers are organized into regular repeating cellobiose units to form cellulose chains as shown in Figure 1. Cellulose has a degree of polymerization of about 10,000 for native wood to 2000 for

pulp (Sjostrom and Westermark 1999). Intra- and intermolecular hydrogen bonding allow cellulose chains to form crystalline regions that can account for up to 65% of the biopolymer's structure in wood (Rowell, Pettersen, Han et al. 2005) and 40-50% for elemental chlorine free (ECF) bleached pulps (Liitia, Maunu, Hortling *et al.* 2003).

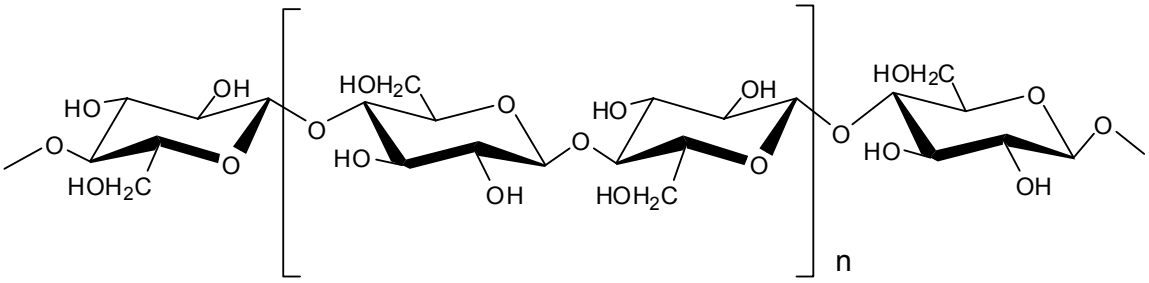

Figure 1 – Cellobiose
The repeating cellobiose unit and the β-1,4-glycosidic linkages (Sjostrom and Westermark 1999).

Unlike cellulose, hemicelluloses are linearly branched heteropolysaccharides comprised of a variety of different sugars depending on their species of origin (Sjostrom 1993). They make up approximately 20-30% of the cell wall in wood (Saka 2001). Softwood hemicelluloses are composed mainly of galactoglucomannans (Willfor, Sundberg, Hemming *et al.* 2005b) while hardwoods are predominately glucuronoxylans (Willfor, Sundberg, Hemming *et al.* 2005a). Table 1 lists the major hemicelluloses for softwoods and Table 2 lists them for

hardwoods. Hemicelluloses are amorphous and have a degree of polymerization of approximately 200 (Sjostrom 1993). Figure 2 and Figure 3 show the major softwood and hardwood hemicellulose structures, respectively.

Table 1 - Major Softwood Hemicelluloses
The major hemicellulose in softwoods are shown as a percent in wood (Rowell, Pettersen, Han *et al.* 2005).

Hemicellulose Type	Degree of Polymerization	Percent (%)
Galactoglucomannan	100	11-25
Arabinoglucuronoxylan	100	7-10

Table 2 - Major Hardwood Hemicelluloses
The major hemicellulose in hardwoods are shown as a percent in wood (Rowell, Pettersen, Han *et al.* 2005).

Hemicellulose Type	Degree of Polymerization	Percent (%)
Glucuronoxylan	200	15-30
Gluccomannan	200	2-5

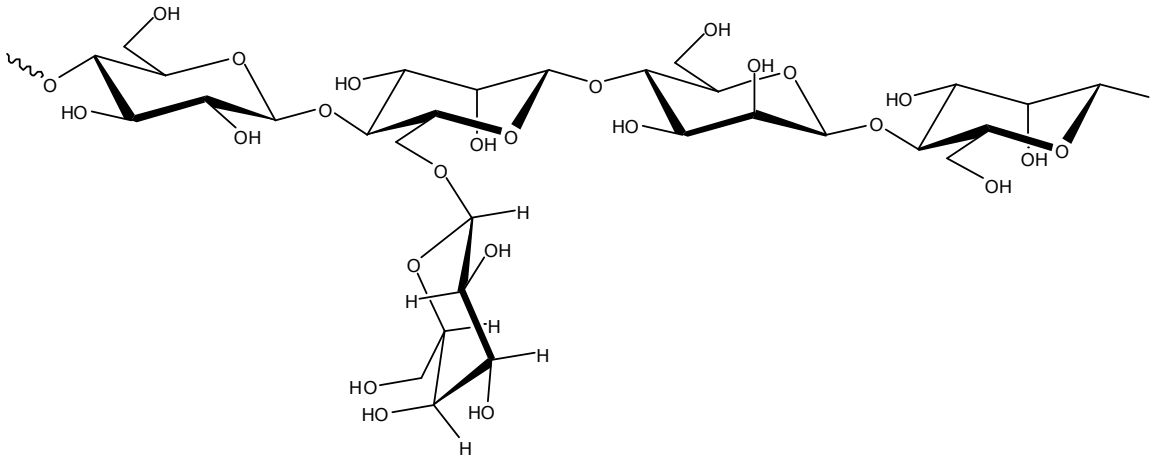

Figure 2 – Galactoglucomannan
The predominate hemicellulose in softwoods (Sjostrom 1993).

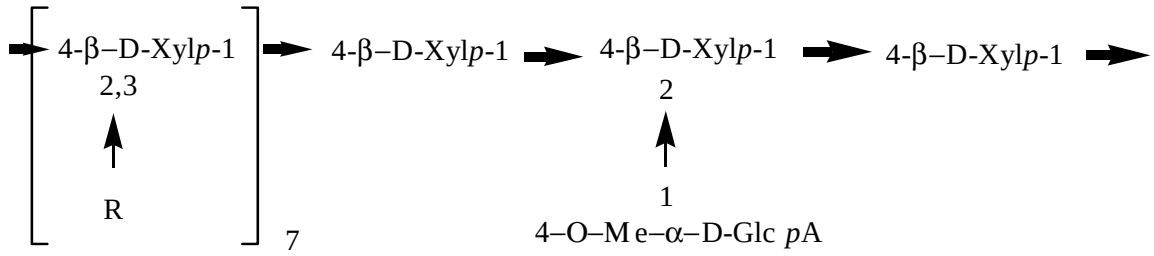

Figure 3 – Glucuronoxylan
The predominate hemicellulose in hardwoods. Sugar units: β-D-xylopyranose (Xyl*p*); 4-O-methyl-α-D-glucopyranosyluronic acid (Glc *p*A); R = Acetyl group (CH_3CO) (Sjostrom 1993).

The remaining 20-30% of the cell wall is composed of lignin (Saka 2001). Lignin is an amorphous polymer consisting of the phenylpropane structures: coniferyl, sinapyl, and *p*-coumaryl alcohol (Chakar and Ragauskas 2004). The three basic units of lignin are shown in Figure 4.

Hardwood lignin has a methoxyl content of 18-21% and is composed of all three precursors. Softwood has a methoxyl content of 15-16%. Coniferyl alcohol is the main SW precursor with a minor contribution from the coumaryl alcohol subunit (Rowell, Pettersen, Han et al. 2005).

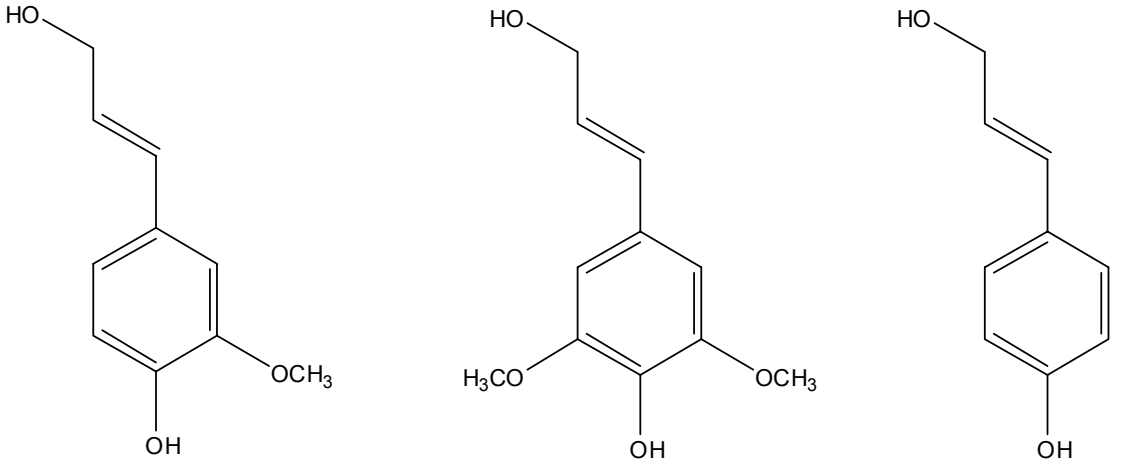

Figure 4 - Lignin Precursors
The three building blocks of lignin are coniferyl alcohol (softwood/hardwood), synapyl alcohol (hardwood), and coumaryl alcohol (softwood/hardwood).

2.1.2 Cell Wall Structure

The cell wall consists of a complex intermixing of cellulose, hemicellulose and lignin (Panshin and deZeeuw 1980). Cellulose is generally organized in thin crystalline microfibrils, about 50 nm wide, through hydrogen bonding (Horii 2001). Page *et al* have described the cell wall as a fiber

reinforced composite material. The fibers are the cellulose mircofibrils surrounded by a stress- equalizing matrix of hemicellulose and lignin (Page, Seth and El-Hosseiny 1985).

The composition and organization of the cell wall material varies based on the species of origin and the location in the cell wall. Three main layers make up the structure of the cell wall: the middle lamella, the primary wall, and the secondary wall. Figure 5 shows a wood fiber and the location of the layers of its structure (Cote 1967). Table 3 shows typical layer thickness for two wood species (Fengel and Wegener 1989).

The middle lamella is a highly lignified layer that exists between individual fiber cells. It acts as the "glue" or "cement" that holds the wood ultra-structure together. The primary wall is a layer about 0.1 μm thick consisting of an irregularly woven network of cellulose microfibrils (Panshin and deZeeuw 1980). The secondary cell wall is relatively dense, contains the majority of the fiber's cellulose, and is generally divided into three layers: S1, S2, and S3. The cellulose is organized into microfibrils that have a distinct angle of orientation in each layer. The S1 layer serves as a transition between the primary cell wall and the bulk of the secondary wall. The microfibrils are organized much like the primary cell wall with a definable angle of orientation appearing closer to the S2 layer

(Wiedenhoeft and Miller 2005). The S2 layer makes up the bulk of the cell wall with microfibrils oriented along the axis of the cell. Directly adjacent to the lumen, the S3 layer is made up of cellulose microfibrils that can be parallel to those in the S2 layer (Wiedenhoeft and Miller 2005).

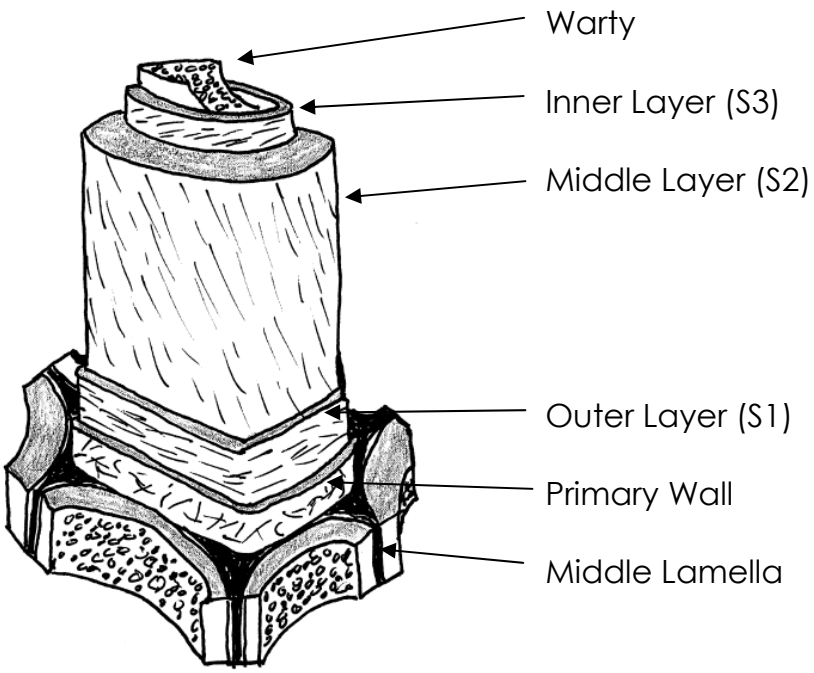

Figure 5 - Cell Wall Structure
A Diagram of the structure of a wood cell wall showing the middle lamella, primary wall, S1, S2, S3, and the warty layers. Adapted from Cote (Cote 1967)

Table 3 - Cell Wall Layer Thicknesses
Cell wall layer thicknesses for earlywood spruce tracheids (*Picea abies*) and beech (*Fagus crenata*) fiber tracheids (Fengel and Wegener 1989)

Wall Layer	Softwoods		Hardwoods	
	µm	%	µm	%
Primary	0.09	4.3	0.07	5.0
S1	0.26	12.4	0.24	16.0
S2	1.66	79.0	0.99	67.0
S3	0.09	4.3	0.17	12.0
Total Wall	2.10		1.47	

The polymeric constituents of the cell wall are not uniformly distributed. Figure 6 illustrates the composition of each cell wall layer and how the distribution of lignin, hemicelluloses, and cellulose varies. The highest concentration of lignin occurs in the middle lamella, but, because of the thinness of this layer (see Figure 6), only about 10% of the cell's total lignin content is located here. The bulk of the cell wall material is in the S2 layer, due to its size in comparison with the other layers.

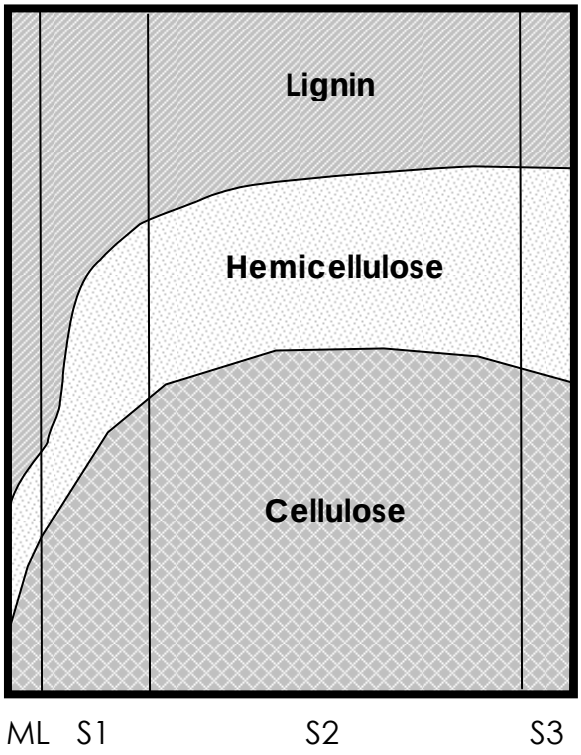

Figure 6 - Cell Wall Composition
Graph illustrating known and inferred data about the composition of the cell wall (Panshin and deZeeuw 1980).

The species of origin and kraft pulping also play a large role in the distribution of the cell wall components in the final papermaking fiber (Rowell, Pettersen, Han et al. 2005). Hardwoods tend to contain less lignin and more hemicelluloses and cellulose than typical softwood species. Table 4 shows a typical range of values for hardwoods and softwoods before and after kraft pulping (Gullichsen 1999).

Table 4 - Species/Pulping Variation for Unbleached Cell Wall Composition The average composition and the general range for cellulose, hemicelluloses, lignin and extractives expressed as a percentage of original wood (Gullichsen 1999).

Component	Wood Component		Kraft Pulp Component	
	Pine	Birch	Pine	Birch
	%	%	%	%
Cellulose	38-40	40-41	35	34
Hemicellulose	25-30	30-35	10	17
Lignin	27-29	20-22	2-3	1.5-2
Extractives	4-6	2-4	0.25	<0.5

2.1.3 Fiber Charge and Its Origin

The charge of a pulp fiber plays a major role in determining the final properties of a paper sheet and influences its behavior in a pulp suspension. The negative charge of a fiber is generally from acid groups on the surface and in the bulk of its structure. The charge for wood and pulp fibers comes from carboxyl groups, sulfonic acid groups, phenolic groups, or hydroxyl groups that are part of the fiber's polymeric constituents (Lindstrom 1989). The ability of these groups to be ionized is dependent on the conditions of the system in which they are placed. For normal papermaking conditions, only carboxyl and sulfonic acid groups contribute to the charge of a fiber (Lindstrom 1989). The quantity of acid groups is affected by the makeup of a fiber's polymeric constituents

and/or the chemical treatment it undergoes during pulping, bleaching, or other topochemical modification. Table 5 describes typical fiber charge values for several ECF, total chlorine free (TCF) bleached, and unbleached pulps (Laine and Stenius 1997a; Risen, Hulten and Paulsson 2004).

Table 5 - Fiber Charge for Unbleached and Bleached Kraft Pulps
The total fiber charge for bleached and unbleached hardwood and softwood pulps (Laine and Stenius 1997a; Risen, Hulten and Paulsson 2004)

Pulp Sample	Total Charge (μeq/g)
SW Unbleached Kraft	113
TCF SW - OQ(OP)(ZQ)(OP)*	57
ECF SW – DEDED*	40
HW Unbleached Kraft	166
TCF HW - OQ(OP)(ZQ)(OP*)	117
ECF HW – DEDED*	58

*see Nomenclature for bleaching abbreviations.

Only carboxyl groups are ionized at pH values normally present during the papermaking process (Sjostrom 1989). For fibers in their native state (*i.e.*, fibers that have not been subjected to any chemical treatment), the bulk of the charge comes from the acid side groups attached to the hemicellulose backbone (Sjostrom 1989). Phenolic units are somewhat

ionizable at neutral pH, but their contribution to the total fiber charge is limited (Sjostrom 1989).

The industrial production of chemi-thermomechanical pulp (CTMP) can also introduce charge groups to the fiber structure. Chips that undergo a CTMP process are generally subjected to a sulfite pretreatment. This pretreatment, as well as normal sulfite chemical pulping, introduces sulfonic acid groups to the fiber's lignin (Lindstrom 1992a). The amount of sulfonic acid groups introduced is dependent on the pulping conditions (temperature, pH, *etc.*). The effect of initial pH is shown in Table 6 (Sjostrom 1989).

Table 6 - The effect of pH on Sulfonic Acid Groups for TMP
The effect of pH on the sulfonic acid groups of softwood and hardwood TMP is shown (Sjostrom 1989).

Pulp Sample	Sulfonic Acid Groups (mmol/100g)
SW – initial pH = 2	10
SW – initial pH = 4	7
SW – initial pH = 6	12
HW – initial pH = 2	4
HW – initial pH = 4	3
HW – initial pH = 6	4

Changes in the cell wall composition during kraft pulping are accompanied by changes in the total fiber charge. Chai *et al* have reported that as kraft pulping progresses (e.g. lower kappa numbers), the concentration of charged acidic groups is reduced (Chai, Hou and Zhu 2003). Table 7 shows that a 50% reduction in kappa number can reduce carboxyl groups by almost 13%. Other reactions that occur during alkaline delignification (lignin fragmentation, cellulose peeling, *etc.*) modestly contribute to the acid group content (Lindstrom 1992a). It has also been demonstrated that kraft pulping can reduce the amount of hemicellulose in a pulp fiber by 30-50% (Suckling, Allison, Campion *et al.* 2001; Kim, Allison, Carter *et al.* 2005) leading to a reduced fiber charge. Zhang *et al* have shown that if oxidative chemicals are used during the pulping process (e.g. an oxygen based extended delignification) The reduction in acid groups in the residual lignin can be minimized (see Table 7).

Table 7 - Carboxyl Groups and Kappa Number
A reduction in kappa number leads to fewer carboxyl groups for lab cooked loblolly pine (Chai, Hou and Zhu 2003).

Kappa Number	Oxygen Delignification time (min)	Carboxyl Groups (μmol/g fiber)
30 – pulp	--	105
20 – pulp	--	97
15 - pulp	--	93
26 – residual lignin	10	400
20 – residual lignin	30	350
15 – residual lignin	80	350

Uronic acids, particularly 4-O-methylglucuronic acid (MeGlcA), make up a large portion of the carboxyl groups found in native wood (Sjostrom 1989). Table 8 Reports typical MeGlcA and carboxyl group content of wood for several species (Sjostrom 1989). During kraft pulping MeGlcA is converted to a hexenuronic acid as described in Figure 7 (Jiang 2000).

Table 8 - MeGlcA and Carboxyl Content for Several Species
MeGlcA and carboxyl content are reported for wood samples from several species (Sjostrom 1989).

Species	MeGlcA (mmol/100g)	Total Carboxyl Groups (mmol/100g)
Picea abies	7	15-25
Pinus sylvestris	8	15
Betula verrucosa	15	25-35

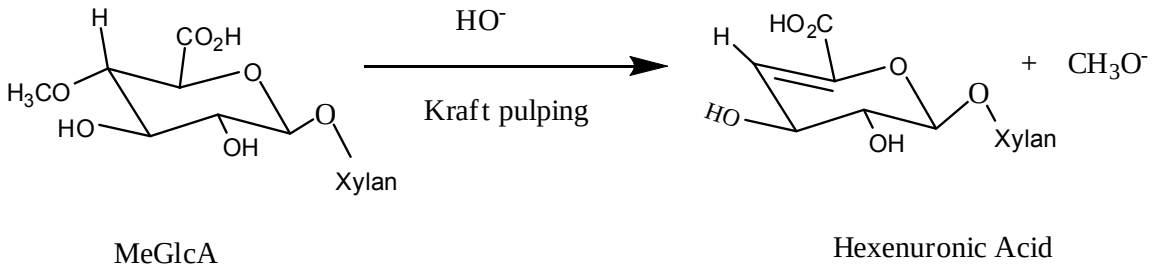

MeGlcA Hexenuronic Acid

Figure 7 - Formation of Hexenuronic Acid
During kraft pulping MeGlcA can lead to the formation of hexenuronic acid (Jiang 2000).

Hardwoods generally contain more hexenuronic acid because of the have higher xylan content (Jiang 2000). Table 9 shows typical hexenuronic content for unbleached kraft pulps. Hexenuronic acid content is of industrial importance because it consumes bleaching chemicals, decreases brightness, increases brightness reversion and prevents efficient metal removal (Jaing 2000).

Table 9 - Hexenuronic Acid Content for SW and HW Kraft Pulps
MeGlcA and hexenuronic acid content are reported for unbleached hardwood and softwood kraft pulps (Jiang 2000).

	Hardwood Kraft	Softwood Kraft
Kappa Number	18	26
MeGlcA (mmol/100g)	42	14
Hexenuronic Acid (mmol/100g)	76	54
Total	118	68

2.1.4 The Role of Charge in Fiber and Paper Properties

Fiber charge is important in determining the properties of a sheet during its formation and after drying. Many researchers have looked at the relation of bond strength to the presence of acid groups. Ampulski, Engstrand, and Barzyk have all shown that the presence of acid groups contributes to the development of sheet strength (Ampulski 1985; Engstrand, Sjogren, Olander *et al.* 1991; Barzyk, Page and Ragauskas 1997a). Barzyk, in particular, has shown that acid groups on the surface of a fiber can increase the fiber-to-fiber specific bond strength (Barzyk, Page and Ragauskas 1997a). The work of Barzyk was the impetus for Lanie's extensive investigation into the effect of surface and bulk charge on the physical and optical properties of paper sheets (see Section 2.1.6).

Fiber charge can also influence other aspects of papermaking such as dewatering and pressing, fiber flocculation, and response to wet end chemicals (retention aids, strength additives, *etc.*) (Lindstrom 1992a). The effect of fiber charge (mainly in the bulk of the fiber structure) on dewatering and pressing is an indirect consequence of fiber swelling; swollen fibers are more difficult to dewater (Busker and Cronin 1982). Finally, fiber charge can have direct impact on flocculation and the response of fibers to wet end additives. Wet end additives are usually cationic and are generally more effective in fibers with more negative charge (Lindstrom 1989).

2.1.5 Fiber Charge and Fiber Swelling

When placed in water, a dry fiber will imbibe the liquid and increase its volume by the amount of water taken in. Scallan has offered a model for the progression of swelling in a fiber (Scallan 1974). In his model, Scallan considers a pulp fiber made only of cellulose microfibrils (a low yield pulp fiber). He further states that the microfibrils are bonded in a tightly packed array. Water gains access to these fiber bundles because of chemical or mechanical action and progressively begins to swell the fiber. The hydrogen bonds between the fiber bundles continue to break down until the wall is concentrically delaminated (Scallan 1974).

The presence of acid groups in the structure of a fiber influences fiber swelling. It has been known for many years that the presence of cations during the papermaking process can have a beneficial effect on sheet properties. There are generally enough cations in the pulp to create a concentration gradient between the fiber and the surrounding solution (Scallan and Grignon 1978; Scallan 1983). The ions must stay near the anionic groups to remain electrically neutral; therefore, to maintain equilibrium, water must enter the cell wall (Scallan and Grignon 1978; Scallan 1983). This process continues until the osmotic pressure generated by the presence of the counterions is balanced by the resistance of the cell wall to swell any further (Scallan and Grignon 1978; Scallan 1983). Figure 8 demonstrates this concept.

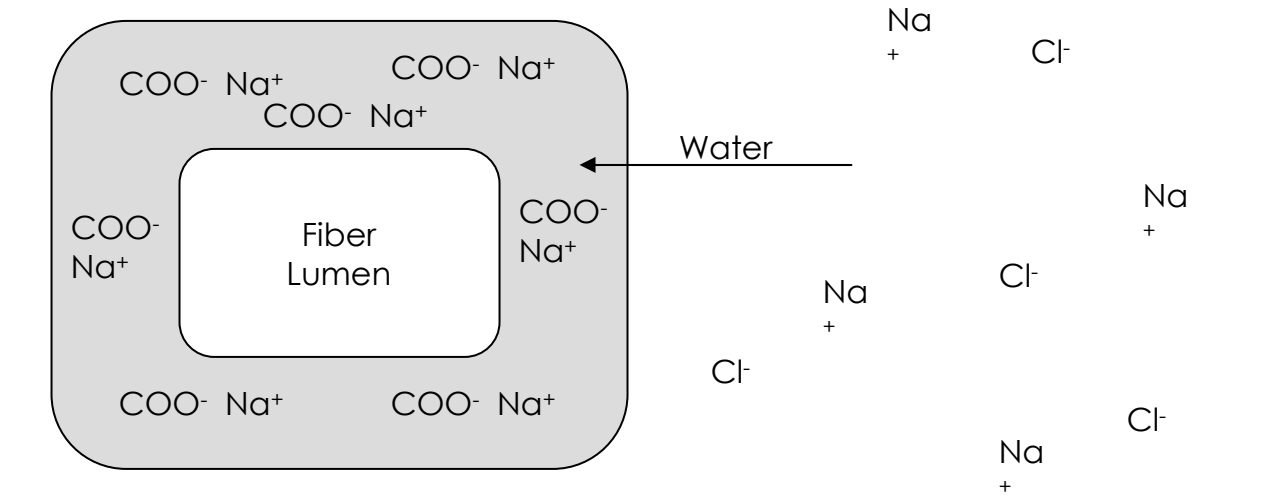

Figure 8 - Fiber Swelling
A fiber will imbibe water until the osmotic pressure is balanced by the resistance of the cell wall to swell further. Adapted from Barzyk (Barzyk 1996).

The total amount of charge present in a fiber exerts some control over the amount of swelling a fiber undergoes. Laine and Stenius have shown that a 30% increase in fiber swelling results when the total charge of a fiber is doubled (Laine and Stenius 1997b). Scallan and Grignon have demonstrated that the interaction between the acid groups and the cations can enhance the swelling of a fiber (Scallan and Grignon 1979). They investigated this by first removing all the trace metals that are normally present in a pulp and then systematically replacing them with different ionic species. By replacing all the cations in a fiber with a single

species, Scallan and Grignon found that fibers with certain ions made sheets of higher strength. In order of increasing strength, the species tested were: $Al^{+++} < H^{+} < Mg^{++} < Ca^{++} < Li^{+} < Na^{+}$ (Scallan and Grignon 1978). Figure 9 shows the relationship between the swelling caused by ion exchange and the breaking length.

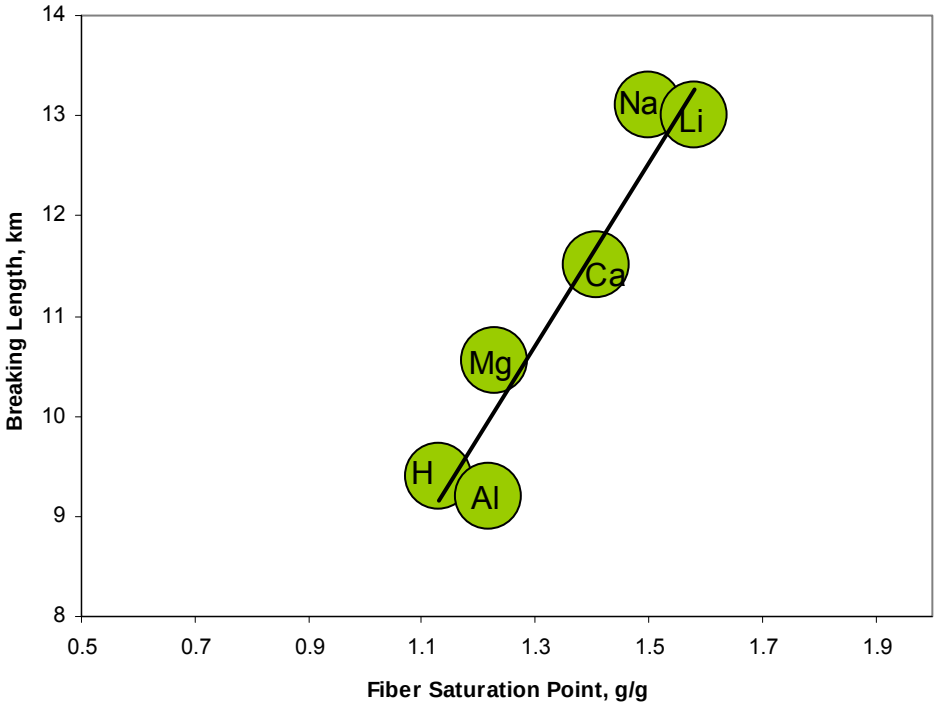

Figure 9 - The Effect of Cations on Swelling and Strength
The changes in fiber swelling (g of water per g of oven dried fiber) and sheet strength as a result of cation exchange. Data from Scallan and Grignon (Scallan and Grignon 1978).

Water retention value and fiber saturation point are two ways in which researchers have chosen to report the degree of swelling of pulp fibers.

Water retention value (WRV) is a method developed by Jayme to measure the ability of a pulp to hold water (Jayme 1958). WRV is determined by centrifuging a pulp mat at 3000 g force for 15 minutes, recording its weight, oven-drying the mat, and then recording the OD weight (Jayme 1958). The WRV is defined as:

$$WRV(\%) = \frac{\text{moist weight after centrifuging} - \text{oven-dry weight}}{\text{oven-dry weight}} \times 100$$

Equation 1 - Water Retention Value

Typical values of WRV can range from 100-200% depending on the species and degree/type of treatment. WRV is a simple method that does not require any special equipment; therefore, it has become the most prevalent means to measure fiber swelling. Nonetheless, WRV is subject to some limitations. WRV does not differentiate between water retained because of swelling and water retained between the fibers because of surface tension (Yiannos 1965). Yiannos has proposed a method that exchanges the water in the pulp mat for isopropanol to prevent skewed measurement due to inter-fiber water being retained (Yiannos 1965). Table 10 lists some typical results from using the isopropanol retention method.

Table 10 - Pulp Swellability via Isopropanol Retention
The effect of beating on the isopropanol retention of never-dried unbleached softwood kraft pulp is shown (Yiannos 1965).

Beating Time (min)	Swellability ($cm^3/100g$)
5	115
10	141
20	165
35	205

Stone and Scallan propose another method to measure the degree of swelling, the fiber saturation point (Stone and Scallan 1967). The fiber saturation point is the amount of water contained within the water saturated cell wall(Stone and Scallan 1967). Stone and Scallan use a solute exclusion technique whereby the change in concentration of a polymer placed in solution with fibers is equated to the fiber saturation point (Stone and Scallan 1967). This method works on the principle that large polymers are not able to enter the fiber through the fiber pores; therefore, the water is not available to dilute the polymer's concentration (Stone and Scallan 1967). Typical values for fiber saturation point are shown in Table 11 which illustrates the effect of yield on the fiber saturation point for a kraft cooked spruce fiber.

Table 11 - Kraft Yield and FSP
The effect of yield on fiber saturation point for a kraft cooked spruce (Stone and Scallan 1967).

Pulp Yield (%)	Fiber Saturation Point (g/g)
wood	0.40
92.4	0.67
89.0	0.74
80.0	0.86
77.8	0.84
70.4	1.06
61.4	1.16
53.4	1.21
48.7	1.14

2.1.6 Fiber Charge Modification

The importance of fiber charge and swelling to fiber and paper properties has been well recognized. Recently, paper scientists have developed research programs to explore how the distribution of fiber charge influences paper and fiber physics.

The early work of Walecka utilized chloroacetic acid in an isopropyl alcohol solution to carboxymethylate the pulp at a low degree of substitution (Walecka 1956). Table 12 shows that Walecka's pulps exhibit an increase in strength with increased carboxymethylation. Unfortunately, his method could not control the topochemical distribution of the charge groups. This limited any fundamental investigation into the mechanism of strength development.

Table 12 - Carboxymethylcellulose Substitution and Tensile Strength Data from Walecka shows that increasing the CMC substation on a bleached hard rag stock leads to increased tensile strength (Walecka 1956).

Chloroacetic Acid Concentration (%)	Degree of Substitution (DS)	Tensile Strength (lb/in)
0.00	0.002	13
0.10	0.006	17
0.25	0.014	19
0.50	0.022	23
1.50	0.053	27

Barzyk later controlled the degree of fiber swelling to selectively place the carboxylic acid groups onto the surface of the fiber (Barzyk, Page and Ragauskas 1997b). Neverdried and solvent exchange dried pulp samples were substituted throughout the fiber structure while once dried fibers were selectively substituted on the surface. In Table 13, the surface substituted fibers show higher Scott-Bond values at the same scattering coefficient indicating an increase in specific bond strength (Barzyk, Page and Ragauskas 1997a).

Table 13 - Surface Carboxyl groups and Specific Bond Strength
Data from Barzyk *et al*. show that an enrichment of surface acid groups leads to higher specific bond strength (Barzyk, Page and Ragauskas 1997a).

Light Scattering Coefficient ($cm^2/100g$)	Scott-Bond (J)	
	Bulk	Surface
270	0.05	0.07
230	0.08	0.11
190	0.13	0.22

Laine continued to investigate the impact of fiber charge and its distribution on the physical and optical properties of paper. His work employed two techniques that selectively introduce carboxyl groups to the fiber structure. Surface charge was introduced by irreversibly attaching carboxymethyl cellulose (CMC) to the fiber (Laine, Lindstrom,

Nordmark *et al.* 2000). As long as the CMC has a high enough molecular weight (M_w>10^5), the attachment will only be on the surface. The second method was much like that of Walecka to introduce carboxyl groups throughout the fiber structure (Laine, Lindstrom, Bremberg *et al.* 2003a).

The negative charge of CMC and the anionic nature of the fiber surface make deposition of CMC onto the fiber difficult. Laine found that if pH and the electrolyte concentration are controlled, the charge interaction can be screened out (Laine, Lindstrom, Nordmark *et al.* 2000). Surface deposition of CMC onto the fiber leads to increased fiber swelling as shown in Table 14 (Laine, Lindstrom, Nordmark *et al.* 2002). Also, the sheet tensile index was increased 150% with only a 3% decrease in light scattering coefficient and a 4% decrease in sheet density. Therefore, surface CMC served to only increase the specific bond strength of the fiber-fiber bonds.

Table 14 - CMC Attachment and WRV
A higher amount of surface CMC (M_w = 1.0x10^6, DS = 0.52) results in increased water retention value for ECF bleached softwood kraft pulps (Laine, Lindstrom, Nordmark *et al.* 2002).

Attached CMC (mg CMC/g fiber)	Water Retention Value (%)
0	133
5	155
10	165
15	180
20	185

Laine also investigated the differences in CMC surface deposition and bulk carboxymethylation (Laine, Lindstrom, Bremberg *et al.* 2003a; Laine, Lindstrom, Bremberg *et al.* 2003b). For bulk carboxymethylated pulps, the contribution of the surface charge groups to swelling was much more significant than the contribution of the charge groups in the bulk of the fiber. Finally, Laine compared the effect of surface CMC and bulk carboxymethylation on the physical and optical properties of handsheets. He concluded that the impact of surface swelling was more important to the fiber bond strength than to the change in cell wall flexibility and sheet consolidation (Laine, Lindstrom, Bremberg *et al.* 2003b).

2.2 Wet Fiber Deformability

Wet fiber deformability is one of the most fundamental and important fiber properties. Depending on the author, deformability has also been referred to as flexibility (Emerton 1957; Van Den Akker 1959; TamDoo and Kerekes 1981; Steadman and Luner 1985; Kuhn, Lu, Olson *et al.* 1995), conformability (Mohlin 1975b), collapsibility (Page 1967) and compactability (Brodeur and Runge 1995). All types of deformation are interrelated and contribute to sheet consolidation and/or the formation of fiber bonds. Most research has focused on the importance of wet fiber flexibility. Flexibility has been thought to affect almost every optical and physical property of a paper sheet (Clark 1985).

Most methods used to quantify wet fiber flexibility treat the fiber as a beam subject to pure elastic deformation. Classical mechanics defines the flexibility of a body as the inverse of its flexural stiffness, EI, where E is the modulus of elasticity and I is the second moment of area. The modulus of elasticity is a material property while I is a physical property (TamDoo and Kerekes 1981). Following is a discussion of wet fiber flexibility, how it has been measured, its influence over paper properties, and recent developments.

2.2.1 Measuring Wet Fiber Flexibility

The importance of wet fiber flexibility to sheet properties has been studied for some time. In 1959 Van den Akker discussed the importance of fiber flexibility on the formation of fiber-to-fiber bonds and stated that "there is a great need for a more accurate, more direct measurement of the wet flexibility of fibers." (Van Den Akker 1959). Researchers have developed several ways to quantify a fiber's wet flexibility. These methods can be separated into three main groups based on the length scale most critical to their measurement: macro-scale (mm), micro-scale (μm), and nano-scale (nm).

Macro-Scale Techniques

Much of the work on fiber deformation has been on the macro-scale where single fibers were deflected in some manner. Early work treated the fiber as a cantilever. Fibers were either held in place by a clamp while a quartz spiral spring was used to deflect a fiber (Seborg and Simmonds 1941) or deflected using a stream of water (Samuelsson 1963). There are two significant drawbacks to this type of method. First, the test is done on single fibers making it very tedious and cumbersome. Second, the technique of clamping a fiber into place is very much an art. If clamped too tightly, the fiber may be locally damaged. If clamped too

loosely, the fiber may slip and produce very large errors (Kuhn, Lu, Olson et al. 1995).

Forgacs and Robertson classified fiber flexibility based on its behavior in a controlled fluid flow (Forgacs and Mason 1958; Robertson, Meindersma and Mason 1961). They suspended pulp fibers in a liquid that is subjected to laminar shear. The fibers would assume rotational orbits that are related to their flexibility. Fibers that bend over themselves the most are considered more flexible. A pulp sample with a large percentage of fibers with flexible orbits was determined to have high average fiber flexibility.

There are several problems associated with classification methods such as the one presented by Robertson *et al.* Most importantly, these methods are not direct measurements of flexibility. They rely on subjective determination of the orbital type by the operator. Also, these methods can only describe the flexibility of undamaged fibers. Fibers that are permanently deformed assume orbits that can not be clearly assigned.

Later researchers utilized capillary tubes to support fibers in various fluid flows and measure flexibility. These methods model the fiber as a simply supported elastic beam and examine each fiber independent from any

interactions with other fibers or objects. Tam Doo and Kerekes have developed a method in which a fiber is simply supported and deformed by a stream of water (Tam Doo and Kerekes 1981). In their method a fiber is placed across a notch at the end of a capillary tube. The fiber is deformed by water flowing around the fiber and into the capillary tube. Like the Seborg and Simmonds method the major drawback of the Tam Doo and Kerekes method is the testing of single fibers. Single fiber testing is tedious and can lead to artificial results because of the selection of "good" or undamaged fibers by the operator. Particular to the Tam Doo and Kerekes method, the length of fiber is dictated by the inner diameter of the capillary tube; therefore, this method is not suitable for hardwood fibers. See Table 15 for a representative flexibility result from Tam Doo and Kerekes.

Kuhn *et al.* have developed a method where a fiber travels down a capillary tube to a main channel (Kuhn, Lu, Olson *et al.* 1995). As the fiber enters the main channel, it encounters a hydrodynamic force that is normal to its initial direction. A digital camera, placed at the junction of the capillary and the main channel, captures an image of the fiber as it is deflected by the normal hydrodynamic force.

The method of Kuhn *et al.* does address most of the concerns of previous methods. The flexibility of a large population of fibers can be measured in a relatively short amount of time without any operator bias. The method does have some built in bias, though. Kuhn only reports the flexibility data for relatively long, straight fibers (Kuhn, Lu, Olson et al. 1995). Short fibers tend not to contact both walls of the capillary tube as they exit into the main channel. Also very flexible fibers do not contact the walls of the capillary tube (Kuhn, Lu, Olson et al. 1995). The Kuhn method is a direct measure of the flexibility of a fiber, but it is not very representative of what is occurring during the formation of a paper sheet and it may give flexibility results that are higher than expected. Table 15 compares representative results for unbleached softwood pulp using the methods developed by Tam Doo and Kuhn (TamDoo and Kerekes 1981; Kuhn, Lu, Olson *et al.* 1995).

Table 15 - Flexibility Results from Macro-scale Techniques
Representative flexibility results from two methods using unbleached Canadian Softwood kraft pulp (TamDoo and Kerekes 1981; Kuhn, Lu, Olson *et al.* 1995).

	Average Flexibility (10^{11} $N^{-1}m^{-2}$)
Tam Doo and Kerekes	1.70
Kuhn, Olson and Robertosn	3.70

Nano-scale Techniques

With atomic force microscopy (AFM) becoming more prevalent in paper research laboratories, nano-scale techniques are now being reported in the literature. Most recently, Nilsson *et al* have described a method to investigate the fine structure of a water swollen lignocellulosic fiber using AFM (Nilsson, Wagberg and Gray 2001). In essence, they used an AFM probe to perform a nano-indentation to measure the local conformability or pliability of wet fibers. The pulp fibers were found to have variations in local conformability due to the differences in material properties at the fiber surface. Table 16 describes some stiffness values (S_{MS}) for softwood fibers and illustrates their variability. This method yields detailed information about the polymeric constituents and their heterogeneous distribution on the fiber surface; however, it's implications to the physical and optical properties of a paper sheet are still unclear.

Table 16 - Nano-scale Results for Local Fiber Stiffness
The mean fiber stiffness (S_{MS}) and the range of values demonstrate the heterogeneous nature of a fiber surface (Nilsson, Wagberg and Gray 2001).

Fiber	S_{MS} Mean Value (N/m)	S_{MS} Range (N/m)
TCF Bleached, 2 fibers	2.1	1.6-2.8
Kraft (kappa = 61), 3 fibers	3.8	2.5-5.3
Kraft (kappa = 88), 7 places on 3 fibers	4.3	0.6-9.0
Kraft (kappa = 110), 3 places on 2 fibers	4.5	2.5-8.1

Micro-scale Techniques

Micro-scale methods rely on measurements of fiber deformations with fibers or other objects. Mohlin introduced the idea of measuring the conformability of a fiber instead of directly measuring the flexibility (Mohlin 1975b). Conformability, stiffness, flexibility, and collapsibility are interrelated properties because they all depend on the Young's modulus of the cell wall (Mohlin 1975b). Mohlin's conformability is the ability of a fiber to conform to a glass fiber (diameter = 60 μm) that has been placed on a glass plate. A pulp fiber is placed across the glass fiber in a drop of water and then allowed to dry. The distance between the two glass plate-fiber contact points was measured, and the inverse of this difference was used as the measure of the fiber's conformability (Mohlin

1975b). Representative conformability, shown in Table 17, illustrate that sulfite fiber conformability is more sensitive to yield than kraft fibers.

Table 17 - Conformability of Kraft and Sulfite Pulps
The conformability of kraft and sulfite pulps is shown (Mohlin 1975b).

Pulp	Conformability (mm^{-1})
Unbleached SW Kraft (Yield = 46.9%)	0.42
Unbleached SW Kraft (Yield = 68.4%)	0.43
Unbleached SW Sulfite (Yield = 51.5%)	0.60
Unbleached SW Sulfite (Yield = 59.6%)	0.39

Mohlin's method is closer to an actual flexibility measurement; however, the method is still not ideal. Fibers are manipulated in the wet condition and allowed to dry before being evaluated. This method most likely does not approximate what happens in the paper structure because there is no pressure applied to the fiber and the scale (60 µm) is not very close to what is occurring in paper (pulp fibers are generally 4-12 µm thick).

Steadman and Lunar offered the next iteration by determining the "effective fiber flexibility" of fibers crossing a 25 µm stainless steel wire (Steadman and Luner 1985). It uses the conformability of the fiber and relates it to the bending stiffness to derive the fiber flexibility as shown in

Equation 2. The Steadman method is the closest method thus far to representing what is actually occurring during the formation of a paper sheet.

$$\frac{1}{EI} = \frac{72d}{PWS^4}$$

Equation 2 – Steadman's Calculation of Effective Fiber Flexibilty

Where
E = modulus of elasticity (Nm^{-2})
I = moment of inertia (m^4)
d = wire diameter, (m)
P = pressing pressure (Nm^{-2})
W = projected fiber width (m)
S = mathematical estimate of the loaded span (m)

The Steadman Technique

A very low basis weight sheet is initially formed in a standard handsheet mold. A high speed (coarse) filter paper is placed on the mold's wire. The mold is closed and then filled from the top with deionized water. An aliquot of dilute stock is added and then stirred as usual. The mold is drained and the filter paper is placed on several wet blotters in the handsheet press. The flexibility slides are placed on the sheet and then covered with several more wet blotters. After pressing, the flexibility slides are removed and allowed to air dry (Steadman and Luner 1985).

Once the slides have dried, they are imaged using a microscope capable of using both reflected and transmitted light. Just as Mohlin did, the

length of non-contact, L, is measured. To equate the length of non-contact, Steadman treats the fiber as a uniformly loaded, homogeneous elastic beam. Figure 10 shows a schematic used by Steadman in the treatment of the fiber as a cantilever beam where q is the load, d is the diameter of the stainless steel wire, and L is the length of non-contact.

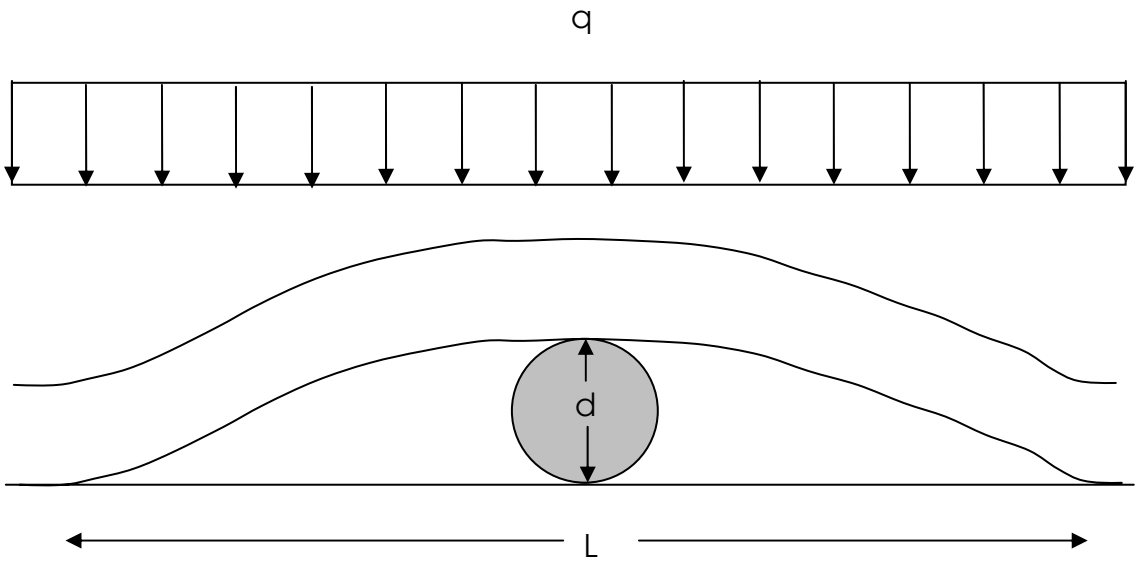

Figure 10 - Geometry of the Steadman Method
A schematic used by Steadman in the treatment of a fiber as a uniformly loaded, homogeneous elastic beam (Steadman and Luner 1985).

The method presented by Steadman is intended to measure the flexibility of the whole pulp (*i.e.*, both damaged and undamaged fibers); therefore one must take care when comparing fiber flexibilities that have been determined with different methods. Steadman compared his results to those measured by the Tam Doo and Kerekes method. Table 18 shows

flexibility measurements by the Steadman Method and the Tam Doo and Kerekes Method.

Table 18 - Comparison of Flexibility Results
Flexibility results obtained by the Steadman and TamDoo methods for unbleached kraft pulps (Steadman and Luner 1985).

Pulp	Median Flexibility Value ($N^{-1}m^{-2}$)	
	Steadman	Tam Doo and Kerekes
Black Spruce	4.5×10^{11}	6.7×10^{10}
Douglas Fir	1.7×10^{12}	2.6×10^{11}

The Tam Doo and Kerekes method is a single fiber method that cannot measure short fibers (< 2mm). The operator may artificially select longer and, hence, coarser fibers, leading to a lower flexibility number for the same pulp. Kuhn reports values of about 2×10^{11} $N^{-1}m^{-2}$ for black spruce (Kuhn, Lu, Olson et al. 1995). This value is on the same order of magnitude as the value reported by Steadman. The Kuhn method's bias toward longer fibers may also lead to slightly stiffer fiber measurements.

2.2.2 Fiber Properties/Treatments and Wet Fiber Flexibility

Tam Doo and Kerekes state that there are three major variables that have a great effect over wet fiber flexibility: species, yield, and beating (TamDoo and Kerekes 1981). Drying history is also very important. Each of

these in some form or fashion exerts control over the parameters E and I (TamDoo and Kerekes 1981). Species, yield, beating, and drying history serve as a convenient way of discussing the effect of fiber properties on wet fiber flexibility. Fiber collapse will also be discussed.

Species

The tree species from which pulp fibers come obviously has a major effect on most fiber properties. The species source controls the fiber composition and structure. The fiber composition will influence swelling and cell wall elasticity. Hemicelluloses and lignin contribute the majority of the acid groups in a fiber. The content and structure of both hemicellulose and lignin is dependent on species. In general, hardwoods are going to have more hemicelluloses and softwoods are going to have more lignin (see Table 4). Katz, Liebergott, and Scallan have shown that increasing the acid groups by 88% will lead to a 40% swelling improvement for spruce pulps (Katz, Liebergott and Scallan 1981). Greater swelling changes the structure of the cell wall and can affect fiber flexibility. With regard to the species, cell wall elasticity is going to be most affected by the S2 microfibril angle and the crystallinity of the cellulose (Paavilainen 1993).

Fiber coarseness is related to the thickness and density of the cell wall. It is another way in which different species may influence wet fiber flexibility.

Cell wall thickness is probably the most important wood fiber property with regard to wet fiber flexibility. Paavilainen measured cell wall thickness visually with a projection microscope and found thicker cell walls are less flexible and more difficult to collapse as shown in Table 19 (Paavilainen 1993). This was also shown earlier by Page (1967).

Table 19 - Cell Wall Thickness and Flexibility
Thicker cell wall are less flexible for unbleached softwood kraft pulp (Paavilainen 1993).

Cell Wall Thickness (μm)	Wet Fiber Flexibility (10^{10} $N^{-1}m^{-2}$)
5.5	80
7.0	30
9.0	10

Many other authors have described a similar trend (Steadman and Luner 1985; Abitz and Luner 1991; Laine and Stenius 1997b). Forgacs has reported that, as fiber length increases, the flexibility of the fiber increases (Forgacs and Mason 1958). This is contrary to the expected result. Clark states that the coarseness of a fiber increases with fiber length (Clark 1985). According to data from Paavilainen and other researchers, an increase in fiber length should lead to a decrease of the wet fiber flexibility because of the higher coarseness. Steadman points out longer fibers are

more easily damaged, which could lead to higher than expected flexibility numbers (Steadman and Luner 1985).

Yield

Pulping and bleaching methods can have a great impact on the final fiber composition and structure. The final yield of a pulp is generally an indication of the extent to which the fiber has been processed. Mechanical pulps, with yields generally ranging from 92-96% (Biermann 1996), undergo very little chemical treatment. Fully bleached kraft pulps will have yields around 45% and have the majority of their lignin and hemicelluloses removed. Wet fiber flexibility increases as yield decreases regardless of the method used to determine flexibility (TamDoo and Kerekes 1981; Steadman and Luner 1985; Paavilainen 1993). Some representative results for a hardwood pulp are shown in Table 20 (Paavilainen 1993).

Table 20 - Yield and Flexibility
As yield decreases the wet fiber flexibility increases for unbleached and ECF bleached white birch hardwood kraft pulp (Paavilainen 1993).

Kraft Pulp Yield (%)	Wet Fiber Flexibility (10^{12} $N^{-1}m^{-2}$)
75	0.25
70	0.38
60	0.52
48 – ECF Bleached	0.66

As the pulping process proceeds, material (mostly lignin and hemicellulose) is removed from the cell wall, which decreases cell wall thickness (Stone and Scallan 1967). This has a direct impact on E and I, giving more flexible fibers (TamDoo and Kerekes 1981). In unbleached pulp, lignin acts as a crosslinker in the cell wall and prevents swelling to some extent (Laine and Stenius 1997b). This action could also contribute to reduced wet fiber flexibility because of a "tighter" cell wall structure (Laine and Stenius 1997b).

Beating

The complexity of the beating process is well known. The major effects of beating are (Page 1989):

- Fiber cutting or shortening
- Fines production

- External fibrillation
- Internal fibrillation or delamination
- Inducing fiber curling or straightening
- Addition or removal of kinks and microcompressions
- Redistribution of the hemicelluloses

The extent of each effect is dependent on the type of device used for the refining process. For example, PFI refining has been shown to have higher internal fibrillation, lower external fibrillation, and almost no fiber cutting (Kerekes 2005).

Beating transfers mechanical energy to the fiber. The cell wall is delaminated, thereby decreasing the modulus of elasticity and increasing fiber flexibility (TamDoo and Kerekes 1981; Paavilainen 1993). Emerton states that the ability of a fiber to deform plastically is increased by the presence of internal defibrillation (Emerton 1957). The mechanical action imparted to the fiber could also serve to reduce the cell wall's resistance to swelling by breaking hydrogen bonds between adjacent polysaccharide units.

It is traditionally thought that one of the most important effects of beating is to increase fiber flexibility (Higgins and deYong 1961; Kibblewhite 1973;

Hietanen and Ebeling 1990). The increased degree of fiber flexibility aids in the ability of the paper sheet to consolidate during pressing and drying (Kibblewhite 1973). Kibblewhite also attributes the increased fiber flexibility to the internal defibrillation of the fiber (Kibblewhite 1973).

Emerton is careful to describe the effect of internal fibrillation as contributing to fiber deformation instead of fiber flexibility (Emerton 1957). While fiber flexibility may very well be impacted by the beating process, assigning the main effect to flexibility without regard to other forms of fiber deformation is premature. For instance, fiber collapse is also impacted by beating (Page 1967) and should also be considered when investigating fiber deformation behavior.

Fiber Collapse

During web consolidation, the ability of a fiber to collapse is extremely important. Fiber collapse is influenced by many of the same properties that can affect fiber flexibility such as yield, beating, and cell wall thickness (Page 1967). Page has also shown that never dried fibers are almost completely uncollapsed. Fibers that have been dried and reslushed are generally collapsed, but they can be returned to their uncollapsed state via beating. Refining, however, increases the amount of collapse for a pulp upon drying or re-drying (Page 1967).

The progress of collapse for single fibers is rather difficult to determine because of the damage that can occur to fibers during sample preparation. Hartler and Nyren measured the collapse behavior of single fibers between two optical flats in both the dry and wet state (Hartler and Nyren 1970; Nyren 1971). They found that the fiber first collapses and then the cell wall is compressed. Wild *et al*, however, did not observe two distinct regions and suggest that fiber collapse is a continuous process of dewatering and densification (Wild, Omholt, Steinke *et al.* 2005).

Gorres investigated fiber collapse by measuring the thickness of thin fiber networks which had been pressed to glass slides. His work has shown that wet pressing increases the number of collapsed fibers and that over 85% of the fibers are collapsed at 50 psi for an unbleached kraft pulp. Also, fiber collapse is initiated at the fiber-fiber contact points in a sheet because that is the where the wet pressing pressure is transferred (Gorres, Amiri, Grondin *et al.* 1993).

Drying History

The drying history of a fiber has some effect on the flexibility of low yield pulps. As a fiber is dried, the amount of cross-linking between microfibrils due to new hydrogen bonding increases (Laivins and Scallan 1993). These

new bonds are not broken during rewetting, which leads to a reduction in swelling and fiber stiffening. The progressive loss of swelling and increased fiber stiffening is referred to as hornification (Lainins and Scallan 1993).

The hornification of a fiber increases with each drying cycle. Laivins and Scallan show that the greatest increase in hornification occurs during the first drying cycle and continues to increase with each additional cycle (Laivins and Scallan 1993). In Table 21, Paavilainen has also demonstrated how hornification reduces the flexibility of fibers (Paavilainen 1993).

Table 21 - Hornification and Flexibility
The effect of hornification on the wet fiber flexibility of fibers. The flexibility was determined using the Steadman method (Paavilainen 1993).

	Flexibility ($x10^{12}$ $N^{-1}m^{-2}$)
Southern Pine, Bleached Kraft Never Dried	0.51
Southern Pine, Bleached Kraft Air Dried	0.25
Southern Pine, Unbleached Kraft Never Dried	0.43
Southern Pine, Unbleached Kraft Air Dried	0.15

2.2.3 Wet Fiber Flexibility and Paper Properties

Wet fiber flexibility is traditionally considered significant to almost every physical and optical property of paper. More flexible fibers respond

better to Campbell's forces and form a consolidated sheet with more fiber-to-fiber bonded area (Paavilainen 1993). Higher wet fiber flexibility leads to increases in many sheet properties. Three closely related properties are discussed below: apparent density, tensile index, and light scattering coefficient. The data presented in the following discussion were measured using a method developed by Steadman (Steadman and Luner 1985).

Apparent Density

Apparent density is a fundamental property of paper which is related to most other sheet properties. It is a representation of the amount of sheet consolidation, or how tightly the fibers are packed together in the sheet. Flexible fibers will make sheets that are more consolidated, and, hence, with a higher apparent density. Steadman (Steadman and Luner 1985) and Paavilainen (Paavilainen 1993) have both shown that as fiber flexibility increases, apparent density also increases. Results for a Scandinavian pine sulfite pulp are shown in Table 22. Steadman suggests that, for a particular pulp treatment, a fines-free sheet apparent density can be used as a measure of average fiber flexibility (Steadman and Luner 1985).

Table 22 - Apparent Density and Flexibility
As wet fiber flexibility increases, so does sheet apparent density for unbleached softwood kraft pulp(Steadman and Luner 1985).

Sheet Apparent Density (kg/m^3)	Effective Fiber Flexibility ($x10^{12}\ N^{-1}m^{-2}$)
625	0.9
700	2.0
745	3.1

Tensile Strength

The tensile strength of a sheet is affected by the strength of individual fibers, the bond strength and the relative bonded area (Page 1969). Fibers that are more flexible generally have more opportunities to form fiber-fiber bonds. Paavilainen has shown how tensile index increases linearly with wet fiber flexibility (Paavilainen 1993). Table 23 summarizes some of Paavilainen's data.

Table 23 - Tensile Index and Flexibility
An increase in wet fiber flexibility results in increased tensile index for an unbeaten and unbleached kraft Scandinavian pine (Paavilainen 1993).

Tensile Index (Nm/g)	Wet Fiber Flexibility ($x10^{12}\ N^{-1}m^{-2}$)
8.0	0.13
21.0	0.78
41.0	1.20

Light Scattering Coefficient

If more flexible fibers produce sheets with larger bonded areas, a decrease in light scattering coefficient should also be observed. Paavilainen has shown (see Table 24) how light scattering coefficient decreases with increasing wet fiber flexibility (Paavilainen 1993).

Table 24 - Light Scattering and Flexibility
An increase in wet fiber flexibility results in decreased light scattering coefficient for an unbeaten and unbleached kraft Scandinavian pine (Paavilainen 1993).

Light Scattering Coefficient (m^2/kg)	Wet Fiber Flexibility ($x10^{12}$ $N^{-1}m^{-2}$)
28	0.5
21	1.0
14	1.7

2.2.4 A New Direction: Wet Fiber Deformability

Researchers have attempted to measure the flexibility, conformability, collapsibility, pliability, compactability, *etc.* of pulp fibers. Each of these cases is, in essence, trying to measure the deformability of individual fibers. The most relevant methods to measure any of the above properties have been previously presented (see section 2.2.1). In almost every case the

researcher has treated the fiber as an elastic beam expressing the result as the inverse of fiber flexural stiffness. Recent work by Waterhouse and Page has pointed out that this assumption may not be appropriate (Waterhouse and Page 2004).

A fiber can undergo deformation due to both bending and shear. The controlling mode of deformation depends on the span and the ratio of the longitudinal modulus to the transverse shear modulus (Waterhouse and Page 2004). As the span decreases, the importance of shear deformation increases. Previous methods to measure wet fiber flexibility have used spans ranging from the length of the fiber (up to 4 mm) in the cantilever method of Seborg and Simmonds (Seborg and Simmonds 1941) to approximately 100 μm in the method of Steadman and Luner (Steadman and Luner 1985). As the step height of the underlying fiber (*e.g.*, the stainless steel fiber used by Steadman) decreases, the spans which the deforming fiber must cross also decrease. A collapsed pulp fiber will have a step height ranging from 3-10 μm, which is much smaller than that of any method used to test wet fiber flexibility.

Work by Scallan and Tigerstrom (Scallan and Tigerstrom 1992) and Nilsson, Wagberg, and Gray (Nilsson, Wagberg and Gray 2001) has investigated the wet moduli of pulp fibers. Based on their work, the ratio of longitudinal

elastic modulus to transverse shear modulus may be on the order of 1000 (Waterhouse and Page 2004). This ratio coupled with the short spans most likely present in a paper sheet implies that shear may be the controlling mode of deformation. Waterhouse and Page support this implication by determining the percent of total deformation due to shear for several methods previously used to measure wet fiber flexibility. The results are presented in Table 25. According to these estimations, between 79 and 94% of the deformation of fibers in a paper sheet is due to shear.

Table 25 - Percent of Total Deformation Due to Shear
The percent of total deformation due to shear is described for several wet fiber flexibility measurements. A calculation for real paper is also included (Waterhouse and Page 2004).

Method	Percent of Total Deformation Due to Shear	
	Uncollapsed Fiber (%)	Collapsed Fiber (%)
Samuelson 1963	26.2	0.22
Tam Doo and Kerekes 1981	76.2	1.96
Steadman and Luner 1985	89.6	66.9
Kuhn *et al.* 1995	45.4	0.44
Waterhouse and Page 2004 -estimate for a paper sheet	93.9	78.5

2.3 Light Interference

Light interference is commonly observed in the every day world. The colors of a soap bubble or an oil slick, for instance, are formed from the interference that results from the reflection of light from the front and back surfaces of the thin film (Halliday, Resnick and Walker 1993). The colors are a result of the varying film thickness. The use of monochromatic light allows this thickness to be determined. Consider Figure 11 where an air film of thickness L is shown between two objects that have higher indices of refraction, *n*. Light reflected at *a* to form r_1 will not experience a phase change while light reflected at *b* to form r_2 will shift out of phase by ½ wavelength of light. For the waves to end up exactly out of phase and undergo completely destructive interference, the path length difference, 2L, must be equal to zero or an integer multiple of the wavelength of light being used. Therefore the film will appear dark whenever its thickness, L, is described by Equation 3. In this research, this is applied to the air wedge created by a fiber freespan to measure stepheights in section 4.5.

$$L = m\frac{\lambda}{2} \qquad m = 0, 1, 2, \ldots$$

Equation 3 - Light Interference for a Thin Air Film

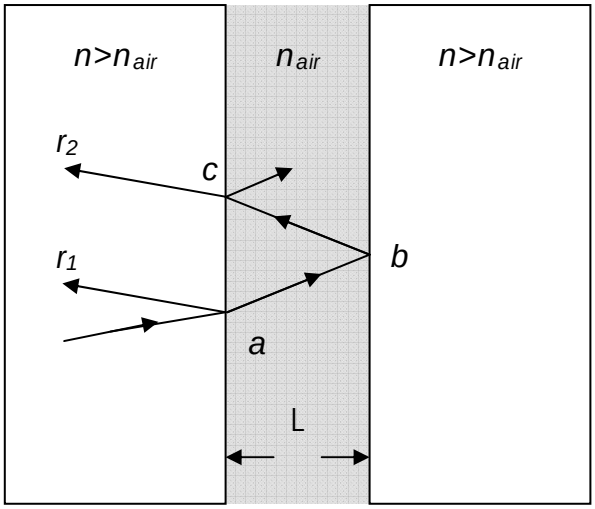

Figure 11 - Light Interference
An air wedge is shown between two objects with a higher index of refraction. The light source is nearly perpendicular and the angles of the rays are exaggerated.

2.4 Fiber-Fiber Bonds

The local deformation behavior of pulp fibers plays a large role in the formation of fiber-fiber bonds. Fiber-fiber bonding is widely regarded as one of the most important properties for the papermaker because it is principally responsible for the internal cohesion of a paper sheet (Retulainen and Ebeling 1993). Bonding is traditionally defined using two independent factors: bonded area and specific bond strength (bond strength per unit bond area) (Nordman 1957). There is significant industrial importance in decoupling these two factors because bonded area is directly related to both optical and strength properties, while specific bond strength has little impact on the optical properties.

Refining and wet pressing are traditional papermaking tools that effect fiber deformation behavior; hence, they can have a direct impact on bonded area (Ingmanson and Thode 1959; Nordman, Aaltonen and Makkonen 1965; Alexander and Marton 1968), and thus they manipulate both strength and optical properties. This trade-off can be overcome by directing research efforts toward enhancing specific bond strength leading to significant benefits for many paper grades. The determination of specific bond strength requires that a true bonded area between fibers be measured. Current methods may not accurately deconvolute the contributions of molecular interactions between fibers from the surface area over which they operate.

2.4.1 Fiber Bonding

The strength of paper is inherently linked to the ability of pulp fibers to form inter-fiber bonds. An inter-fiber bond can be defined as the area between two fibers sufficiently close such that molecular interactions can occur between the surfaces of the fiber. Several mechanisms for inter-fiber bond formation have been reviewed by Lindstrom *et al* (Lindstrom, Wagberg and Larsson 2005).

Hydrogen bonding is a chemical interaction between an electron poor molecular region and an electron rich molecular region. Traditionally, it has been cited as a major component of the cellulose fiber bonding mechanism. Nissan has described this concept at length (Nissan 1961; Nissan and Sternstein 1964). The cellulose fiber surface is rich with the hydroxyl groups which could participate in hydrogen bonding. One problem with attributing the majority of bonding between cellulose fibers to hydrogen bonding is that the hydroxyl groups must be within ~3 Å to form a bond. This is unlikely to occur via pressing the surfaces together (McKenzie 1984).

Recent work by Notley has show that van der Waals interactions could be important to cellulose fiber bonding (Notley, Petterson and Wagberg 2004). Notley measured the interaction force between a 13.5 μm cellulose sphere and a regenerated cellulose film under aqueous conditions. It was found that van der Waals interactions can begin to have effect at a 40 nm separation, much larger than most molecular interactions require. This suggests that long range van der Waals forces may play a larger role in cellulose fiber bonding than previously thought.

The surface of the fiber cell wall is rather soft and malleable (Nilsson, Wagberg and Gray 2001); therefore, it has been postulated that the

actions of wet pressing and drying may manipulate two fiber surfaces such that they interlock with one another. During the drying process Campbell's forces are known to exert significant amounts of force between two surfaces (Clark 1985). This leads to the intimate contact illustrated in Figure 12. It is important to note that the contact depicted here does not necessarily imply that the surfaces are interacting on the molecular level (Lindstrom, Wagberg and Larsson 2005).

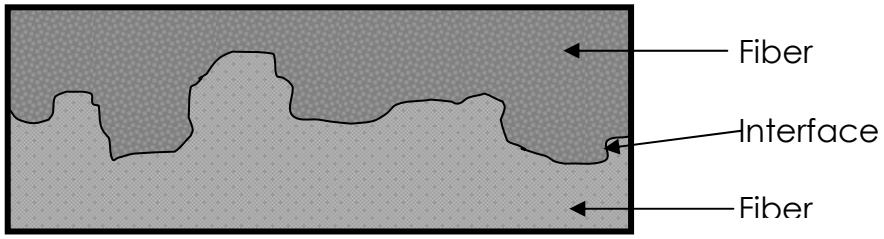

Figure 12 - The Interlocking Mechanism of Bonding
Schematic representation of two fibers surfaces interlocking due to Campbell's forces during drying (Lindstrom, Wagberg and Larsson 2005).

McKenzie has suggested that Voyutskii theory of diffusion controlled adhesion can be applied to inter fiber bonding (McKenzie 1984). Here plasticized polymeric materials that are similar in nature will diffuse across the interface into one another. The plasticizing agents (temperature, pressure, solvent) are removed and the intermingled polymer chains are locked in place. McKenzie examined the potential for hemicelluloses to interdiffuse since they are known to be softened with water (Goring 1963).

Pelton has reported similar results with dextran saturated fibers (Pelton, Zhang, Wagberg et al. 2000). An illustration of the interdiffusion mechanism is shown in Figure 13.

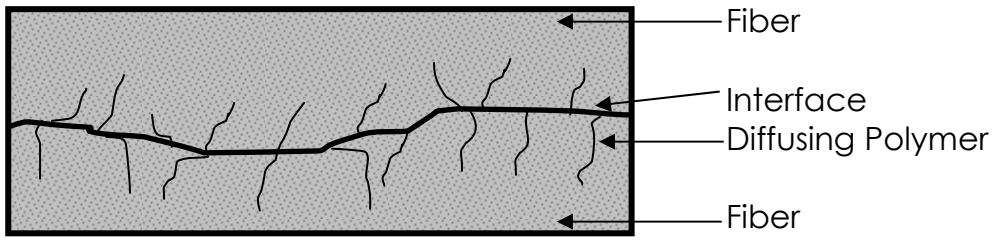

Figure 13 - The Interdiffusion Mechanism of Bonding
Schematic representation of interdiffusion between two fiber surfaces (Lindstrom, Wagberg and Larsson 2005).

While the mechanisms discussed above may operate under different constraints, they each must be accompanied by two fiber surfaces that are in close proximity (on the order of one nanometer) to each other. As the fiber surfaces approach one another, various molecular interactions begin to occur resulting in the formation of a fiber-fiber joint. Ultimately, the number of bonding interactions and the nature of those interactions determine the efficacy of the bonded area to transfer load between fibers. This dictates end product quality in terms of paper optical and strength properties.

2.4.2 Bonded Area

In order to measure the efficiency of the interfacial fiber-fiber area to transfer load, the total bonded area needs to be defined. Many researchers have offered methods (Parsons 1942; Haselton 1955; Ingmanson and Thode 1959; Caulfield 1973; Yang, Eusufzai, Sankar et al. 1978). According to Uesaka *et al.* relative bonded area (RBA) can be measured either directly or indirectly (Uesaka, Retulainen, Paavilainen et al. 2002). Direct methods, such as Yang *et al.* (Yang, Eusufzai, Sankar et al. 1978), depend on the sectioning of sheets followed by an examination of micrographs and computer analysis. However, the accuracy of such methods is directly linked to the quality of sample preparation and the micrograph data collection methodology.

The more commonly used indirect methods were developed to measure the relative bonded area in paper sheets. They generally utilize gas adsorption or light scattering techniques. The scattering coefficient is related to the free specific surface area from which an approximation of the bonded area of a paper sheet can be derived. The most widely used method for measuring relative bonded area, developed by Ingmanson and Thode (Ingmanson and Thode 1959), relies on the use of light scattering coefficient and extrapolation to zero tensile strength.

Support for the use of light scattering as an indication of bonding can be found in several places. Barkas has shown that tremendous pressures can be generated from the Cambell's forces which would deform the malleable fiber surfaces and bring them into intimate contact (Barkas 1950). Asunmaa and Steenberg have directly observed the close contact between bonded fibers down to the resolution limit of their micrographs of 20 Å (Asunmaa and Steenberg 1958) suggesting that the fiber surfaces are within the distance necessary for molecular interactions to occur. The work of Haselton utilized nitrogen gas adsorption and the Brunauer-Emmett-Teller (BET) method to calculate specific surface area (Haselton 1955). Graphs of BET area versus scattering coefficient go through the origin suggesting that the separation between bonded surfaces can not be more that 0.4 nm (the radius of a nitrogen molecule). Since this method does not depend on the use of light scattering, it has been extensively used by scientists for pulp fibers.

Despite the evidence describe above, there is still debate surrounding the use of optical techniques such as light scattering to describe the bonded area (Page and Wagberg 1997). Currently, there is no definitive method to measure bonded area. A new, preferably *in situ*, method that does not depend on the scattering of light is needed. Combining the technique of

fluorescence microscopy with the principle of fluorescence resonance energy transfer could provide such an opportunity.

2.4.3 Fluorescence Resonance Energy Transfer

A proper description of FRET requires a full understanding of electronic spectroscopy. For an extensive review of the basic principles of fluorescence spectroscopy and resonance energy transfer, see Lakowicz (Lakowicz 1983) and van der Meer *et al.* (Van Der Meer, Coker and Chen 1994). FRET is a long range dipole-dipole interaction between two fluorescing dye molecules resulting in a non-radiative transfer of excitation energy from a donor to an acceptor dye. FRET can only occur if there is sufficient spectral overlap and the two dye molecules are within 100 Å of one another. The interaction is electrostatic in nature and shows a characteristic inverse sixth power relationship between the energy transfer efficiency and the donor-acceptor distance.

Figure 14 illustrates the relevant spectra and a characteristic FRET response. The unique signature of FRET is the observation of long wavelength emission attributed to the acceptor molecule with donor molecule excitation at a much shorter wavelength. Since the acceptor molecule has low absorbance (and correspondingly low fluorescence quantum efficiency) at the excitation wavelength of the donor, emission

from the acceptor must be due to non-radiative energy transfer. Furthermore, if the nature of the donor and acceptor dye molecules and the index of refraction of the surrounding media are known quantities then the energy transfer efficiency can be used to determine the separation distance between the two molecules.

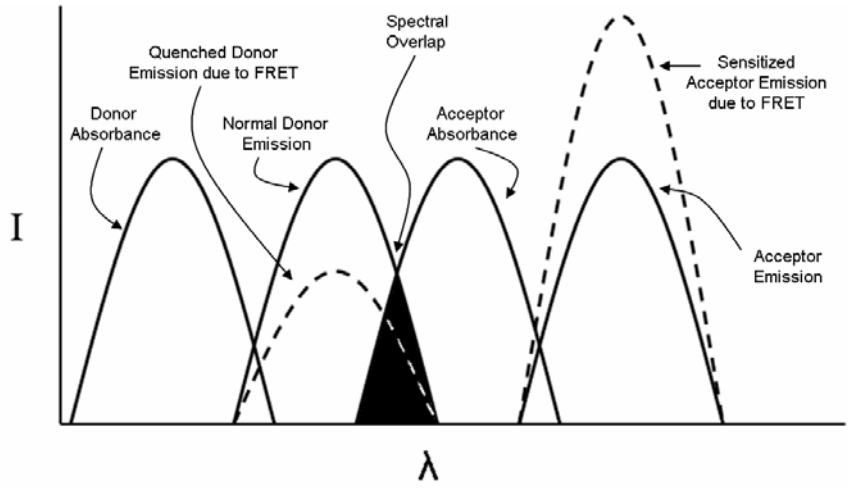

Figure 14 - FRET Spectra
Stylized representation showing decreased donor emission and increased acceptor emission due to non-radiative energy transfer (Herman 1998).

FRET has been widely used in medical and biochemical research as a tool to determine distances and global structural alterations in proteins and DNA (Somogyi, Matko, Papp et al. 1984; Hoppe, Christensen and Swanson 2002; Yapoudjian, Ivanova, Douchet et al. 2002). FRET gains new applications daily in a variety of fields, particularly material science. The technique is powerful because it can be used in imaging applications

when a fluorescence microscope is employed (Jares-Erijman and Jovin 2003). Currently, FRET is not being utilized in the study of pulp and paper and more specifically it has not been used to probe the nature of the fiber-fiber bond.

An illustrative example of how FRET could operate in a paper system is shown in Figure 15. Two fibers, independently dyed with the donor and acceptor dyes, are brought into close proximity via capillary forces and wet pressing. When illuminated with the appropriate wavelength of light to excite the donor dye molecule, acceptor fluorescence can be detected if the two molecules are within 100 Å. Variations in the intensity of acceptor and donor fluorescence allow the FRET response to be used as a "spectroscopic ruler" to provide spatial information about the fiber-fiber interface.

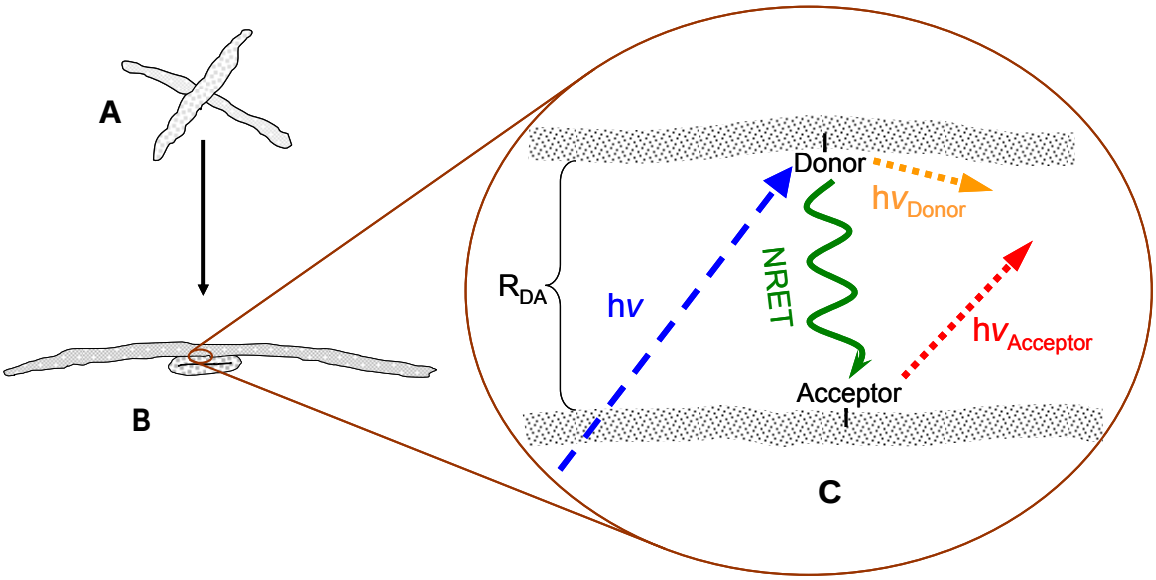

Figure 15 - FRET in a Paper System
Illustration of excitation energy transfer in a paper system. (A) A fiber crossing composed of a donor dyed and an acceptor dyed fiber. (B) A side view of the crossing. (C) A representation of the fiber-fiber interface indicating the donor-acceptor distance (R_{DA}), donor excitation ($h\nu$), donor emission ($h\nu_{Donor}$), non-radiative energy transfer (NRET) between the dye molecules, and acceptor emission ($h\nu_{Acceptor}$) due to NRET.

CHAPTER 3: PROBLEM ANALYSIS AND OBJECTIVES

Within this thesis, the main objective was to better understand the contribution of physical and chemical modifications of lignocellulosic fibers to deformation behavior and the formation of fiber-fiber bonds. Many researchers have worked on developing an understanding of fiber deformation behavior, fiber-fiber bond formation, and their relationship to the physical and optical properties of a paper sheet. The seminal works have been reviewed in the previous chapter in order to establish a salient experimental program.

The methods that have been developed to examine fiber deformation behavior have generally modeled a fiber as a linearly elastic beam expressing the result as the inverse of fiber stiffness. Recent work has shown that this assumption may be inappropriate (Waterhouse and Page 2004). In fact, the primary mode of deformation may be shear.

The local deformation behavior of pulp fibers plays a large role in the formation of fiber-fiber bonds. Fiber-fiber bonding is widely regarded as one of the most important properties because many of the physical and optical properties of paper sheets are derived from the ability of lignocellulosic fibers to form bonds. Despite all the work investigating the

structure and formation of inter-fiber bonds, no method currently exists that can resolve the fine structure of the molecular interactions between two fiber surfaces involved in a bond.

Therefore, the objectives of this thesis were to:

- Develop a new technique to investigate the deformation behavior of lignocellulosic fibers that better approximates what is occurring during the formation of a paper sheet.
- Investigate how traditional industrial processes (refining, bleaching, drying, *etc.*) impact fiber deformation behavior.
- Examine how chemical fiber modification techniques impact fiber deformation behavior.
- Develop a method to study the molecular interactions of a fiber-fiber bond while two fiber surfaces are bonded.

Steadman's method to measure wet fiber flexibility appeared to be the closest to approximating what occurs in real paper. Hence, it served as the basis for the method described in Chapter 4. This new technique allowed the implications of changing wet fiber deformation behavior to be observed. Specifically, wet fiber deformability is the tendency of fibers to deform elastically and plastically in the z-x and z-y direction under stress in the z direction while in a water-swollen state.

Observing the fine structure of a fiber-fiber bond required a novel approach borrowed from the analysis of protein structures. Combining the technique of fluorescence microscopy with the principle of fluorescence resonance energy transfer provided the opportunity to observe an inter-fiber bond *in situ* without any dependence on light scattering or the destruction of the fiber-fiber joint for analysis.

The remainder of this thesis is dedicated to describing the methods, materials, and results of two new methods that investigate fiber deformation behavior and the formation of fiber-fiber bonds. Chapter 4 describes the materials and methods used for this work in detail. The methods are developed and applied in Chapters 5-8 each of which was written such that they could be read independently of the thesis. Finally, the overall conclusions and some recommendations for future work are included as Chapter 9 and Chapter 10, respectively.

CHAPTER 4: EXPERIMENTAL MATERIALS AND PROCEDURES

The materials, methods, and equipment utilized during the research program are described below. Portions of the following chapter are reproduced with the kind permission of The Pulp and Paper Fundamental Research Society[i].

4.1 Pulp

Mill produced northern Canadian black spruce (*Picea mariana*) unbleached kraft pulp was provided by SFK Pulp in Saint Félicien, Québec. A mill produced birch (*Betula papyrifera*) pulp was provided by Oy Metsä-Botnia Ab in Äänekoski, Finland. A mill produced white spruce (*Picea glaucal*) was provided by Alberta Pacific in Alberta, Canada. A regenerated cellulose viscose pulp (13.3 mg/100m) was supplied by Lenzing AG, Austria. The pulp samples came from various points in the mill operation. Table 26 list the various pulp samples, its origin, and the mill sample point. The bleached birch pulps were ECF bleached with a A O Z/D E_{OP} D Z P sequence. The bleached white spruce pulps were ECF bleached with a standard D E_{OP} D E D sequence. Bleaching abbreviations are described in the Nomenclature section.

[i] Initially presented at the 13th Fundamental Research Symposium, September 11-16, 2005, Robinson College, Cambridge, England and published in the Transactions of that meeting. See Appendix C for copyright permission.

Table 26 - Pulp Sample Descriptions and Nomenclature
A list of the various pulp samples used in this research is shown. Each pulp's origin, drying history, bleaching history is also shown. ISO brightness and kappa number are shown where applicable. Average fiber length is for the medium long fraction.

Species	Origin	Drying	Bleaching	Length Weighted Average Fiber Length (mm)	ISO Brightness	Kappa #
Black Spruce	Canada	Never Dried	Unbleached	3.07	--	19.9
Birch	Finland	Dried	Mill Bleached	1.01	84.1	--
Birch	Finland	Never Dried	Unbleached	1.05	--	15.0
Birch	Finland	Never Dried	Mill Bleached	1.02	84.3	--
White Spruce	Canada	Never Dried	Mill Bleached	3.10	88.2	--
Viscose	Austria	NA	NA	1.90*	--	--

* Manually cut from the original staple fiber length of 39 mm

4.2 Chemicals

Two fluorescent dyes were purchased from Molecular Probes (Eugene, OR, USA): 7-diethylaminocoumarin-3-carboxylic acid hydrazide (DCCH) and fluorescein-5-thiosemicarbazide (FTSC). All other chemicals in this

research were purchased from Sigma-Aldrich, VWR, or Fischer Chemicals and used as described below.

4.3 Standard Procedures

4.3.1 Laboratory Refining

All refining in this research was performed in a standard PFI mill following the TAPPI Standard Method T 248 sp-00. A beating gap of 0.2 mm was used. Pulps were generally refined to 300, 1000, 2000, and 4000 revolutions.

4.3.2 Canadian Standard Freeness

Canadian standard freeness (CSF) was measured for each pulp after refining using TAPPI Standard Method T 227 om-04. The correction factors for temperature and consistency cited in the standard method are for groundwood pulps only. The CSF method requires that the sample consistency and temperature to be at 0.30% and 20.0°C, respectively. When these requirements are not met, the CSF must be corrected to the standard using the equations for chemical pulps (Sundrani, Hill and Biermann 1993). Two tests are performed and the results are averaged if they are within 5.0%. When the two samples do not agree, another sample is taken and the test is repeated. Results are reported in mL.

4.3.3 Fiber Quality Analysis and Fiber Coarseness

Fiber length and coarseness were determined using fiber quality analyzer developed by OpTest Equipment, Inc. Standard methods described in the operation manual, Fiber Quality Analyzer, Code LDA96 were used. A dilute fiber suspension (~0.0008% consistency) is prepared and the average fiber length is determined optically via an internal image analysis program. Fiber length is reported in mm as a length weighted average of 5000 fibers. Fiber coarseness is reported in mg/100m. Two tests are performed and the results are averaged if they are within 5.0%. When the two samples do not agree, another sample is taken and the test is repeated. Data are reported in Table 26, Chapter 6, and Appendix D.

4.3.4 Moisture Analysis

A Mettler Toledo HR73 moisture analyzer was used for all consistency measurements. Samples were generally measured three times and then averaged. The results are reported in percent and were accepted if the standard deviation was less than 5.0%

4.3.5 Handsheet Forming

Handsheets were prepared using TAPPI Standard Method T 205 sp-06. A standard TAPPI handsheet mold and press at 50 psi were generally used.

When it was necessary to vary the handsheet pressing pressure (1.75 psi – 300 psi) a modified press was used (see Figure 17).

4.3.6 Tensile Strength

Tensile strength was measure with a Lorentzen and Wettre Alwetron TH1 following TAPPI Standard Methods T 220 sp-06 (physical testing), T 494 om-01 (tensile properties), and T 402 sp-03 (laboratory conditioning). Generally, 10 strips were measured from each sample. The average and standard deviation were calculated for each set. The results are reported in Nm/g in Appendix D.

4.3.7 Caliper

Caliper was measured using a EMVECO Electronic Microgage 200A with soft platens following TAPPI Standard Method T 411 om-05. The average and standard deviation were calculated for each set. The results are reported in μm.

4.3.8 Basis Weight

Basis weight or grammage was determined using TAPPI Standard Method T 410 om-02. The weight of each air dry handsheet is recorded in g. The sheet is used for physical testing as long as the oven dry weight is between 1.140 g and 1.260 g. The standard handsheet area (200 cm^2) is

then used to calculate the basis weight of each sheet. The average and standard deviation were calculated for each set. The results are reported in g/m^2 in Appendix D.

4.3.9 Scattering Coefficient

Scattering coefficient was determined using a Technidyne Opacimeter BNL-3 following TAPPI Standard Method T 425 om-06. R_o and R_∞ are determined for each handsheet. The results are corrected for the basis weight of each sample. The average and standard deviation were calculated for each set. The results are reported in m^2/kg in Appendix D.

4.3.10 Kappa Number

Kappa number was measured following TAPPI Standard Method T 236 om-99. Two tests are performed and the results are averaged if they are within 5.0%. When the two samples do not agree, another sample is taken and the test is repeated.

4.3.11 Pulp Screening

Mill pulps were screened upon receipt using a Valley Screen with 0.008 inch slot screen following TAPPI Standard Method T 278 sp-04. The rejects were discarded.

4.3.12 Water Retention Values

The water retention values were measured at STFI by Elisabeth Duker following the Scandinavian Pulp, Paper, and Board Testing Committee standard SCAN-C 62:00. Two tests were performed and the results were averaged if they are within 5.0%. When the two samples do not agree, another sample is taken and the test is repeated. The results were reported as g of water retained/g oven dry fiber.

4.3.13 Equipment List

The following equipment was used. When available, a model, part, or catalogue number is also stated.

- Valley Screen (0.0008 in Slotted Screen)
- PFI Mill
- Bauer-McNett Classifier
- Buchner funnel
- Vacuum flask
- Ultrasonic Cleaner (Branson 3510)
- Filter paper (VWR #: 28320-143)
- Blotter paper (XPEDEX Grade 240, 8"x8" sheets)
- Glass slides (VWR #: 48300-025)
- Grade V-1 Mica (Structure Probes, Inc #:1872)

- Microscopic immersion oil (Richard Allen Scientific #: M3000)
- Leica DM-IRM microscope (Vashaw Scientific)
- EFOS X-Cite 50 W metal halide lamp (Vashaw Scientific)
- Hamamatsu ORCA-ER digital camera (Vashaw Scientific)
- Simple PCI image analysis software (Verison 5.3, ComPix and Vashaw Scientific)
- Custom Fluorescence Filter Cubes (Chroma Tech and Vashaw Scientific)
- MATLAB (Verison 7.2, MathWorks)

4.4 Sample Preparation for Deformability Analysis

4.4.1 Fiber Refining and Classification

Each pulp sample was washed upon receipt in a Buchner funnel with deionized water until the filtrate ran clear. The pulps were then screened using a Valley screen with 0.008 inch slot screen as describe in section 4.3.11 and then refrigerated at 4°C until required.

Samples were PFI refined to 300, 1000, 2000, and 4000 revolutions followed by Canadian standard freeness measurement. Ten grams (oven dry basis) were then fractionated using the Bauer-McNett Classifier. Table 27

describes the screens used for softwood (black spruce, white spruce) and hardwood (birch) pulps.

Table 27 - Bauer-McNett Classifier Screens
The screen sizes for fiber classification are listed. The screen sizes were set such that the average fiber length was captured in the medium long fraction.

Sample	Fraction	Screens
Softwood	Longs	R12
	Medium Longs	R14
	Medium Shorts	R28
	Shorts	R35
Hardwood	Longs	R28
	Medium Longs	R35
	Medium Shorts	R48
	Shorts	R200

All fractions were saved, but generally only the medium long fraction was tested. Water was removed from the unfractionated fibers with a Buchner funnel and filter paper to bring the pulp mat to approximately 20% consistency.

4.4.2 Fiber Dyeing

Approximately 0.2500 g (oven dry basis) was weighed from the medium long sample. Using a calibrated pipette, 5.000 mL of a 0.20 weight percent solution of Chlorazol Black dye was added to the pulp in a plastic

digestion vile. The total volume was brought to 25.0 mL and then capped. The fiber suspension was thoroughly mixed via shaking and then refrigerated overnight at 4°C. The fibers were then exhaustively washed with deionized water in a Buchner funnel until the filtrate was free of color before being suspended in 1000.0 mL of deionized water for slide making.

4.4.3 Slide Making

An 18.5 cm diameter 415 qualitative filter paper was placed onto a wet screen in a TAPPI handsheet mold. Once closed, 5000 mL of deionized water and approximately 20.0 mL of the fiber suspension were top-filled into the mold. The sample was drained onto the filter paper and wet pressed onto four (25mm x 75mm) glass slides for two minutes at 50 pounds per square inch as illustrated in Figure 16. A modified press used to apply pressure is shown in Figure 17. A metal coupon cut to the exact size of 4 glass slides was used to ensure that the pressure applied to the glass slides was 50 psi. Once the pressure was released, the filter paper was removed. The slides were allowed to dry and were kept under TAPPI Standard Conditions before and during imaging.

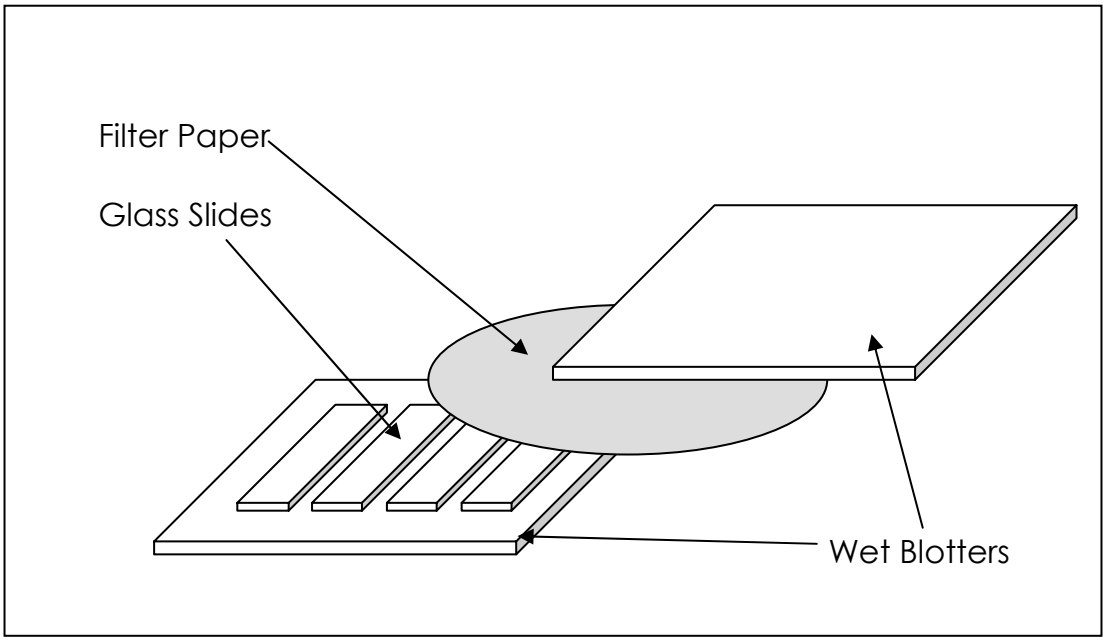

Figure 16 - The wet pressing setup
An illustration describing the wet pressing setup with the placement of wet blotters below the glass slides (25 mm x 75 mm) and above the filter paper.

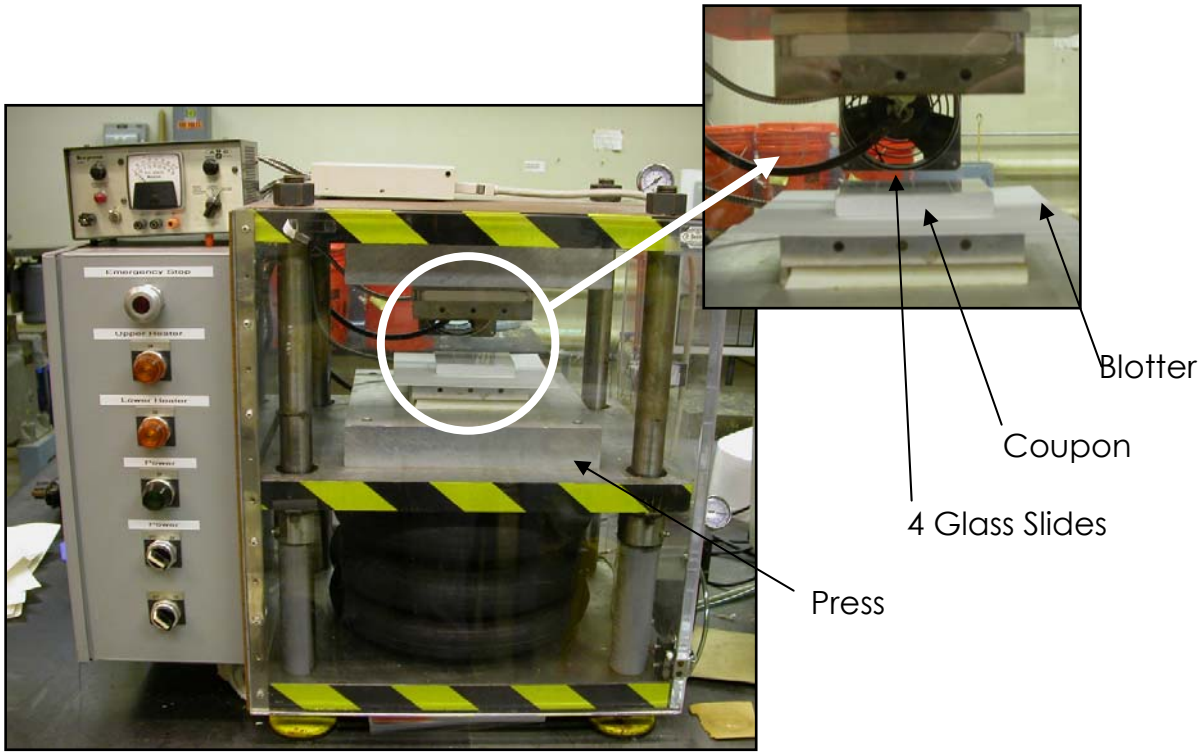

Figure 17 - The Press
A metal coupon was used to assure the entire load was being transferred through the glass slides.

4.5 Optical Microscopy for Wet Fiber Deformability

The research utilized a Leica DM-IRM inverted, reflected light microscope equipped with a Hamamatsu ORCA-ER digital camera and a 50 watt metal halide lamp (see Figure 18). A Leica 40X objective with a correction collar to allow imaging through a glass slide was also utilized for this research. A mica sheet was brought into optical contact with the glass slide by applying microscopy immersion oil (Resolve M3000, Richard-Allan Scientific) to the underside of the glass slide as shown in Figure 19. The specimen was then illuminated and viewed in crossed polars. The optical axis of the mica is set at 45° to the plane of polarization.

Figure 18 - The Microscopy Equipment
The Leica microscope, digital camera, computer, and light source are shown.

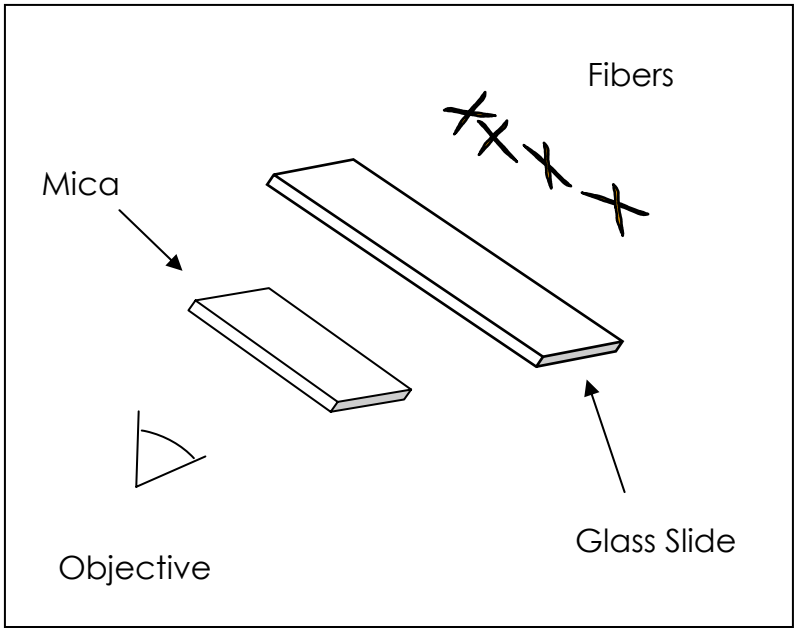

Figure 19 - The Imaging Setup
A piece of mica split to the appropriate thickness is applied to the bottom of the glass slide with microscopy immersion oil.

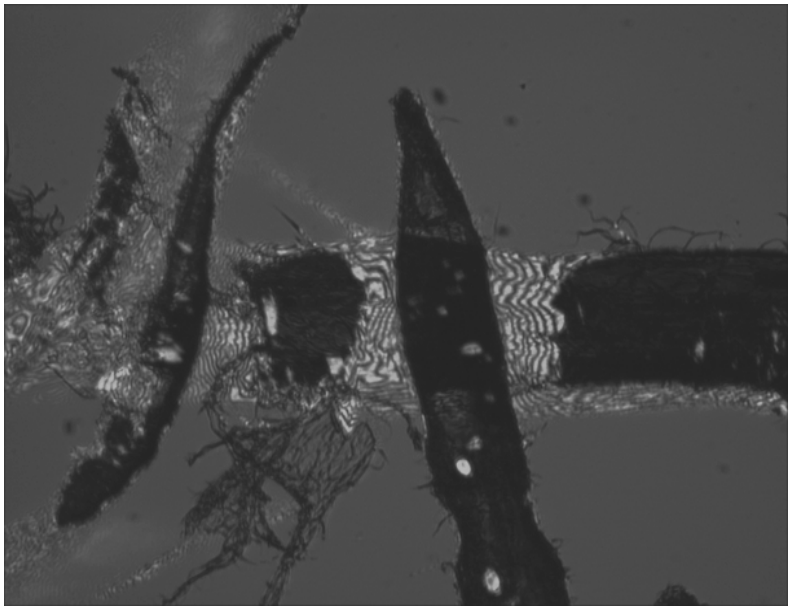

Figure 20 - Image of a Fiber Crossing
A micrograph showing the dark regions of the fiber that are in contact with the glass slide and the interference fringes.

Figure 20 is a micrograph of a fiber crossing. The areas of bonding between the fibers and the glass appear dark compared with the bright regions of non-contact. A narrow band filter (λ=547±10 nm) allows interference fringes to be observed. Figure 21 illustrates the geometry of a fiber crossing. F is the freespan and H is the stepheight.

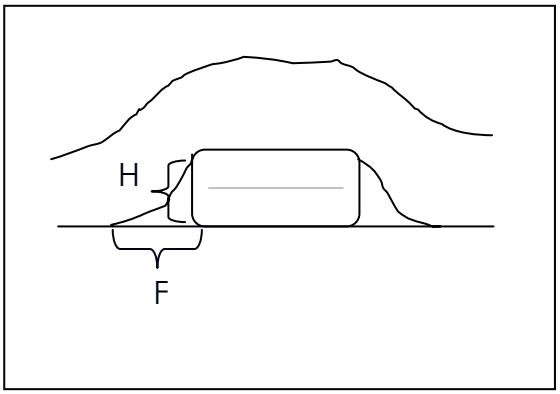

Figure 21 - Stepheight and Freespan in a Fiber Crossing
An illustration showing the location of stepheight (H) and freespan (F) measurements.

To determine the local height of the air wedge, H, Equation 4 is used. Where *n* is the number of black fringes counted from where the fiber leaves the glass slide and λ is the wavelength of light. Equation 4 is derived from the behavior of light in thin films (Halliday, Resnick and Walker 1993)

$$H = n\frac{\lambda}{2}$$

Equation 4 – Calculating Stepheight

4.6 Image Analysis for Wet Fiber Deformability

Between 30 and 50 fiber crossing micrographs were captured for each sample condition. Only undamaged fibers crossing at 90±30° were analyzed. Freespans were generally measured along the central axis of the fiber using the Simple PCI image analysis software. Figure 22 indicates where the freespan and stepheight were measured on this micrograph. The interference fringe pattern was used to deduce the stepheight and determine the shape of the lower surface of the crossing fiber in the freespan region.

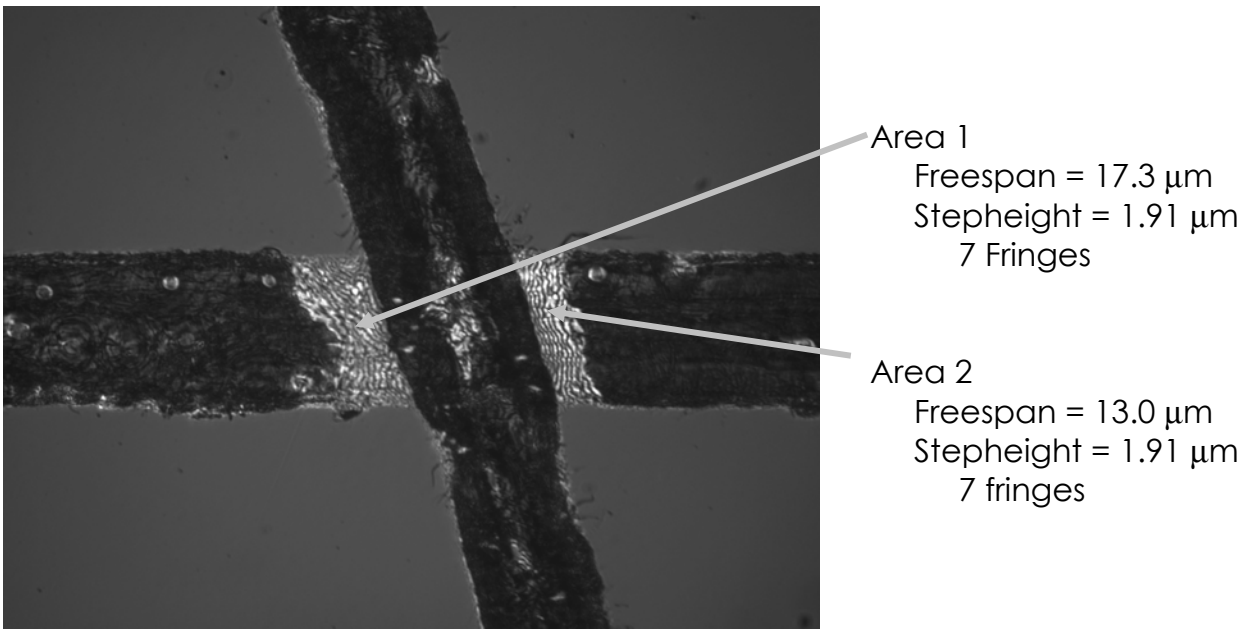

Figure 22 - Measuring Stepheight and Freespan
The freespan and stepheight of a fiber crossing was generally measured along the crossing fibers central axis. The micrograph is of a black spruce fiber crossing.

In most instances, the fringes could be easily counted. However, with increased refining the fiber surface can become damaged leading to difficulty in counting the interference fringes. When this situation arose, Simple PCI (ComPix, Sewickley, PA) was utilized to help count fringes. A line of pixels was selected on the image and the intensity data was graphed. Figure 23 shows a region where it was difficult to distinguish the fringes. The dashed line indicates the line of pixels (160 in total) that were analyzed. Each pixel is assigned a value based on its intensity. Line A represents where the overlying fiber leaves the glass slide, while line B represents where the underlying fiber begins. Both line A and B are zeroth order fringes, or fringes that are caused by optical contact between a fiber and the glass slide. Dark and light fringes are indicated by a definitive change in the direction of the intensity profile. Each successive line between A and B indicates where a dark fringe occurs and its corresponding position on the intensity profile.

Once all of the micrographs for a condition were analyzed, the average stepheight and freespan were calculated from the collected data. Standard deviations, standard errors, and the 95% confidence intervals were also determined (see Appendix D).

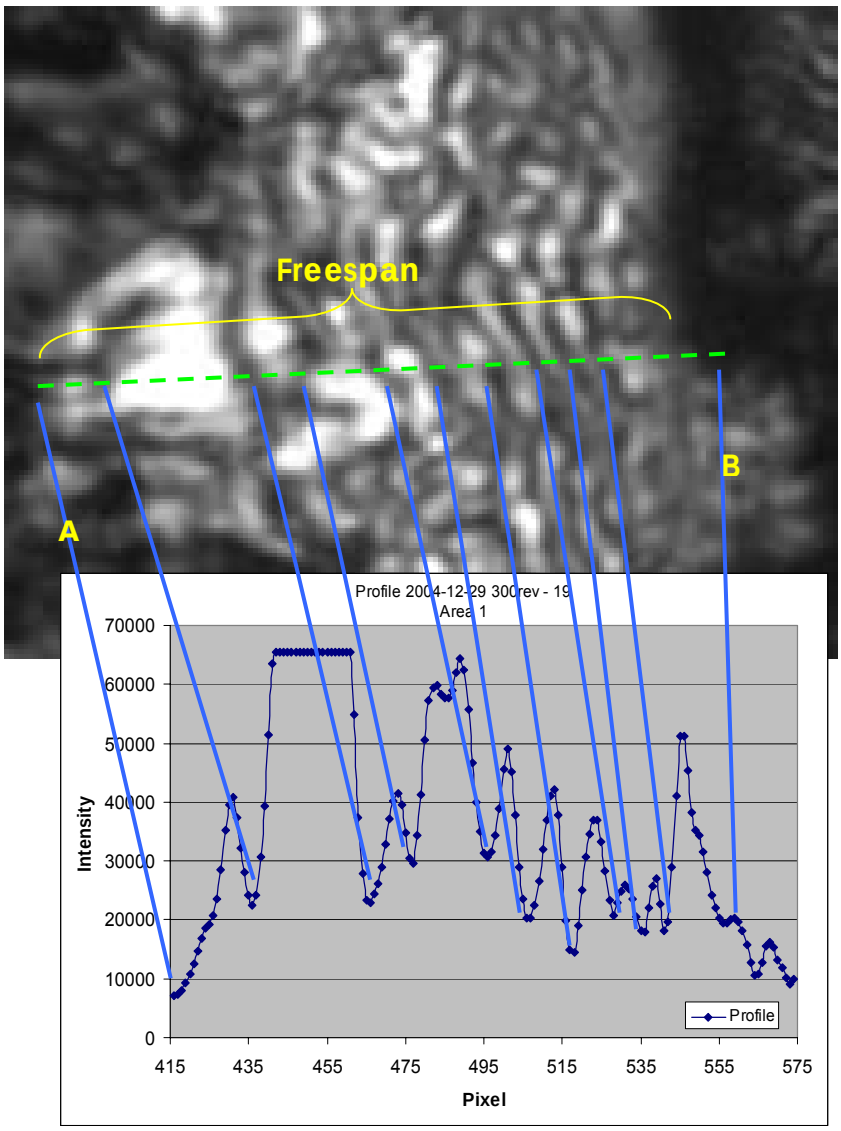

Figure 23 - Counting Interference Fringes with Simple PCI. Only the freespan region is shown. The dashed line indicates the line of pixels that was analyzed. The intensity profile is used to indicate where fringes actually occur. A and B are the zeroth order fringes of the crossing and underlying fiber, respectively.

4.7 Sample Preparation for FRET Analysis

4.7.1 Pulp Preparation

Bleached white spruce fibers were PFI refined to 3000 revolutions and then fractionated in a Bauer-McNett classifier. All fractions were saved. Water was removed from the reserved fibers using a filter paper and a Buchner funnel to bring the pulp mat to approximately 20% consistency. The long fiber fraction with an average fiber length of 3.1±0.1 mm was dyed. Viscose staple fiber (39 mm length, 1.2 denier) was supplied by Lenzing AG (Austria). The fiber was manually cut to an average fiber length of 1.9 mm, washed with deionized water and then air dried in a fume hood before use.

4.7.2 Fiber Dyeing

The hydrazide dyes were applied to the white spruce and viscose fibers using a method adapted from Anderson (Anderson 1986). A 2% suspension of cellulose fiber (oven dry basis) in the appropriate solvent (FTSC: N,N,-dimethylformamide, DCCH: methanol), containing 1.600 mmol/L of dye, and 1.800 mmol/L of HCl was magnetically stirred in the dark overnight at room temperature. The resultant dyed fibers were briefly washed with their respective solvents and then subjected to a mild sodium borohydride reduction. Finally, to assure that only covalently

linked dye remained on the fibers, they were Soxhlet extracted with acetonitrile overnight.

4.7.3 Slide Making

Slides were prepared as describe in Section 4.5.3 with the exception that ~0.100 g (oven dry basis) of a 50/50 weight percent mixture of DCCH and FTSC dyed fibers were diluted to 1000.0 mL. The FTSC dye has a pH dependence, therefore, a 0.025M sodium tetraborate buffer solution was used to maintain pH 9 during the slide making process. The fibers were couched onto glass slides and then wet pressed as described in Table 28. Slides were allowed to dry and condition at 50% relative humidity and 23°C before being imaged.

Table 28- Wet Pressing Conditions for Viscose and White Spruce Samples

Sample	Wet Pressing Conditions		
Viscose	Couched Only	Couched Only	80°C, 3.4 MPa, 5 min
White Spruce	Couched Only	23°C, 0.35 MPa, 5 min	23°C, 2.1 MPa, 5 min

4.8 Fluorescence Microscopy for FRET

A Leica inverted reflected light microscope, a 50 watt metal halide lamp, and a Hamamatsu ORCA-ER digital camera were used to acquire images. The microscope was equipped with a fluorescence disc allowing a quick change of the filter sets without disturbing the sample. The filter sets are described in Table 29. The appropriate exposure time was determined for each crossing and held constant between filter set changes. It varied from 0.15 – 0.50 seconds depending on the initial sample intensity. During image acquisition, fiber crossings were minimally exposed to excitation light to prevent photobleaching. Intensity data was analyzed using a MATLAB program coupled with the MATLAB Image Analysis Toolpack to calculate a normalized FRET (FRETN) value at each image pixel in the fiber-fiber interface. This process is described in section 4.9.

4.9 Image Analysis for FRET

Approximately 20 fiber crossings were analyzed for each sample condition. Only undamaged fibers crossing at 90±20° were analyzed. Each fiber crossing was analyzed by collecting three fluorescence micrographs using three different custom filter sets manufactured by Chroma Technology Corp. (Brattleboro, VT). The custom filter sets were designed to capture three distinct signals from the fiber crossing: the

donor emission (D), the directly excited acceptor emission (A), and the acceptor emission due to FRET (F). Figure 24 shows four grayscale images of white spruce fibers using polarized light (Standard), donor excitation with donor emission (Donor), acceptor excitation with acceptor emission (Acceptor), and donor excitation with acceptor emission (FRET).

Table 29 describes each filter set.

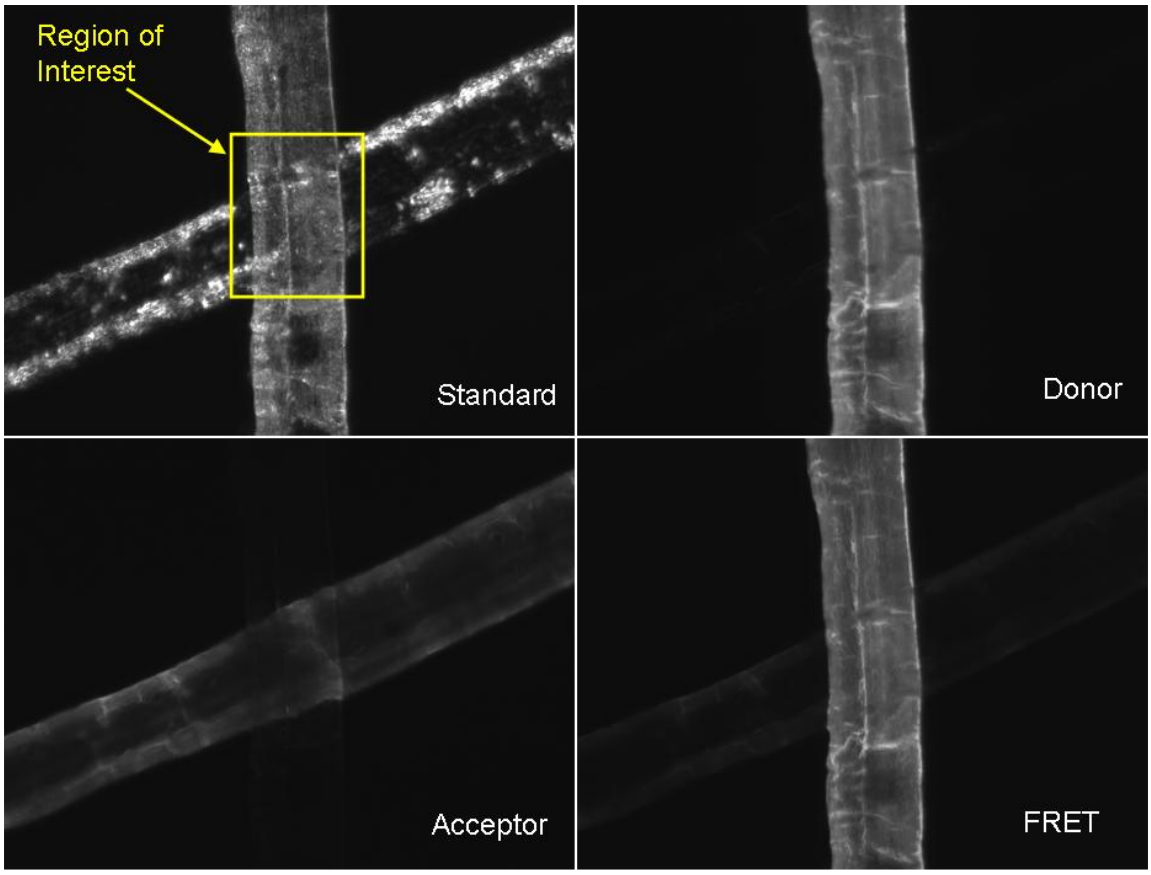

Figure 24 - Standard and FRET Images of a Fiber Crossing
Four grayscale images of white spruce fibers using polarized light (Standard), donor excitation with donor emission (Donor), acceptor excitation with acceptor emission (Acceptor), and donor excitation with acceptor emission (FRET).

Table 29 – Excitation/Emission Specifications for the Custom Filter Sets

Filter Set	Description	Excitation	Emission
D	Donor Excitation and Donor Emission	440±5 nm	485±5 nm
A	Acceptor Excitation and Acceptor Emission	500±5 nm	535 nm long pass
F	Donor Excitation and Acceptor Emission	440±5 nm	535 nm long pass

The main region of interest is the fiber crossing area in which FRET can occur. FRET is very sensitive to local changes in the donor and acceptor dye concentrations. Gordon *et al.* have developed the FRETN correction algorithm to correct for these variations (Gordon, Berry, Liang *et al.* 1998). Equation 5-Equation 8 show the pixel by pixel FRETN calculation used in the fiber crossings. The variables are systematically defined. The first capital letter identifies the filter set used to capture the micrograph (A= acceptor filter set, D= donor filter set, and F= FRET filter set). The subscript lower case letter identifies the fiber in the micrograph (a= acceptor fiber, d=donor fiber, x=the fiber crossing). For example, D_a identifies the average acceptor fiber intensity while using the donor filter set. The values are total fiber averages of grey scale intensity except for the crossings (*e.g.* F_x, D_x, A_x) which are the pixel by pixel gray scale values for

the fiber crossing. Use of the FRETN correction algorithm to normalize the FRET signal requires the collection of data from several other regions in the image.

$$Afa = \frac{A_x - \frac{F_x A_d}{F_d}}{1 - \left(\frac{F_a}{A_a}\right)\left(\frac{A_d}{F_d}\right)}$$

Equation 5 - Calculation of *Afa* for *FRETN*

$$FRET1 = \frac{F_x - D_x \frac{F_d}{D_d} - Afa\left[\frac{F_a}{A_a} - \left(\frac{F_d}{D_d}\right)\left(\frac{D_a}{A_a}\right)\right]}{G\left[1 - \left(\frac{D_a}{F_a}\right)\left(\frac{F_d}{D_d}\right)\right]}$$

Equation 6 - Calculation of *FRET1* for *FRETN*

$$Dfd = D_x + FRET1\left[1 - G\left(\frac{D_a}{A_a}\right)\right] - Afa\left(\frac{D_a}{A_a}\right)$$

Equation 7 - Calculation of *Dfd* for *FRETN*

$$FRETN = \frac{FRET1}{Afa \bullet Dfd}$$

Equation 8 - Calculation of *FRETN*

Figure 25 shows a representation of a fiber crossing and indicates the areas of interest: the fiber crossing, an area where only donor exists, a region where only acceptor exists, and a region to determine the background signal. Grayscale images using each of the filter sets were acquired and saved for image analysis. An average grayscale value was calculated based on each fluorescence micrograph for the DCCH Only, FTSC Only, and the Background region using MATLAB. This gives a total of nine values that are used to calculate the FRETN value at each image pixel in the fiber crossing.

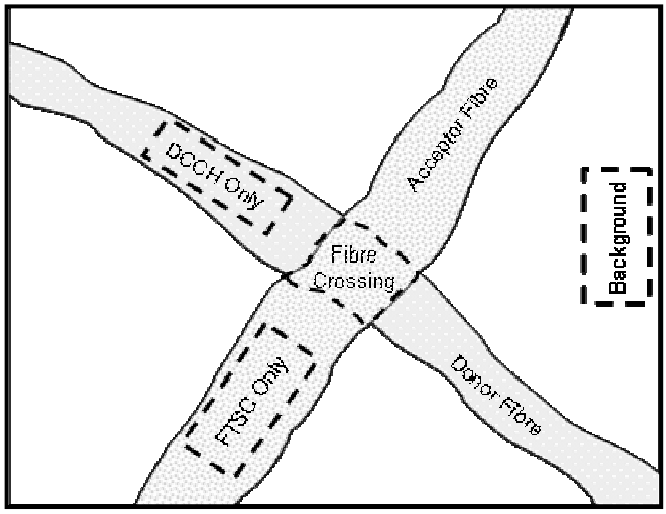

Figure 25 - Areas Used for FRET Normalization
DCCH only, FTSC only, and background averages from each of three micrographs are used to calculate a FRETN value for each pixel in the fiber crossing.

4.10 Preparation of Surface CMC Fibers

The following work was completed at STFI by Elisabeth Duker. The northern Canadian unbleached kraft black spruce pulp was used for this study. Approximately 30 g (oven dry basis) was measured out for each level of CMC treatment described in Table 30. The CMC, Aqusorb A-500 (Hercules, Sweden), had a DS = 0.5-0.7 and molecular weight of about 250,000.

Table 30 - CMC levels of Treatment

Sample	CMC Added
1	0 mg/g pulp
2	12 mg/g pulp
3	40 mg/g pulp

Prior to grafting the pulp was converted to its calcium form as follows:

1. *Hydrogen form:* The pulp was placed in 0.01 M HCl at 2.5% consistency. The pH was adjusted to 2 and remained at this level for 30 minutes. Then the pulp was washed with deionized water in a Buchner funnel until the conductivity of the filtrate was less then 5 µS/cm.

2. *Sodium form:* The pulp was then brought to 2.5% consistency using 1 mM $NaHCO_3$. Sodium hydroxide was used to adjust to pH 9 and held constant for 30 minutes. The pulp was then washed with deionized water in a Buchner funnel until the conductivity of the filtrate was less then 5 µS/cm.
3. *Calcium form:* Finally, the pulp was placed in 0.05 M $CaCl_2$ at 2.5% consistency for 15 minutes and then washed with deionized water in a Buchner funnel until the conductivity of the filtrate was less then 5 µS/cm.

CMC (Aquasorb A 500, Hercules, Sweden) for each treatment level was measured out as described in Table 30, dissolved in 100.0 mL of deionized water, and allowed to stir overnight. The pre-washed pulp was brought to 2.5% consistency with a 0.05 M $CaCl_2$ solution and the dissolved CMC. The pH was adjusted to 8 with 0.01 M $NaHCO_3$ and sealed in a 2.0L autoclave vial. The pulp mixture was place in a preheated glycol bath at 120°C for two hours.

The pulp was then washed with deionized water in a Buchner funnel until the conductivity of the filtrate was less then 5 µS/cm. The total charge and the attached amount of CMC was determined by conductometric titration (Katz, Beatson and Scallan 1984). Polyelectrolyte titration was

performed to determine the surface charge of the fibers (Wagberg, Winter and Lindstrom 1985).

4.11 Preparation of Bulk Carboxymethylated Fibers

The following work was completed at STFI by Elisabeth Duker. The northern Canadian unbleached kraft black spruce pulp was used for this study. Approximately 30 g (oven dry basis) was measured out for each level of carboxymethylation treatment described in Table 31.

Table 31 - Monochloroacetic Acid Added for Bulk Carboxymethylation

Sample	$ClCH_2COOH$ Added
1	0.404 g
2	3.640 g

Prior to treatment the pulp was converted to its calcium form in the same manner described in section 4.11. The pulp was then disintegrated at 1.5% consistence for 10000 revolutions is a standard disintegrator. The pulp was then solvent exchanged with 95% ethanol and filtered after 10 minutes. The solvent exchange was repeated three times.

The monochloroacetic acid amount describe in Table 31 was dissolved in 500 mL of isopropanol and used to impregnate the solvent exchanged

pulp for 30 minutes. The 16.2 g of sodium hydroxide was dissolved in 500 mL of methanol and added to 2000 mL of isopropanol. The methanol/isopropanol solution was heated to boiling and the impregnated pulp was added. The reactants were refluxed for one hour.

The pulp was then filtered and washed with deionized water, then 0.1 M acetic acid, and then deionized water again. Finally the pulp was placed in 4.0% $NaHCO_3$ for one hour and then washed with deionized water. The total charge and the attached amount of CMC was determined by conductometric titration (Katz, Beatson and Scallan 1984). Polyelectrolyte titration was performed to determine the surface charge of the fibers (Wagberg, Winter and Lindstrom 1985).

CHAPTER 5: METHOD DEVELOPMENT: THE EFFECT OF REFINING

The following chapter is reproduced with the kind permission of The Pulp and Paper Fundamental Research Society[ii].

5.1 Introduction

Fiber flexibility (Emerton 1957), conformability (Mohlin 1975b), compactability (Clark 1985), collapsibility, pliability, and deformability are all words that have been used to describe properties which are linked to the ability of a paper sheet to consolidate and form a well bonded network. Fiber flexibility has become the predominant term used to describe the ability of pulp fibers to deform over one another. Many researchers have described methods to quantify fiber flexibility (e.g. (Seborg and Simmonds 1941; Forgacs and Mason 1958; Mohlin 1975b; TamDoo and Kerekes 1981; Steadman and Luner 1985; Kuhn, Lu, Olson *et al.* 1995)). The most relevant and straightforward method was developed by Steadman and Luner (Steadman and Luner 1985). In this method fibers are pressed and dried across a 25 μm diameter stainless steel wire wound around a glass slide. Figure 26 shows the geometry of the Steadman system (A) and the acquired image (B). The region of optical contact

[ii] Initially presented at the 13th Fundamental Research Symposium, September 11-16, 2005, Robinson College, Cambridge, England and published in the Transactions of that meeting. See Appendix C for copyright permission.

between the fiber and the glass slide is observed, and it is deduced that the closer the optical contact regions are to the wire the more flexible is the fiber. The length of the unbonded span is taken as a measure of flexibility.

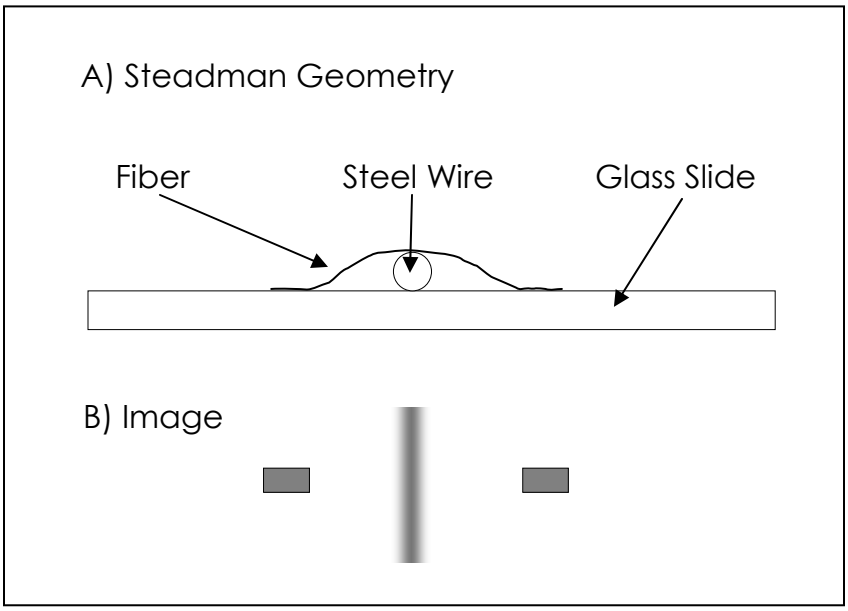

Figure 26 - The Steadman Geometry
A schematic of the Steadman's geometry (A) and an illustration of an acquired image (B) (Steadman and Luner 1985).

One drawback of the Steadman and Luner method is that in a paper sheet the fiber deforms over a much smaller stepheight than 25 μm. While 25 μm is the approximate diameter of an uncollapsed pulp fiber, fibers in paper are always collapsed either partially or completely so that the step height is generally in the range 1-10 μm. As a consequence, the span over which the fiber is unbonded in actual paper should be much lower

than in the Steadman and Luner experiments. It likely is on the order of a fraction of a fiber width (35 μm) rather than the 100 μm or so observed by Steadman and Luner (Steadman and Luner 1985).

It is more relevant to measure the deformation of a fiber when pressed against a glass slide crossing a fiber similar to itself rather than a 25 μm wire. This would simulate more closely the structure in a paper sheet. The unbonded span length under these conditions will be much lower than in Steadman's method and is more typical of the value that would occur in a paper sheet. Thus any measurement of fiber flexibility by this technique is more relevant to the fiber deformations that occur in actual paper. Because of the higher demands on magnification, resolution and contrast, the method has been modified so as to optimize the optical conditions.

5.2 Methods and Materials

5.2.1 Imaging Fiber Intersections

This study utilized a Leica DM-IRM inverted, reflected light microscope equipped with a Hamamatsu ORCA-ER digital camera and a 50 watt metal halide lamp. Samples were prepared by draining a dilute suspension of refined unbleached never dried black spruce pulp fibers onto a piece of filter paper. The fibers were then wet pressed in a

standard handsheet press onto four glass slides for two minutes at 50 pounds per square inch (see Figure 16). The slides were allowed to dry and were kept under TAPPI Standard Conditions before and during imaging.

In order to acquire high contrast and high resolution images of the optical contact regions, several optical modifications were made. The first area of concern was the choice of an objective lens. When long spans (>100μm) are observed (e.g. with the Steadman and Luner method), low magnification objectives are suitable. However, with spans on the order of a few microns a high magnification objective is required. Unfortunately, objective lenses of high numerical aperture suffer from spherical aberration when imaging though a glass slide (Jenkins and White 1976). The off-axis light rays are focused in a different plane than the axial light rays. Modern objectives can be corrected for this spherical aberration via a correction collar, even when viewing through the thickness of a glass slide. A Leica 40X objective with such a correction collar was used for this research.

The second area of concern was the low contrast in the acquired image because of light arising from regions in the specimen that do not contribute to a useful image. First, light is reflected from the bottom of the

glass slide. This light is of similar intensity as the actual image leading to low contrast. The reflection can be eliminated by utilizing a quarter wave plate fashioned from a split sheet of mica. The mica sheet was brought into optical contact with the glass slide by applying microscopy immersion oil to the underside of the glass slide (see Figure 19). The specimen was then illuminated and viewed in crossed polars. The optical axis of the mica is set at 45 degrees to the plane of polarization. The polarized light reflected by the bottom of the glass slide is eliminated by the crossed polars. The light rays forming the image first pass through the mica sheet becoming circularly polarized. After reflection from the fiber-glass interface, they pass back through the mica sheet and become plane polarized in the direction of the analyzer. This technique only permits the desired reflected light (that from the fiber-glass interface) to reach the objective lens.

The final modification was to the fibers themselves. Pulp fibers transmit light that is in part reflected at their top surface and returned to the objective lens, thus reducing the image contrast. This source of unwanted light can be eliminated by dyeing the fibers before application to a glass slide.

5.2.2 Observing Interference Fringes

By incorporating these methods, high resolution images of fiber crossings can be obtained. The areas of bonding between the fibers and the glass are dark compared with the bright regions of non-contact (see Figure 29). It has also been found that if a narrow band filter (λ=547±10 nm) is incorporated, interference fringes can be observed. Figure 27 illustrates how the interference fringes are formed. Light at A passes through the glass slide and is absorbed by the dyed fiber if it is in optical contact with the glass slide; therefore, the intensity of the reflected light is zero. Light at B is reflected at the top glass-air interface and again at the fiber-air interface leading to an interference fringe. The local height of the air wedge, H, at each black fringe is given by:

$$H = n\frac{\lambda}{2}$$

Where n is the order of the black fringe and λ is the wavelength of light.

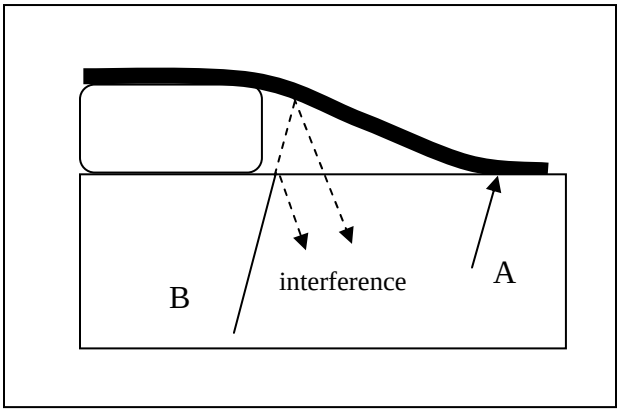

Figure 27 - Interference fringe formation
An illustration of how interference fringes are formed in the freespan region. Light at A cannot be reflected, while light at B reflects at the glass-air interface and the fiber-air interface creating interference.

Analysis of the fringe pattern thus allows an extremely accurate measurement of the height of the lower surface of the fiber in the freespan. These data have been used to determine the shape of the lower surface of the crossing fiber in the freespan region as well as the stepheight and the total freespan. Figure 28 illustrates the geometry of a fiber crossing. The stepheight (H) is defined as the height of the lower surface of the crossing fiber as it leaves underlying fiber. The freespan (F) is defined as the length of the fiber not in optical contact with the underlying fiber or the glass slide.

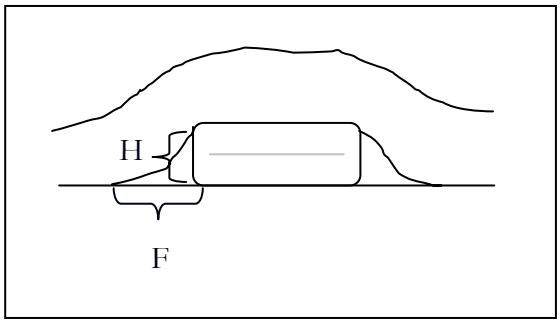

Figure 28 - The Geometry of a Fiber Crossing
A schematic showing the stepheight (H) and freespan (F) in a fiber crossing.

5.2.3 Experimental Procedure

A mill produced, never dried, northern Canadian black spruce (*Picea mariana*) unbleached kraft pulp was washed and screened in a lab screen with 0.008 inch (0.2 mm) slots. The pulp's kappa number was 19.9. Four pulp samples were refined using a lab PFI mill with a 0.2 mm gap to 300, 1000, 2000, and 4000 revolutions. Five grams of wet pulp were removed from each sample and dyed using Chlorazol Black. Imaging slides were prepared as describe above after thoroughly washing the dyed pulp with deionized water. TAPPI standard handsheets were made with the remaining pulp. Freespans and stepheights were measured using image analysis software (see Appendix A). Tensile strength, density, and scattering coefficient were measured and are given in Appendix B.

5.3 Results and Discussion

5.3.1 Micrographs

High contrast, high resolution images have been acquired using the methods described above. Over 200 images were collected and analyzed. Figure 29-33 are representative micrographs showing fibers refined to 300, 1000, 2000, and 4000 revolutions respectively.

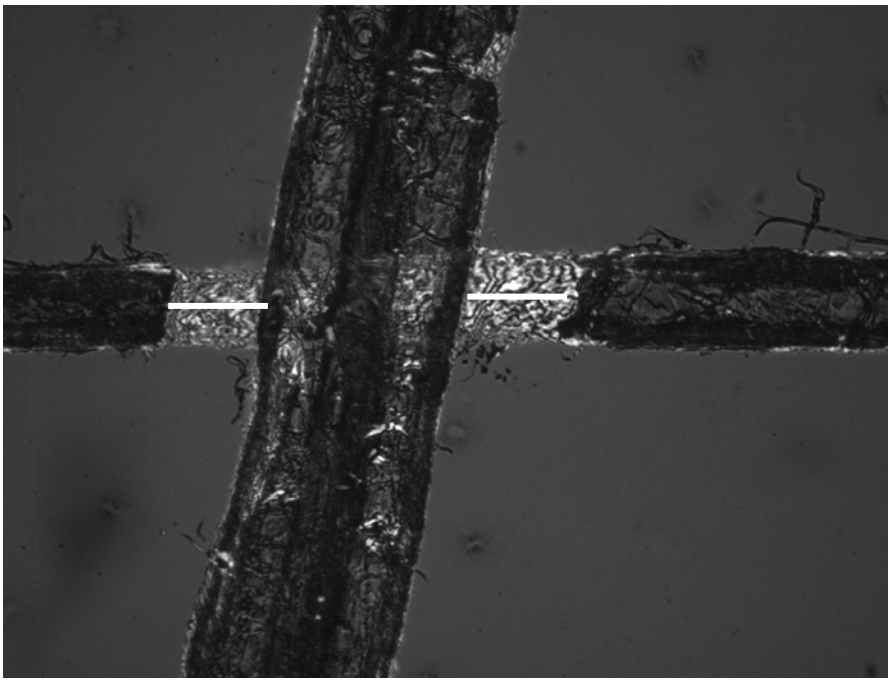

Figure 29 - Freespans on a Black Spruce Micrograph
Dyed black spruce fibers refined to 300 revolutions. Two freespans are indicated by the white lines.

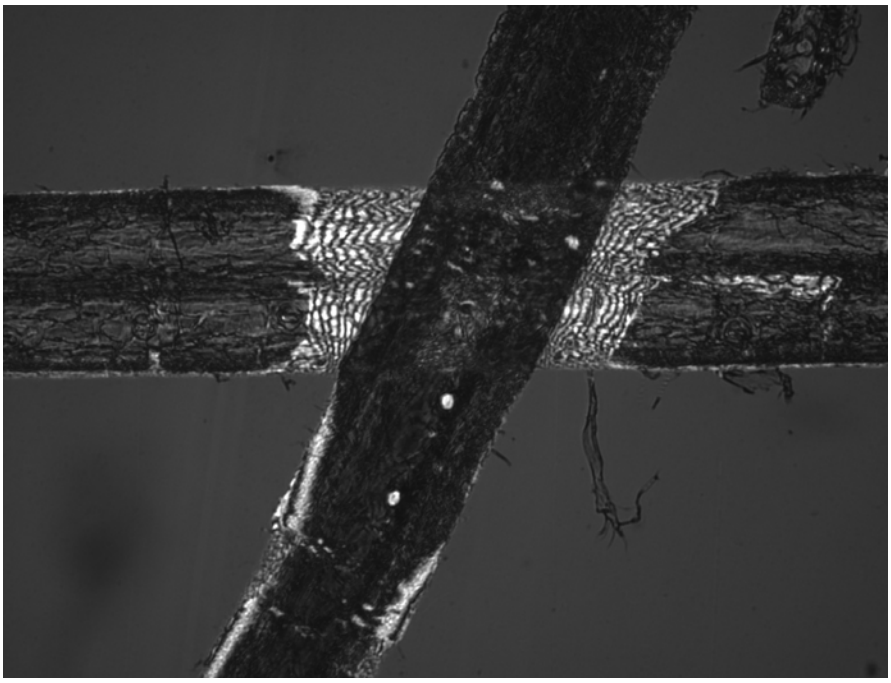

Figure 30 - Black Spruce - 1000 Revs
Dyed black spruce fibers refined to 1000 revolutions.

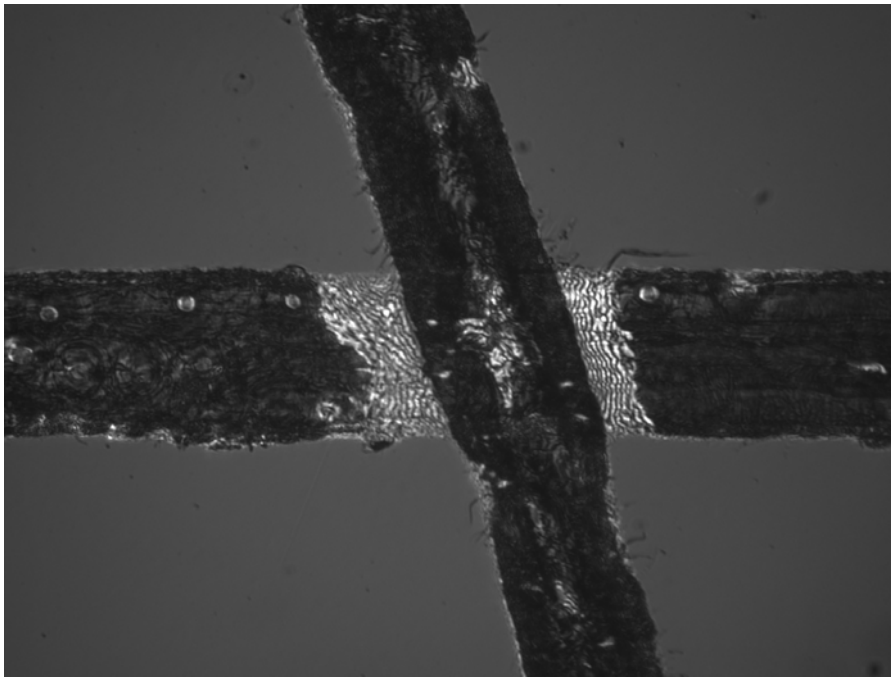

Figure 31 - Black Spruce - 2000 Revs
Dyed black spruce fibers refined to 2000 revolutions.

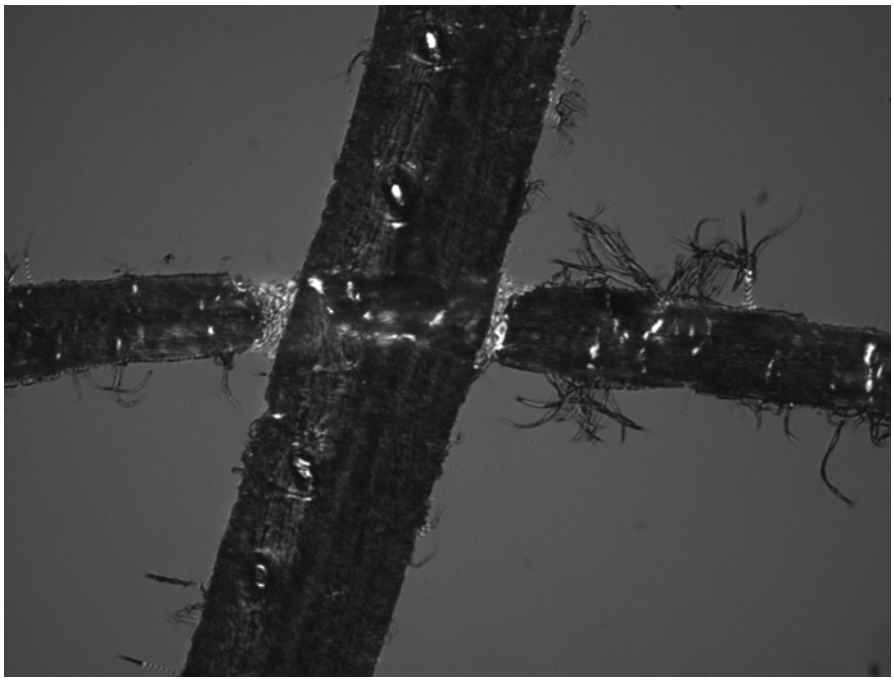

Figure 32 - Black Spruce - 4000 Revs
Dyed black spruce fibers refined to 4000 revolutions.

5.3.2 Stepheight versus Freespan for a Lightly Refined Pulp

Unbleached kraft black spruce fibers were refined in a PFI mill to 300 revolutions. Images were acquired and were analyzed by dividing each image into two areas of interest, one for each side of the intersection. Image analysis software was used to measure freespans and stepheights. The results are shown in Figure 33. A regression analysis line passes through the origin indicating that higher stepheights generally have higher freespans.

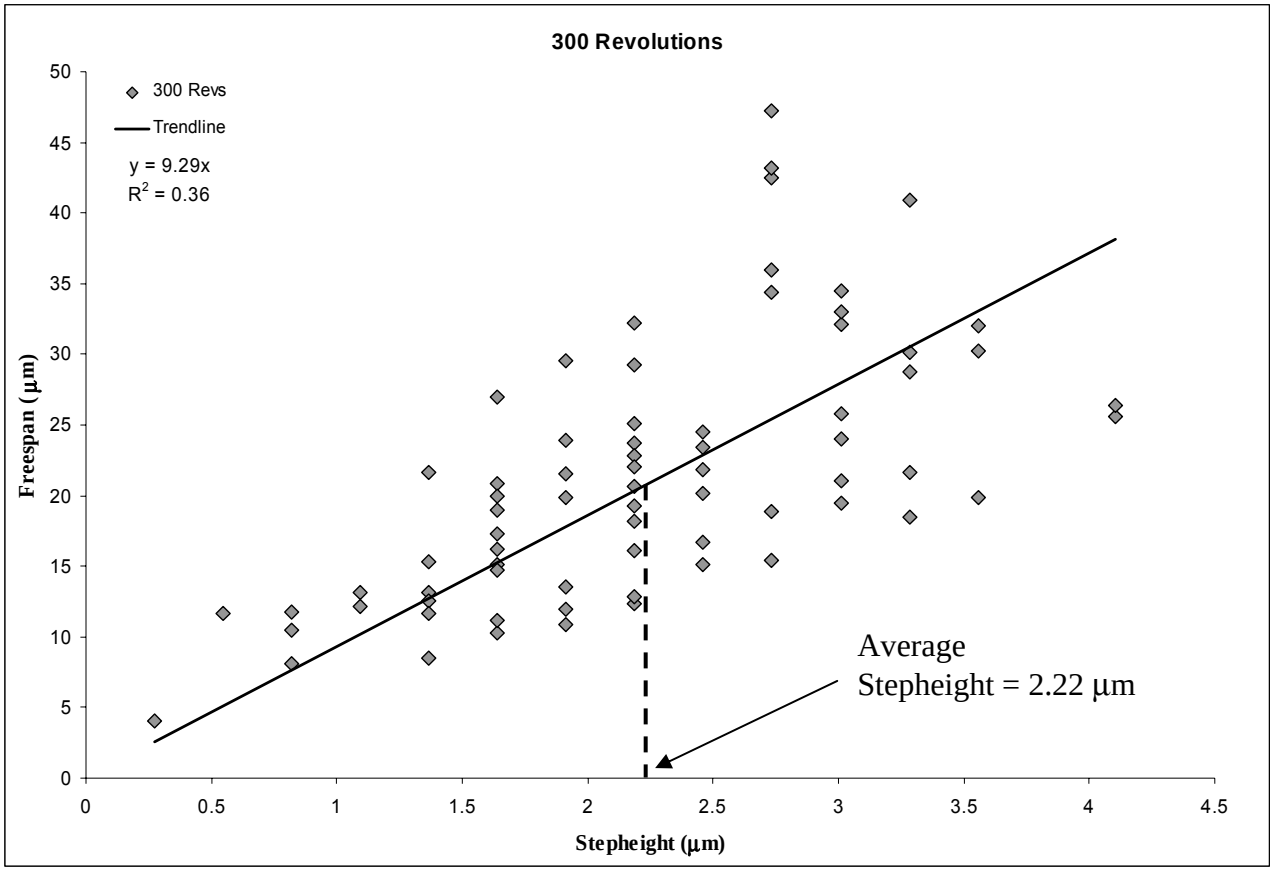

Figure 33 - A Lightly Beaten Pulp
Stepheight versus freespan for lightly beaten (300 revolutions) black spruce fibers. The regression line is indicated as well as the average stepheight.

Figure 34 offers an interpretation of this result. Fibers in the unbeaten state after pressing are often uncollapsed (Page 1967) (Figure 34A) resulting in a high stepheight. Collapsed fibers will have a lower stepheight Figure 34B). Assuming that all the fibers have the same flexibility, the stepheight controls the length of the freespan.

There is some scatter in the freespan data which is likely due, in part, to the differences in fiber flexibility of the crossing fibers. The double wall thickness of an unbleached black spruce kraft fiber is about 2 μm which is slightly less than the average stepheight shown in Figure 33. While stepheight may primarily control the length of the freespan, flexibility also has some influence.

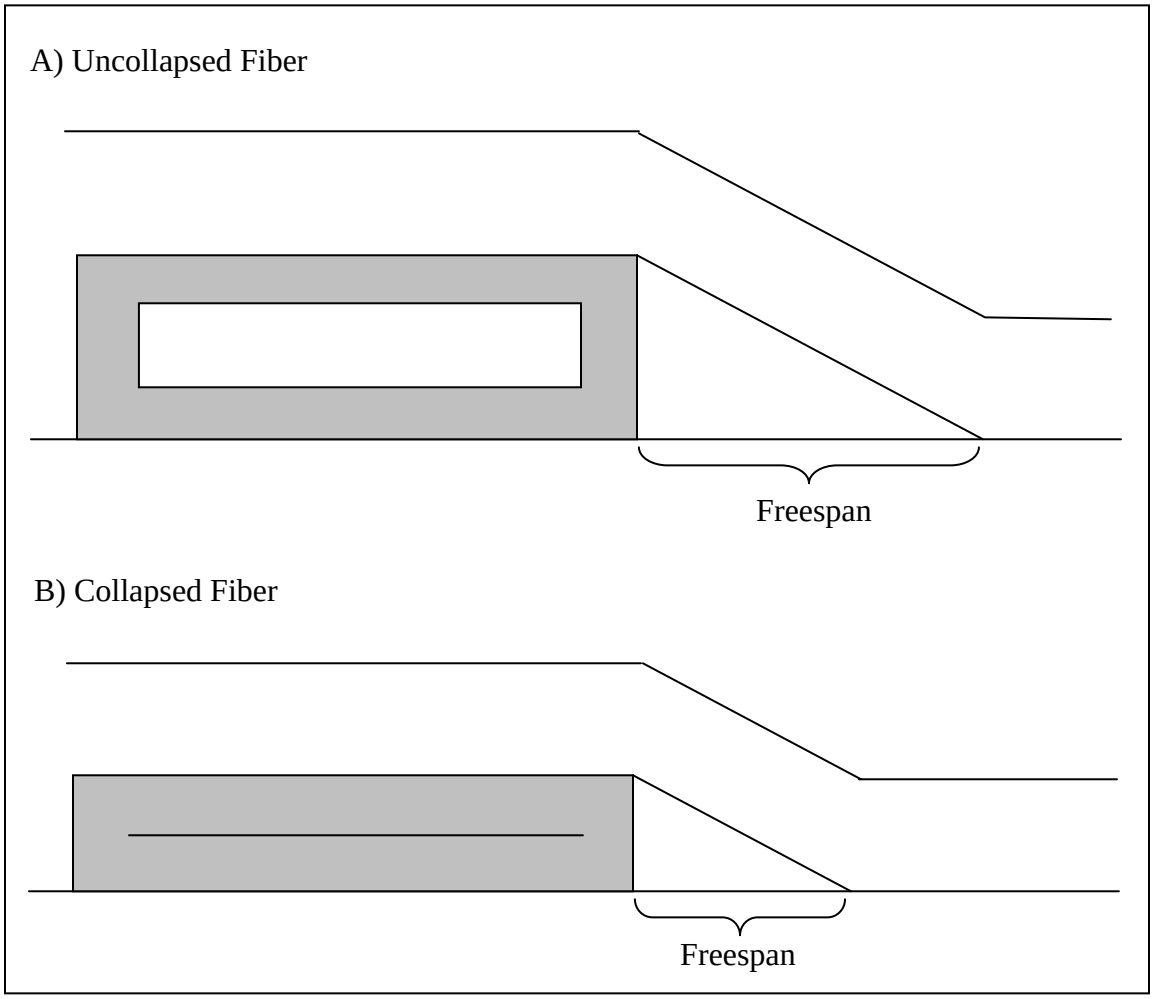

Figure 34 - The Effect of Fiber Collapse
Uncollapsed fibers (A) will have longer freespans than collapsed fibers (B).

5.3.3 Stepheight versus Freespan for Refined Pulps

Figure 35 illustrates two hypothetical extremes of the effect of refining. In Figure 35A, refining only serves to increase the flexibility of fibers reducing the freespan at a given stepheight. In Figure 35B, refining makes fibers more collapsible reducing the stepheight and, hence, the freespan. Figure 36 shows a plot of stepheight versus freespan for each refining level. Figure 37 shows the average for the same data. Clearly, the effect of refining is to lower the stepheight as proposed in Figure 35B. There is no indication that refining increases the longitudinal flexibility of fibers which would lead to a lower freespan at a given stepheight.

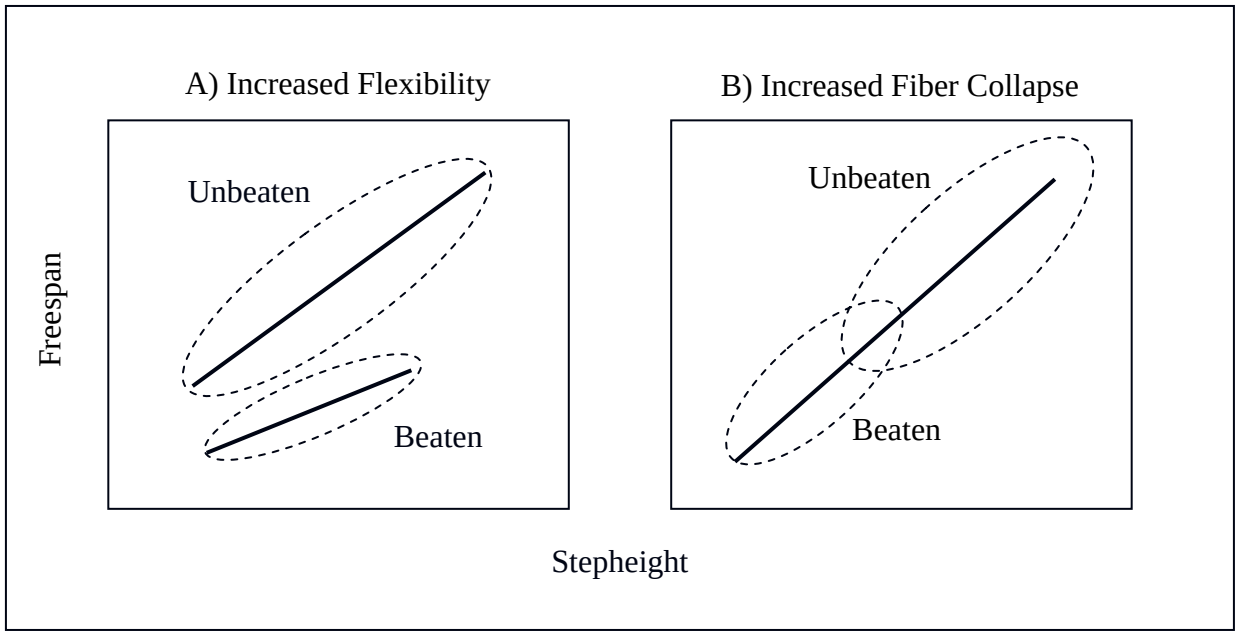

Figure 35 - The Potential Effects of Refining on Stepheight and Freespan Two potential effects of refining are shown. If refining only serves to make fibers more flexible (A), the average stepheight should remain the same with decrease in freespan. If reefing only serve to increase fiber collapse (B), both the average stepheight and freespan should decrease.

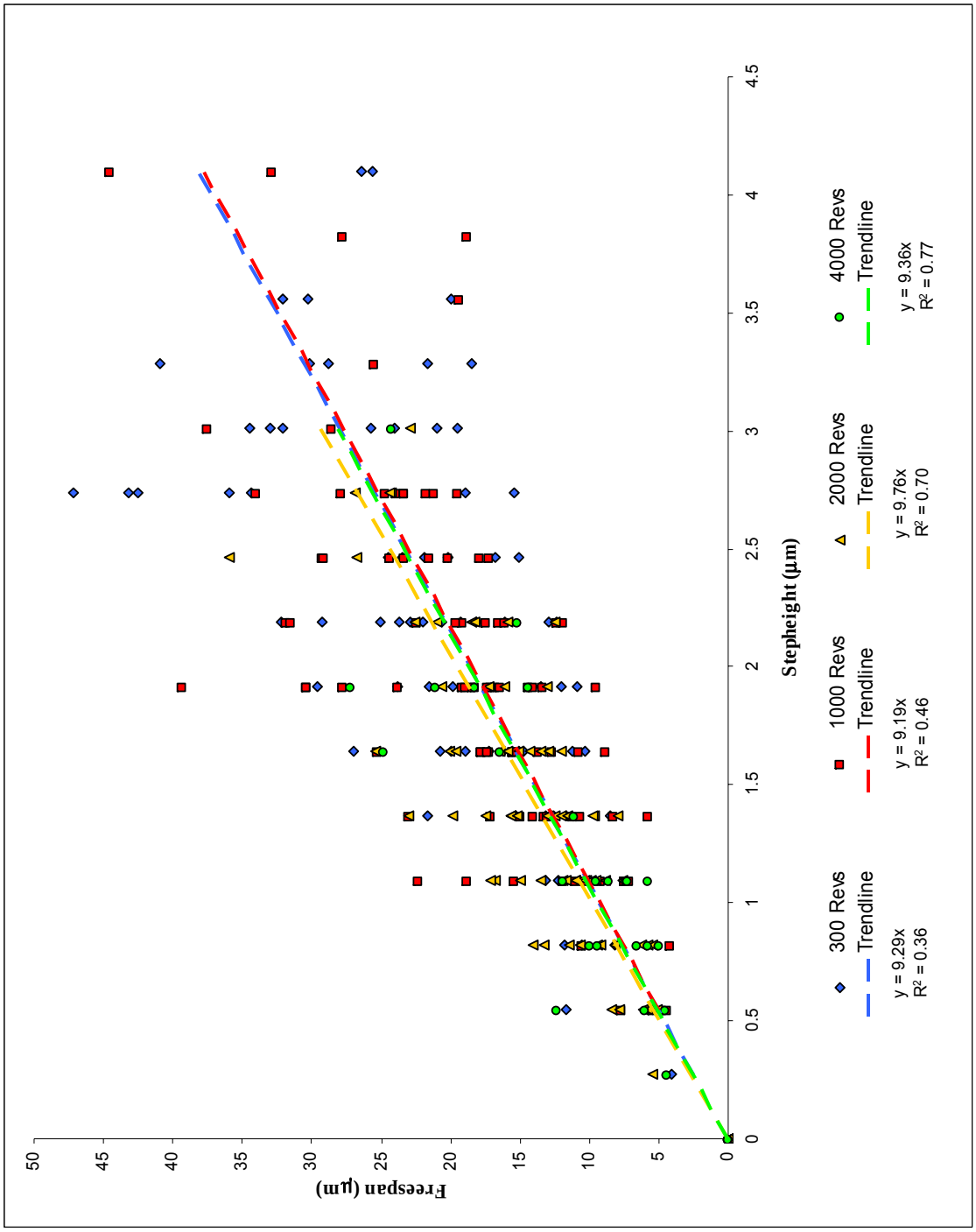

Figure 36 - The Effect of Refining for Black Spruce
The effect of refining is to increase fiber collapse.

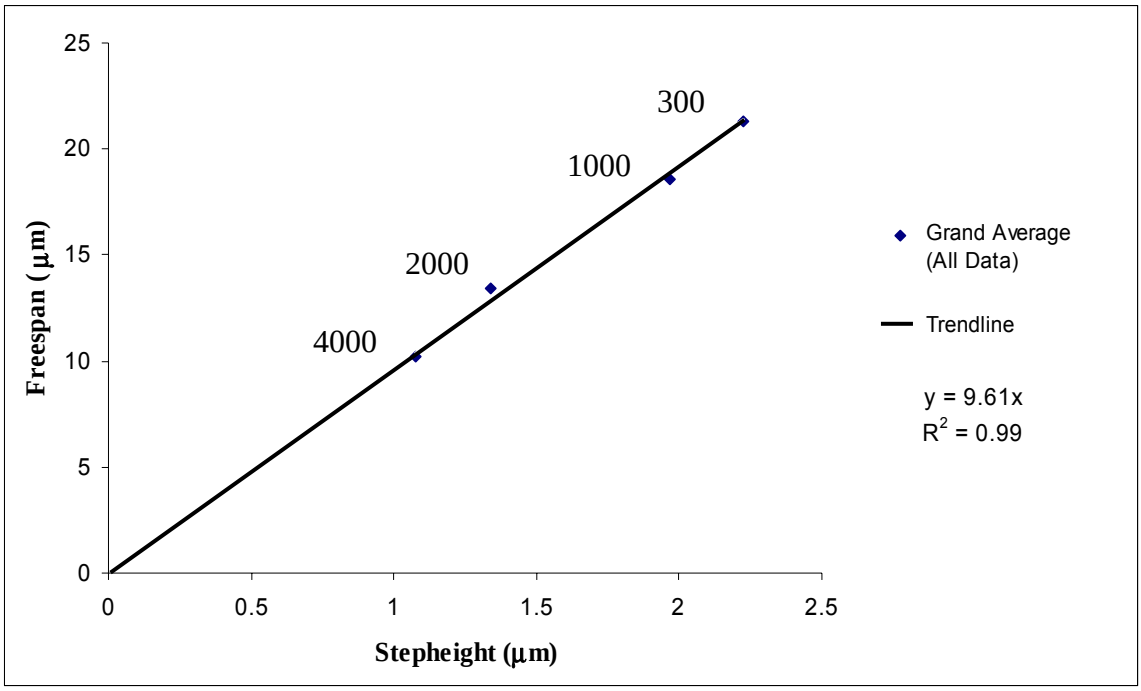

Figure 37 - Average Stepheights vs. Freespans
Average stepheight versus average freespan is shown for 300, 1000, 2000, and 4000 revolutions with the regression analysis going through the origin.

5.3.4 Conformability/Deformability in a Fiber Intersection

The data for the refined pulps do present a challenge in interpretation. Upon refining the average stepheight falls to 1.1 μm (see Figure 37) and many values of stepheight are below 0.5 μm. Indeed, there are cases in which the stepheight is essentially zero as shown in Figure 38. Since this measurement is calibrated to the wavelength of light, there can be little doubt as to its accuracy.

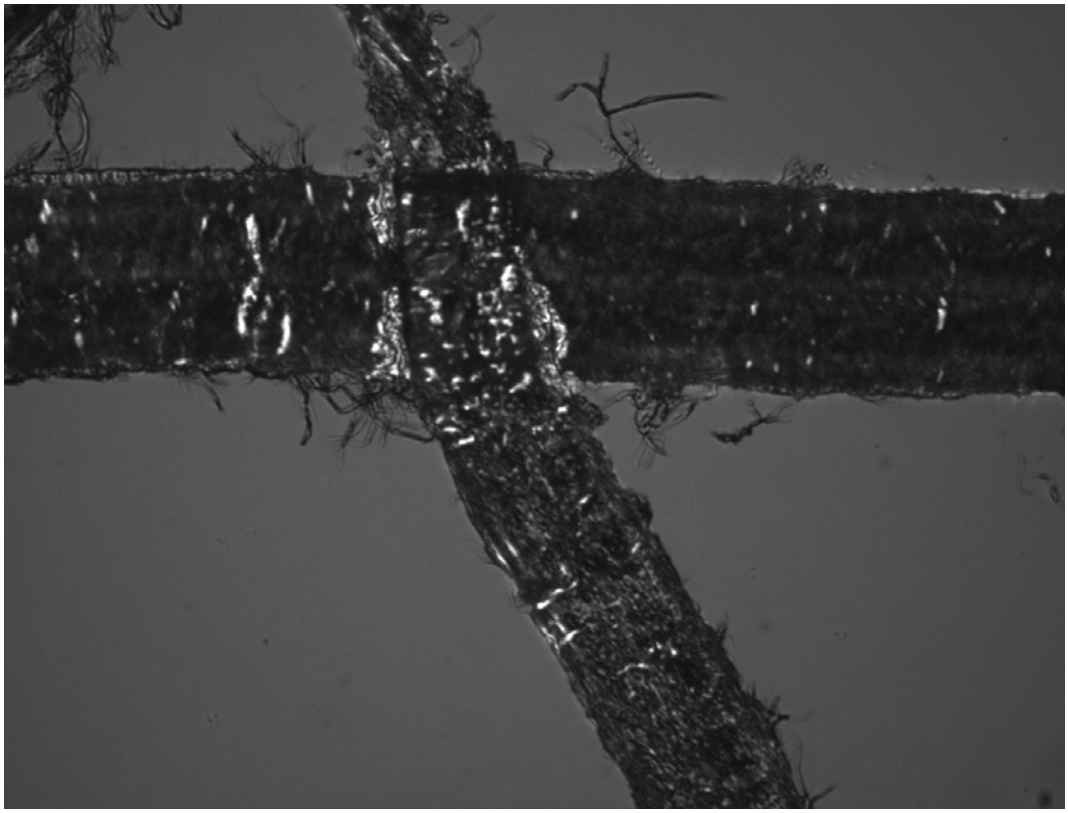

Figure 38 - Zero Stepheight and Freespan
Dyed black spruce fibers refined to 4000 revolutions showing essentially no freespan or stepheight.

A stepheight of zero presents some difficulty when one considers that the double wall thickness of a collapsed unbleached black spruce kraft fiber is about 2 μm. The lower bound on stepheight should be 2 μm not approaching 0 μm. Two mechanisms can help explain this apparent anomaly. First, the overlying fiber may conform to the fiber beneath by overlapping as shown in Figure 39A. Second, the underlying fiber may be

compressed and deformed as shown in Figure 39B. One or both of these phenomena must occur to explain the data, but the extent of each is not certain.

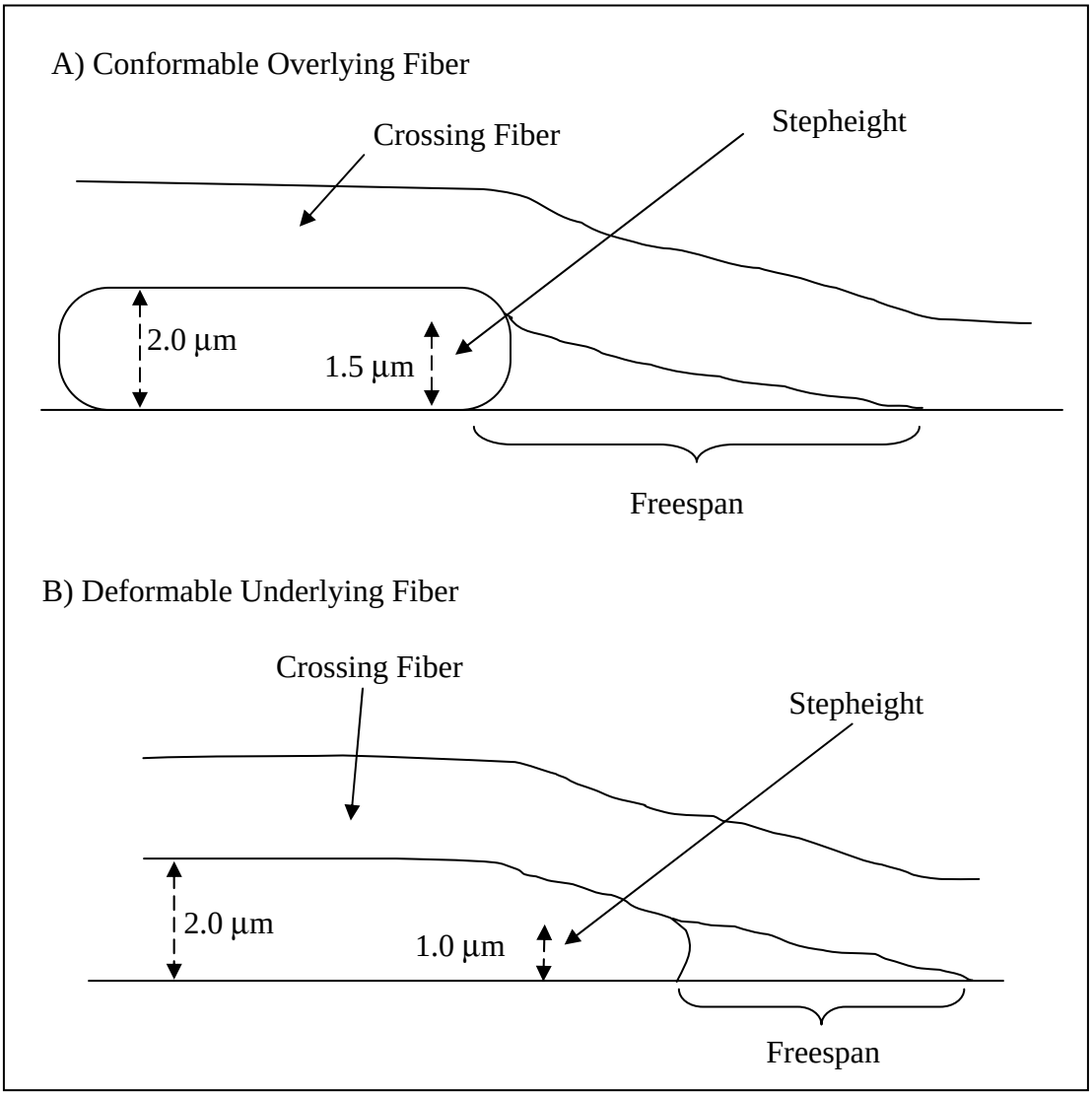

Figure 39 - Conformability and Deformability
Conformability and deformability in a fiber intersection must be occurring to have stepheights less than the double cell wall thickness.

5.3.5 The Shape of the Fiber in the Freespan Region

The shape of the fiber in the freespan region can be determined from the interference fringes. Previously it has been suggested that the fiber deforms via bending and the diagrams (e.g. Figure 2 of Steadman and Luner (Steadman and Luner 1985)) seem to confirm this concept. Recently it has been suggested by Waterhouse and Page that this is incorrect (Waterhouse and Page 2004). In paper the transverse deformation of fibers occurs more by shear than by bending. This work allows the shear deformation hypothesis to be checked by analyzing the spacing of interference fringes in the freespan region. The two modes would show different spacing between the interference fringes as shown in Figure 40. Shear deformation will result in more evenly spaced fringes. Bending deformation would show fringes that are spaced more closely at the center of the span and further apart near the crossing fiber and near the contact with the glass. Upon close inspection of the micrographs, the fringes appear approximately evenly spaced. This physical evidence thus tends to support the theory presented by Waterhouse and Page (Waterhouse and Page 2004).

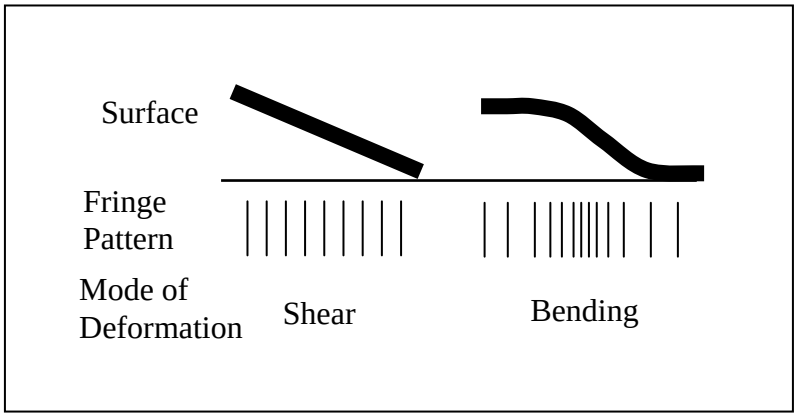

Figure 40 - The Mode of Deformation
Fringe patters for different modes of deformation.

In addition, the stepheight-freespan data further supports the claim by Waterhouse and Page (Waterhouse and Page 2004). Figure 37 shows the regression line going through the origin. While it has been forced to go exactly through the origin, no significant decrease in the R^2 value occurred. In addition, several images show a freespan and a stepheight of zero (see Figure 38). If there is no freespan as the stepheight approaches zero, the mode of deformation must be shear. A significant contribution from bending would lead to some amount of freespan at a stepheight approaching zero.

5.3.6 Imaging of Fiber Intersections in Water

It is also important to note that this technique can capture images of fiber intersections immersed in water. Figure 41 shows the same fiber intersection dry (A) and after re-wetting (B). Although the contrast is

greatly reduced the interference fringes are apparent in both cases. This result has implications with respect to wet pressing. Ultimately, the goal of this research to image fiber intersections during the dynamic conditions that occur during wet pressing.

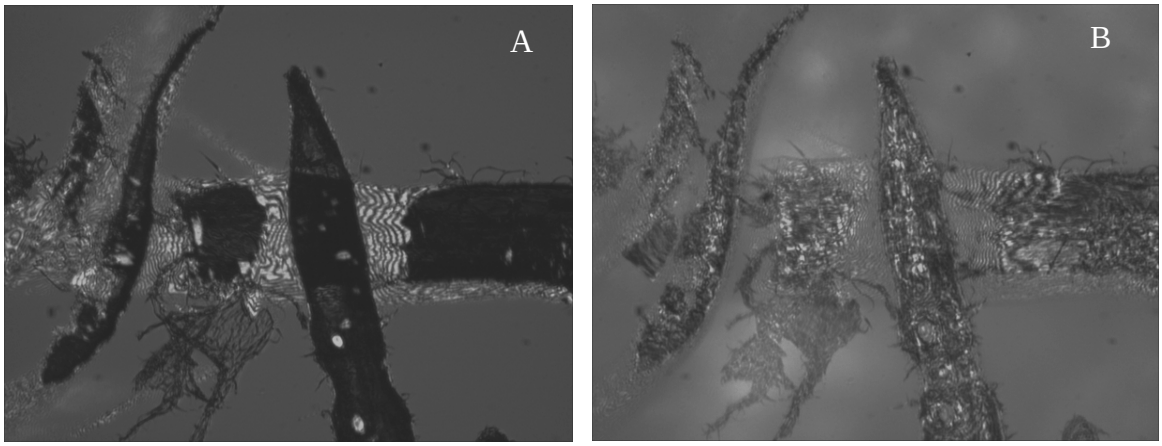

Figure 41 - Rewetting a Fiber Crossing
Dyed black spruce fibers refined to 1000 revolutions dry (A) and wet (B).

5.4 Conclusions

A new experimental procedure has been developed that allows fiber deformability to be measured using geometries that realistically simulate deformations in paper. The freespan of a fiber intersection is not controlled by the flexibility of the overlying fiber. Instead it appears to be controlled partly by the local conformability of the overlying fiber as it wraps around the underlying fiber and partly by the collapse and deformability of the underlying fiber. Observed interference fringe

patterns indicate the predominant mode of deformation of a fiber freespan in a paper sheet is shear.

The technique has provided some surprising results in the light of all the previous work on fiber flexibility. It provides new opportunities to investigate the effect of mechanical and chemical treatment on pulp fibers in both dry and wet states.

CHAPTER 6: THE DEFORMATION BEHAVIOR OF WET LIGNOCELLULOSIC FIBERS

6.1 Introduction

The ability of pulp fibers to deform into a well bonded network controls the extent to which physical and optical properties of a paper sheet can be realized. Research into the deformation behavior of pulp fibers has generally focused on the flexibility, conformability, compactability, collapsibility, *etc*. of lignocellulosic fibers. All types of deformation are interrelated and contribute to sheet consolidation and/or the formation of fiber bonds. However, the controlling mechanism for each is not necessarily the same.

Many techniques have been used to measure fiber deformability. These methods can be separated into three main groups based on the length scale most critical to their measurement: macro-scale (mm), micro-scale (μm), and nano-scale (nm). Much of the work on fiber deformation has been on the macro-scale where single fibers were deflected in some manner. Early work either treated the fiber as a cantilever (Seborg and Simmonds 1941; Samuelsson 1963) or classified fiber flexibility based on its behavior in a controlled fluid flow (Forgacs and Mason 1958; Robertson, Meindersma and Mason 1961). Later researchers (TamDoo and Kerekes 1981; Kuhn, Lu, Olson *et al.* 1995) utilized capillary tubes to support fibers in

various fluid flows and measure flexibility. All of these methods model the fiber as a simply supported elastic beam and examine each fiber independent from any interactions with other fibers or objects.

Micro-scale methods rely on measurements of fiber deformations with fibers or other objects. Mohlin first described a technique to measure the conformability of single pulp fibers by measuring the distance required for a fiber to cross over a 60 μm glass fiber (Mohlin 1975b). Steadman and Lunar offered the next iteration by determining the "effective fiber flexibility" of fibers crossing a 25 μm stainless steel wire (Steadman and Luner 1985). Other methods such as the bulk fiber stiffness method (Frolander and Hartler 1970) or the acousto-optical compaction method (Brodeur and Runge 1995) determined fiber deformation by examining the behavior of a paper sheet or wet fiber mat.

While flexibility has been the most thoroughly investigated deformation behavior, Nilsson *et al* point out that it is one of many contributing factors to the development of fiber and paper properties (Nilsson, Wagberg and Gray 2001). Their work describes a nano-scale technique to investigate the fine structure of a water swollen lignocellulosic fiber with atomic force microscopy. The pulp fibers were found to have variations in local conformability due to the differences in material properties at the fiber

surface. This method could yield detailed information about the polymeric constituents and their heterogeneous distribution on the fiber surface; however, it's implications to the physical and optical properties of a paper sheet are still being determined.

Many of the methods presented above have treated the fiber as a linearly elastic beam expressing the result as the inverse of fiber stiffness, EI. Where E is the elastic modulus (Nm^2) and I is the moment of area (m^4). Recent work has pointed out that this assumption may not be correct (Waterhouse and Page 2004). As the span decreases and/or the ratio of bending stiffness to shear rigidity increases, the importance of shear deformation increases. With spans similar to what occurs in a paper sheet, the contribution of shear can dominate (Waterhouse and Page 2004).

Most recently, a technique developed by Lowe *et al.* modified the Steadman and Luner method by exchanging the underling stainless steel wire for another pulp fiber (Lowe, Page and Ragauskas 2005). This approach allows fiber deformations to be measured using geometries that more realistically simulate what occurs in a paper sheet. Lowe found that the freespan of a fiber crossing was dependent on the stepheight created by the underlying fiber. Also, the main effect of refining was to

lower the stepheight thus giving a shorter freespan. This study employs a slightly modified method to rigorously investigate the effect of pulp type, wet pressing and refining on the fiber deformation behavior of softwood and hardwood pulps.

6.2 Methods and Materials

6.2.1 Sample Preparation

Kraft hardwood pulps were provided by a Scandinavian mill. Unbleached never dried pulp (kappa number 15.1), fully bleached never dried pulp (ISO Brightness 86.3), and fully bleached market pulp samples were collected within one hour after each relevant unit operation in the mill. An unbleached kraft softwood pulp (kappa number 19.9) was provided by a northern Canadian mill. Upon receipt, pulp samples were exhaustively washed with deionized water and then screened using a Valley Screen with 0.2 mm slot size. Each pulp was then refined in a PFI mill to 300, 1000, 2000, and 4000 revolutions according to TAPPI Standard T 249 sp-00 with a beating gap of 0.2 mm. After refining, ten grams (oven dry basis) from each sample were fractionated using a Bauer-McNett Classifier with the R28, R35, R48, and R200 screens for the hardwood and R12, R14, R28, R35 for softwood. Deformability slides were prepared to investigate the effect of bleaching, drying, refining and wet pressing on fiber crossings. Handsheets were made from unfractionated pulp

following TAPPI Standard T 205 sp-02 to provide density, tensile, and light scattering coefficient data for each sample. Results are reported as average values with standard error.

6.2.2 Deformability Analysis

Approximately 0.25 OD g was weighed from the medium long fiber fraction. 5.00 mL of a 0.20 weight percent solution of chlorazol black dye (Sigma-Aldrich, St. Louis, MO, USA) was added to the pulp. The total volume was brought to 25.00 mL and then capped. The fiber suspension was thoroughly mixed via shaking and refrigerated overnight at 4°C. The fibers were then exhaustively washed with deionized water in a Buchner funnel until the filtrate was free of color before being suspended in 1000 mL of deionized water for slide making.

An 18.5 cm diameter grade 415 qualitative filter paper (VWR, West Chester, PA, USA) was placed onto a wet screen in a TAPPI handsheet mold. Once closed, 5000 mL of deionized water and approximately 20 mL of the fiber suspension were top-filled into the mold. The sample was drained onto the filter paper and wet pressed onto four glass slides for two minutes at 0.34 MPa. The slides were allowed to dry and were kept at 23°C and 50% relative humidity before and during imaging.

Images of single fiber crossings were acquired with a Leica DM-IRM inverted polarized light microscope (Leica Microsystems Inc., Bannockburn, IL, USA). To allow imaging through a glass slide, a 40X objective with a correction collar was used. A mica sheet was brought into optical contact with the bottom of a glass slide with microscopy immersion oil to increase image contrast. The specimen was then illuminated and viewed in polarized light to eliminate light reflected from the underside of the slide from the image. Figure 42 illustrates the imaging setup. Other details of the optical setup and the implications to image quality have been described by Lowe *et al* (Lowe, Page and Ragauskas 2005).

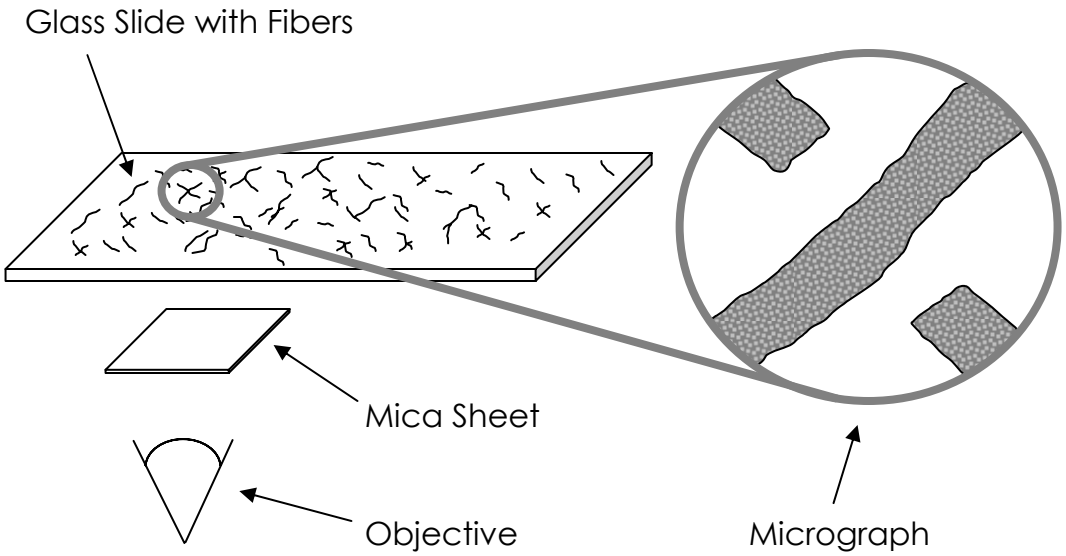

Figure 42 - The Imaging Setup
An illustration of the optical setup using an inverted reflected light microscope to observe fiber crossings through a glass slide is shown.

Regions of the fiber crossing that are bonded to the glass slide appear dark. A narrow band filter (λ=547±10 nm) allows interference fringes to be observed in the region of non-contact. The stepheight and shape of the fiber in the freespan region can be determined by analyzing the fringe patterns (Lowe, Page and Ragauskas 2005). The micrographs were analyzed with Simple PCI 5.3 image analysis software (Compix Inc., Sewickley, PA, USA).

6.2.3 Experimental Design

A 2^3 factorial designed experiment was used to investigate how fiber fraction, refining and wet pressing impact the ratio of stepheight to freespan for the unbleached hardwood pulp. A designed experiment determined the statistical significance of each effect. Deformability slides were prepared with the unbleached never dried hardwood pulp utilizing the conditions described in Table 32. The pulp was refined to 300 and 2000 revolutions then fractionated. The medium long (R35) and short fraction (R200) were reserved for deformability analysis. Slides were prepared as described above except that an additional set was pressed at 2.1 MPa. The significance of each factor was determined using JMP 6 (SAS Institute, Cary, NC, USA) statistical analysis software.

Table 32 - The Experimental Design
The design of experiments listed in standard order. The sample order was randomized for the experiment.

Sample	Refining (PFI Revolutions)	Fiber Fraction	Wet Pressing (MPa)
1	300	Shorts	0.34
2	300	Shorts	2.10
3	300	Med. Longs	0.34
4	300	Med. Longs	2.10
5	2000	Shorts	0.34
6	2000	Shorts	2.10
7	2000	Med. Longs	0.34
8	2000	Med. Longs	2.10

6.3 Results and Discussion

Fiber deformation behavior contributes to most physical and optical properties. The methods described above were used to prepare and analyze micrographs of fiber crossings. Freespans were generally measured along the central axis of each fiber and stepheights were determined by analyzing the interference fringe pattern. Figure 43 illustrates the stepheight (S) and the freespan (F) of a fiber crossing. Average values of freespan and stepheight were calculated for each set of conditions. Table 33 shows these values along with some physical and optical properties.

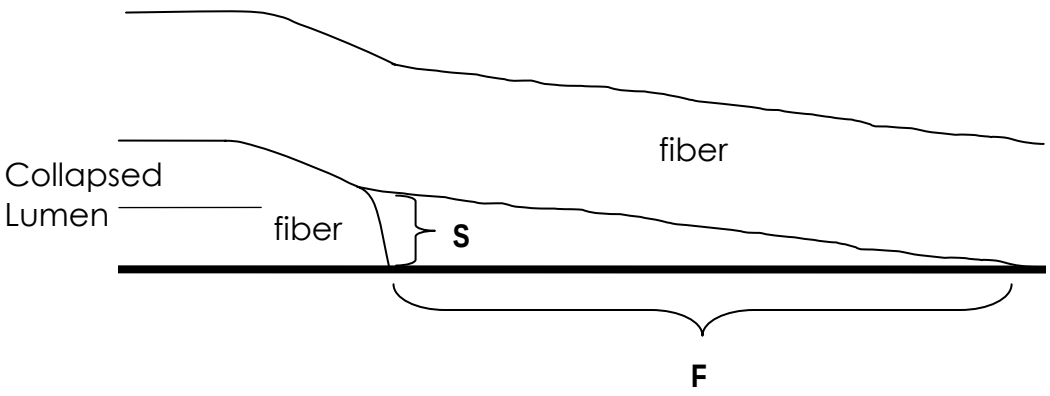

Figure 43 - Stepheight and Freespan Geometry in a Fiber Crossing
An illustration of the geometry of a fiber crossing showing the stepheight (S) and the freespan (F).

Table 33 - Physical and Optical Properties

PFI Revs	Stepheight (μm)	Freespan (μm)	Soft Platen Density (g/cm^3)	Tensile Index (Nm/g)	Scattering Coefficient (m^2/kg)
Unbleached Northern Canadian SW Kraft Slush Pulp (Kappa # 20)					
300	3.41 (0.16)	33.66 (1.73)	0.574 (0.001)	53.3 (1.3)	33.66 (0.22)
1000	3.00 (0.16)	25.67 (1.35)	0.612 (0.006)	72.8 (1.2)	29.15 (0.19)
2000	1.93 (0.13)	18.07 (1.05)	0.687 (0.010)	91.5 (0.6)	25.33 (0.35)
4000	1.76 (0.10)	15.04 (0.91)	0.790 (0.017)	111.7 (2.4)	22.11 (0.14)
Unbleached Scandinavian HW Kraft Slush Pulp (Kappa # 15)					
300	3.43 (0.17)	33.24 (1.53)	0.730 (0.004)	73.1 (2.3)	29.26 (0.45)
1000	2.63 (0.14)	27.05 (1.42)	0.765 (0.003)	80.1 (0.9)	27.51 (0.35)
2000	2.23 (0.14)	21.28 (1.54)	0.797 (0.008)	90.1 (2.8)	24.39 (0.30)
4000	1.74 (0.12)	16.04 (1.19)	0.835 (0.005)	97.8 (1.4)	21.85 (0.32)
Bleached Scandinavian HW Kraft Slush Pulp (ISO Brightness 86)					
300	3.44 (0.23)	30.34 (2.21)	0.740 (0.010)	58.6 (1.5)	34.73 (0.56)
1000	2.62 (0.15)	23.62 (1.35)	0.777 (0.004)	71.8 (1.6)	30.54 (0.29)
2000	2.35 (0.18)	19.15 (1.55)	0.829 (0.006)	83.4 (1.5)	26.91 (0.51)
4000	1.81 (0.15)	15.51 (1.34)	0.851 (0.004)	91.6 (1.6)	24.52 (0.28)
Bleached Scandinavian HW Kraft Market Pulp (ISO Brightness 86)					
300	3.19 (0.19)	27.73 (1.97)	0.677 (0.005)	46.3 (0.7)	37.30 (0.35)
1000	2.49 (0.20)	20.29 (1.86)	0.721 (0.002)	58.4 (0.6)	34.41 (0.30)
2000	1.98 (0.14)	15.62 (1.16)	0.786 (0.002)	68.6 (1.2)	30.39 (0.35)
4000	1.53 (0.13)	11.45 (1.07)	0.819 (0.004)	77.8 (1.1)	28.36 (0.44)

**Standard error is reported in parenthesis.

6.3.1 The Effect of Refining

Figure 44 shows several representative micrographs. Each micrograph was analyzed for stepheight and freespan measurements and the results for unbleached hardwood are shown in Figure 45. The data scatter is due, in part, to the natural variation in the deformation behavior of pulp fibers. The linear regression analyses pass through the origin and nearly coincide with each other. Figure 46 shows the average freespan and stepheight response at each refining level for both hardwood and softwood. The ratio of freespan to stepheight remains approximately constant (*e.g.* the data fall along a single line through the origin). Since the freespan is not reduced independently of the stepheight, refining only serves to decrease the stepheight of the underlying fiber. There is no indication that refining reduces the freespan in a fiber crossing by increasing fiber flexibility. Therefore, a major effect of PFI refining on deformation behavior is to make the fibers more collapsible leading to reduced stepheights. This is similar to the response seen for a softwood pulp (Lowe, Page and Ragauskas 2005).

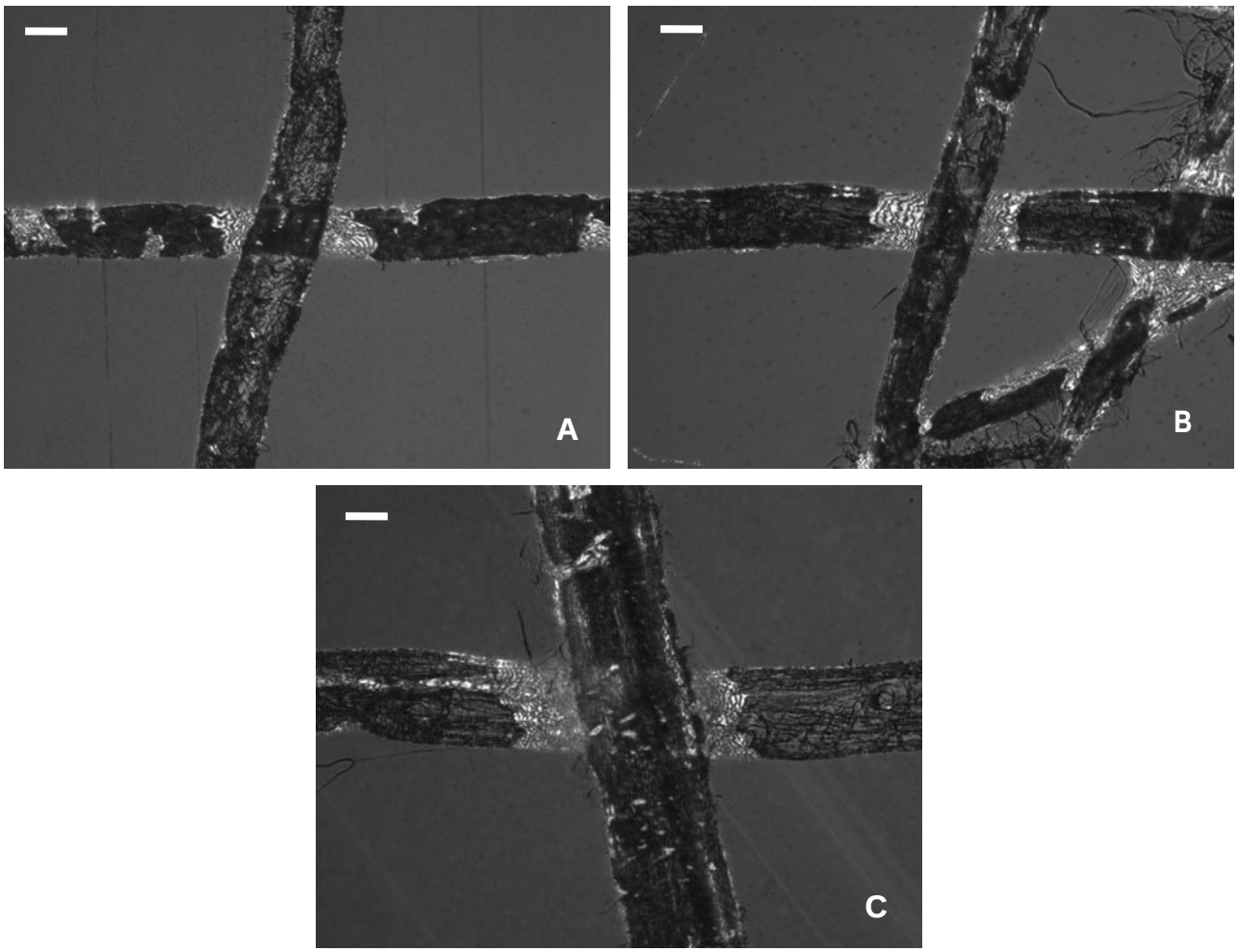

Figure 44 - Hardwood and Softwood Fiber Crossings
Representative micrographs of bleached hardwood (A), unbleached hardwood (B), and unbleached softwood fibers (C). The bar is 15 μm.

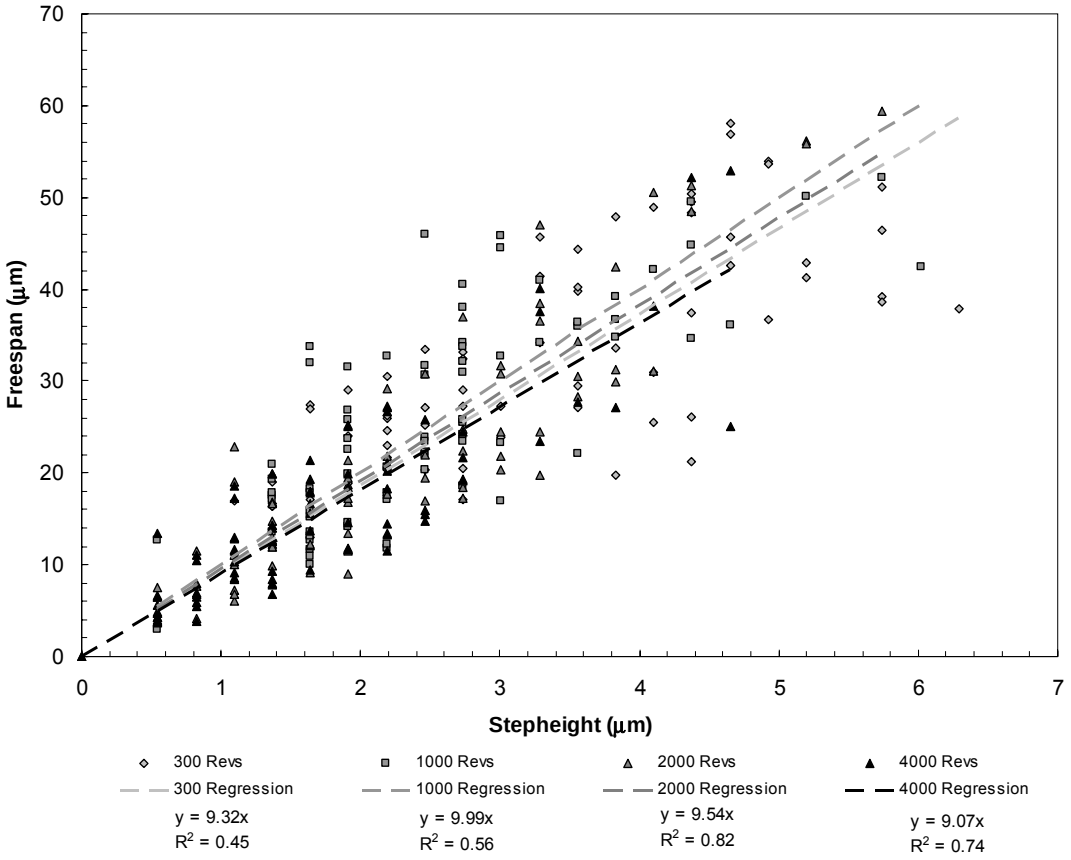

Figure 45 - The Effect of Refining for Unbleached Hardwood Kraft
The effect of refining for unbleached hardwood fibers. Each refining level is shown as well as the linear regression analysis.

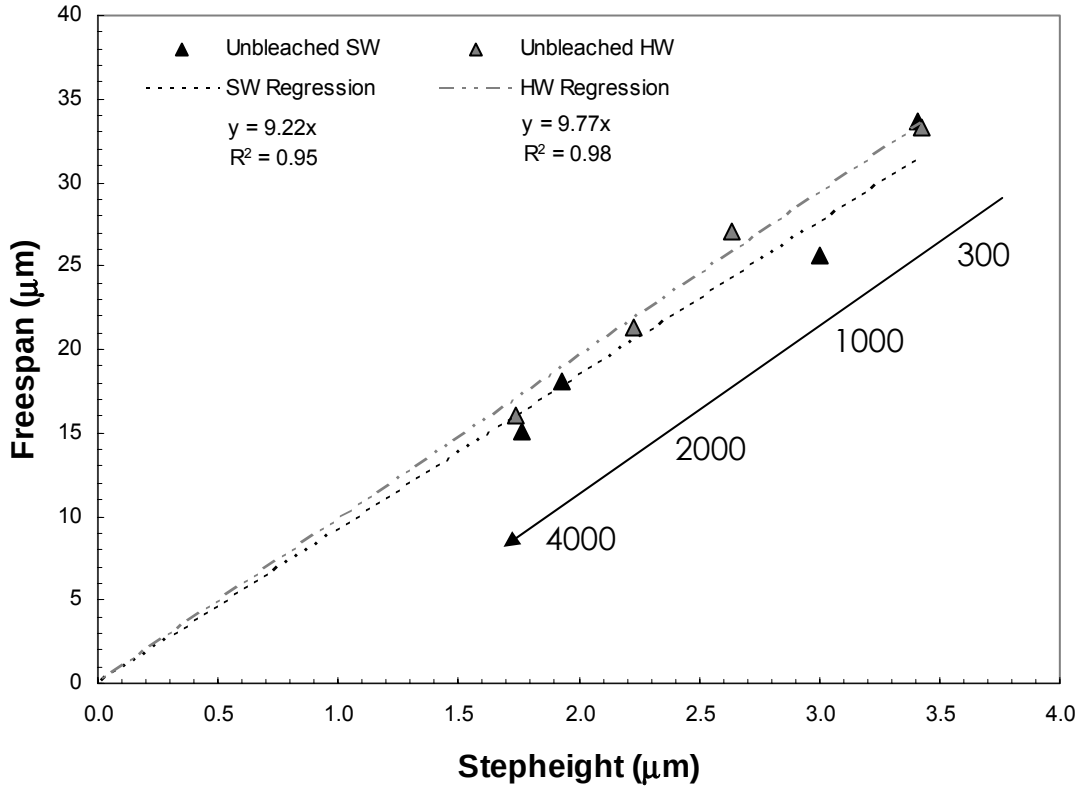

Figure 46 - Average Stepheight and Freespan Values for Unbleached HW and SW Kraft
Average stepheight versus freespan for refined unbleached softwood and hardwood kraft pulps. The regression analysis is shown as well as the effect of PFI refining.

It should be noted that with increased refining the stepheights drop lower than one would expect. The cell wall thickness can range from 2.0-4.0 μm which should lead to stepheights of at least 4.0 μm. In Figure 45, there are several occurrences of stepheights less than 2.0 μm. Lowe *et al* described a similar phenomenon and stated that the underlying fiber is most likely

deforming (Lowe, Page and Ragauskas 2005). These results suggest that the cell wall may deform more readily that previously thought and this deformation behavior is increased with PFI refining. Nanko and Ohsawa have also reported that the cell wall may possess some fluidity which is consistent with our data (Nanko and Ohsawa 1989). The increased deformability allows fibers to assume a lens shape which effectively reduces the stepheight of a fiber crossing. Lens shaped fibers can be seen in many published images of paper cross sections as shown in Figure 47 (Page, Sargent and Nelson 1965).

Figure 47 - A Lens Shaped Fiber
Cross-section of a paper sheet showing a lens shaped fiber(Page, Sargent and Nelson 1965).

6.3.2 The Experimental Design Results

A designed experiment was prepared to investigate the effect of fiber fraction, wet pressing, and refining on the ratio of stepheight to freespan

for the unbleached hardwood pulp. Averages were calculated for each condition set and input to JMP to determine the statistical significance of each variable (refining, fiber fraction, and wet pressing). Table 34 summarizes the results of the designed experiment analysis. A Prob>|t| less than 0.05 is considered a statistically significant effect at the 95% confidence level. Quite unexpectedly, none of the variables had a statistically significant effect on reducing the stepheight/freespan ratio. This result provides some statistical rigor to the initial observation of a constant stepheight/freespan ratio for increased refining. Pulp type and wet pressing are more thoroughly investigated in the following sections.

Table 34 - The Designed Experiment Results
A summary of the experimental design analysis for unbleached hardwood never dried pulp. A Prob>|t| less than 0.05 is considered a statistically significant effect at the 95% confidence level.

	Stepheight/Freespan	
	Prob>|t|	Significant
Refining	0.34	No
Fiber Fraction	0.15	No
Wet Pressing	0.64	No

6.3.3 The Effect of Bleaching, Drying, and Wet Pressing

Figure 48 shows a comparison between unbleached and bleached never dried hardwood fibers. While the stepheights stay virtually the same, reduced freespans at each refining level lower the ratio of freespan to stepheight (i.e. the slope of the regression line is reduced). This is in agreement with work from other researchers. It has been shown that never dried pulps have almost no fiber collapse prior to wet pressing (Page 1967). Also, there is very little difference (~3%) between the transverse elastic modulus of low yield unbleached and fully bleached kraft pulps (Scallan and Tigerstrom 1992). Therefore, it was anticipated that two uncollapsed pulps with similar coarseness values (see Table 35) and a similar transverse elastic modulus would exhibit a comparable amount of fiber collapse with increased refining. Paavilainen has shown that bleached fibers have a higher wet fiber flexibility (Paavilainen 1993); hence, bleached fibers will have shorter freespans.

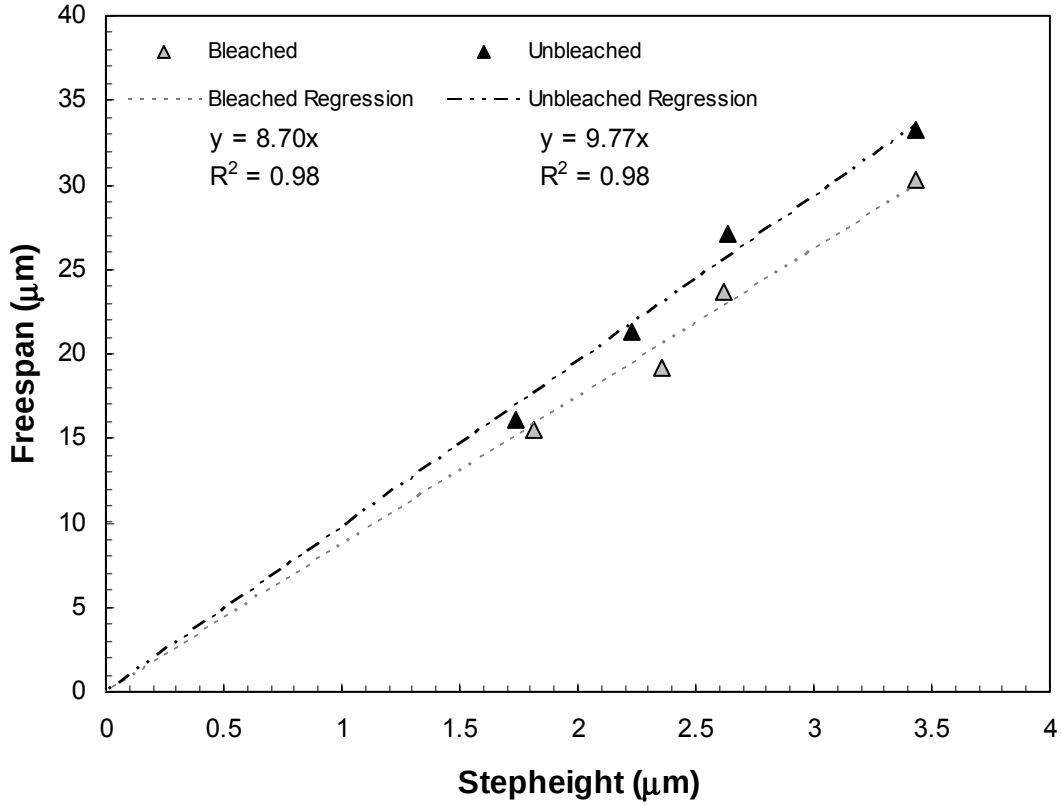

Figure 48 - Bleached and Unbleached Hardwood
Average stepheight versus freespan for unbleached and bleached never dried hardwood pulps. The regression analysis for each set is also shown.

Table 35 - Hardwood Fiber Lengths and Coarseness Values

	Fiber Length (mm)	Coarseness (mg/100m)
Unbleached - R200 (shorts)	0.49	7.0
Unbleached - R35 (medium longs)	1.03	9.9
Bleached – R35 (medium longs)	1.02	9.9

Figure 49 shows a comparison between bleached never dried and a once dried bleached market pulp. The regression analysis for each pulp very nearly overlaps. For each refining level the once dried market pulps fall closer to the origin. The market pulp was pressed and dried prior to being repulped for analysis. Pressing induces fiber collapse (Gorres, Amiri, Grondin *et al.* 1993). Drying does increase the transverse elastic modulus, however, it can be completely recovered with beating (Scallan and Tigerstrom 1992) which increases its tendency to collapse upon re-drying (Page 1967). Therefore, pulp drying reduces stepheight via increased fiber collapse without an impact on the freespan.

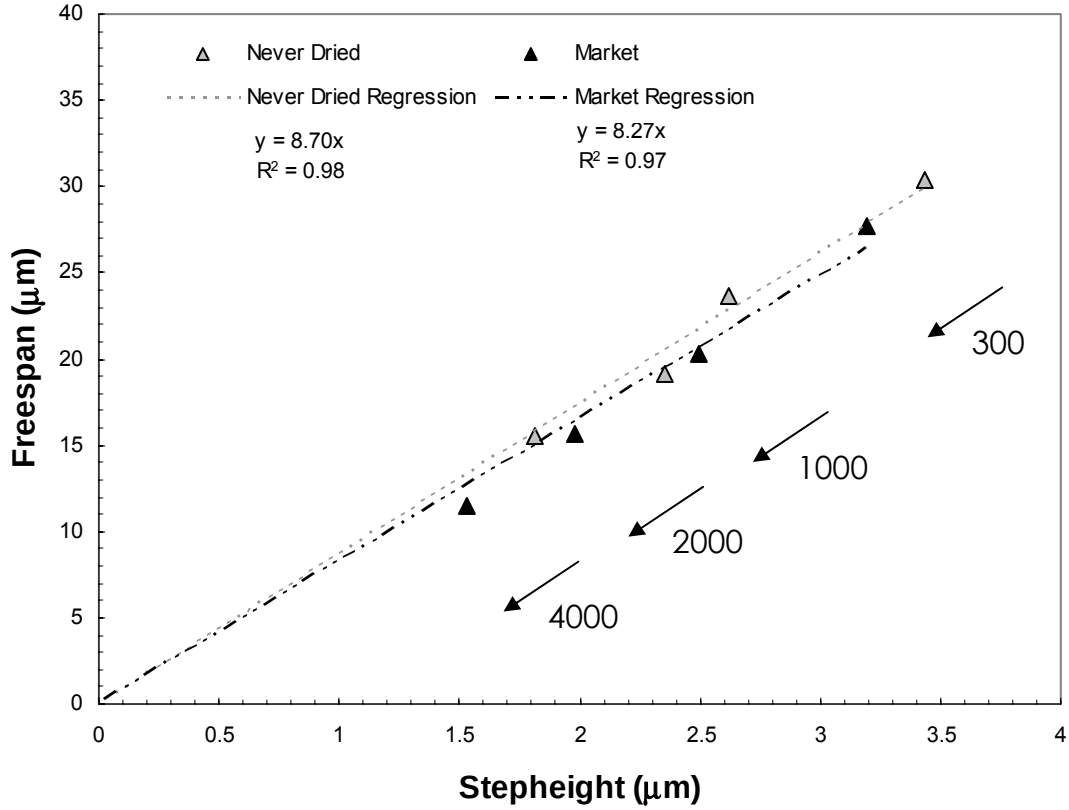

Figure 49 - The Effect of Drying
Average stepheight versus freespan for bleached never dried and market hardwood pulps. The refining level for each point is shown as well as the regression analysis. The arrows indicate the effect of drying for each refining level.

Finally, Figure 50 shows the impact of wet pressing on stepheight and freespan. The data fall along a line through the origin indicating that the flexibility of the overlying fiber is less important than previously thought. As for refining, the wet pressing results indicate the freespan depends only on the stepheight which, in turn, is determined by the deformability of the underlying fiber.

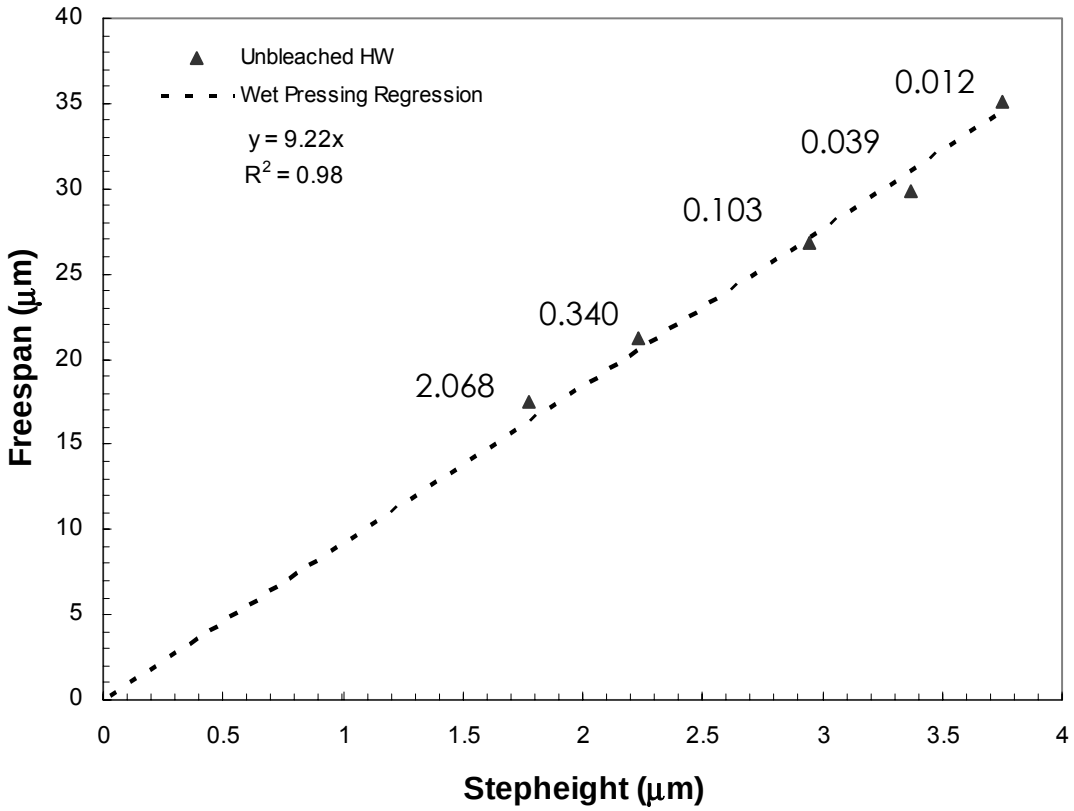

Figure 50 - The Effect of Wet Pressing
Average stepheight versus freespan for an unbleached never dried hardwood pulp. The pressing level (MPa) for each point is shown as well as the regression analysis.

The results taken together are startling. It should be noted that this method uses a wavelength of light as a ruler; therefore, our confidence in the results is high. A constant stepheight/freespan ratio implies that the flexibility of the overlying fiber is largely irrelevant to the formation of fiber crossings. Sheets are densified by pressing or drying via a change in the stepheight of the underlying fiber.

The ratio of stepheight to freespan is constant regardless of pulp species, refining, bleaching, pulp drying, and wet pressing. All of the stepheight versus freespan plots are straight lines through the origin. Theoretical attempts to explain such a remarkable result are lacking. Bending as the controlling mode of deformation has been previously been dismissed (Waterhouse and Page 2004). While it has been shown that the deformation of the freespan is likely controlled by shear (Waterhouse and Page 2004), it has not been demonstrated that the deflection of the freespan is controlled by shear modulus. An extension of the equations developed by Waterhouse and Page (2004) for pure shear to a wet fiber crossing leads to Equation 9. Where d is the deflection or stepheight, q is the fiber distributed load, L is the freespan, f_s is the fiber shape factor, G_{13} is the shear modulus of the fiber, and A is the cross-sectional area. For shear modulus to control the deflection, the stepheight should be proportional to the freespan squared which has not been observed. Since neither bending nor shear is controlling the deflection of the freespan, another mechanism must be at work.

$$d = \frac{qL^2 f_s}{2G_{13}A}$$

Equation 9 - A Shear Modulus Controlled Deflection
For a shear controlled deflection (d), d should be proportional to L^2.

6.4 Conclusions

A method to investigate the deformation behavior of single fiber crossings has been presented. Dyed pulp fibers were pressed onto glass slides and micrographs were acquired. Freespans and stepheights were measured to determine the effects of refining, wet pressing, drying and bleaching on the fiber deformability of unbleached never dried, bleached never dried, and bleached market pulps.

The main effect of refining was to reduce the stepheight in the fiber crossing for both bleached and unbleached fibers by increasing the tendency of the cell wall to collapse and deform. All the pulps and treatments investigated maintained a relatively constant value for the ratio of stepheight to freespan. This result is quite unexpected and suggests the deformation behavior of cellulose pulp fibers may be more universal than previously thought. Work is ongoing to further investigate this phenomenon.

CHAPTER 7: SURFACE AND BULK CHARGE

7.1 Introduction

The importance of surface and bulk charge to fiber and paper properties has been well recognized. Many researchers have looked at the relationship between bond strength and the presence of acid groups. Ampulski, Engstrand, and Barzyk have all shown that the presence of acid groups contributes to the development of sheet strength (Ampulski 1985; Engstrand, Sjogren, Olander *et al.* 1991; Barzyk, Page and Ragauskas 1997a). Barzyk, in particular, has shown that acid groups on the surface of a fiber can increase the fiber-to-fiber specific bond strength (Barzyk, Page and Ragauskas 1997a).

Paper scientists are now developing research programs to explore how the distribution of fiber charge influences paper and fiber physics. Laine *et al.* have recently published their extensive investigation on heterogeneously developing charge in the structure of the fiber (Laine, Lindstrom, Nordmark *et al.* 2000), how the charge distribution impacts fiber swelling (Laine, Lindstrom, Nordmark *et al.* 2002; Laine, Lindstrom, Bremberg *et al.* 2003a), and how fiber charge influences the physical and optical properties of a paper sheet (Laine, Lindstrom, Bremberg *et al.* 2003b).

Laine *et al.* employed two techniques that selectively introduce carboxyl groups to the fiber structure. Surface charge was introduced by irreversibly attaching carboxymethyl cellulose (CMC) to the fiber (Laine, Lindstrom, Nordmark *et al.* 2000). As long as the CMC has a high enough molecular weight (M_w>10^5), the attachment will be only on the surface. The second method was much like that of Walecka (Walecka 1956) to introduce carboxyl groups throughout the fiber structure (Laine, Lindstrom, Bremberg *et al.* 2003a).

Their investigation into the impact of surface and bulk charge groups on the physical and optical properties of handsheet provided some interesting results: 1) Since there was little or no change in sheet density or light scattering coefficient, surface grafted CMC served to primarily increase the specific bond strength of the handsheets. 2) For carboxymethylated pulps, the contribution of the surface charge groups to swelling was much more significant than the contribution of the charge groups in the bulk of the fiber. 3) The impact of surface swelling was more important to the fiber bond strength than to the change in cell wall flexibility and sheet consolidation.

Laine *et al.* based their conclusions on overall impact of surface and bulk charge on the physical and optical properties of handsheets. They did not directly investigate the effect of charge on the deformation behavior of individual fibers. Such an analysis could provide a more fundamental understanding of how fiber charge can shape the development of the physical and optical properties of a paper sheet.

The following study employs a method developed by Lowe *et al.* to investigate the deformation behavior of single fiber crossings (Lowe, Page and Ragauskas 2005). This approach allows fiber deformations to be measured using geometries that more realistically simulate what occurs in a paper sheet. The effect of surface CMC grafting and bulk carboxymethylation on the deformation behavior of unbleached softwood fibers is investigated.

7.2 Methods and Materials

7.2.1 Pulp

A mill produced northern Canadian softwood kraft pulp was provided by SFK Pulp in Saint Félicien, Québec. The pulp was unbleached (kappa number = 19.9) and neverdried. Upon receipt, pulp samples were exhaustively washed with deionized water and then screened using a Valley Screen with 0.2 mm slot size.

7.2.2 Exchange of Counter Ions

Approximately 30 g (oven dry basis) was measured out for each level of CMC treatment. All pulp samples were then washed to the calcium form prior to treatment as follows. The pulp was placed in 0.01 M HCl at 2.5% consistency. The pH was adjusted to 2 and remained at this level for 30 minutes, then the pulp was washed with deionized water in a Buchner funnel until the conductivity of the filtrate was less then 5 µS/cm. The pulp was then brought to 2.5% consistency using 1 mM $NaHCO_3$. Sodium hydroxide was used to adjust to pH 9 and held constant for 30 minutes. The pulp was then washed with deionized water in a Buchner funnel until the conductivity of the filtrate was less then 5 µS/cm. Finally, the pulp was placed in 0.05 M $CaCl_2$ at 2.5% consistency for 15 minutes and then washed with deionized water in a Buchner funnel until the conductivity of the filtrate was less then 5 µS/cm.

7.2.3 CMC Grafting

CMC (Aquasorb A 500, Hercules, Sweden) for each treatment level was measured out as described in Table 36, dissolved in 100.0 mL of deionized water, and allowed to stir overnight. The pre-washed pulp was brought to 2.5% consistency with a 0.05 M $CaCl_2$ solution and the dissolved CMC. The pH was adjusted to 8 with 0.01 M $NaHCO_3$ and sealed in a 2.0L autoclave

vial. The pulp mixture was place in a preheated glycol bath at 120°C for two hours.

Table 36 - Levels of CMC Addition to Unbleached Softwood Kraft Fibers

Sample	CMC Added
1	0 mg/g pulp
2	12 mg/g pulp
3	40 mg/g pulp

The pulp was then washed with deionized water in a Buchner funnel until the conductivity of the filtrate was less then 5 µS/cm. The total charge and the attached amount of CMC was determined by conductometric titration (Katz, Beatson and Scallan 1984). Polyelectrolyte titration was performed to determine the surface charge of the fibers (Wagberg, Winter and Lindstrom 1985).

7.2.4 Carboxymethylation

The pulp was then disintegrated at 1.5% consistence for 10000 revolutions in a standard disintegrator. The pulp was then solvent exchanged with 95% ethanol and filtered after 10 minutes. The solvent exchange was repeated three times.

The monochloroacetic acid amount describe in Table 37 was dissolved in 500 mL of isopropanol and used to impregnate the solvent exchanged pulp for 30 minutes. The 16.2 g of sodium hydroxide was dissolved in 500 mL of methanol and added to 2000 mL of isopropanol. The methanol/isopropanol solution was heated to boiling and the impregnated pulp was added. The reactants were refluxed for one hour.

Table 37 - Bulk Carboxymethylation of Unbleached Softwood Kraft Fibers

Sample	$ClCH_2COOH$ Added
1	0.404 g
2	3.640 g

The pulp was then filtered and washed with deionized water, then 0.1 M acetic acid, and then deionized water again. Finally the pulp was placed in 4.0% $NaHCO_3$ for one hour and then washed with deionized water. The total charge and the attached amount of CMC was determined by conductometric titration (Katz, Beatson and Scallan 1984). Polyelectrolyte titration was performed to determine the surface charge of the fibers (Wagberg, Winter and Lindstrom 1985).

7.2.5 Deformability Analysis

Approximately 0.25 OD g was weighed from each pulp sample. 5.00 mL of a 0.20 weight percent solution of chlorazol black dye (Sigma-Aldrich, St. Louis, MO, USA) was added to the pulp. The total volume was brought to 25.00 mL and then capped. The fiber suspension was thoroughly mixed via shaking and refrigerated overnight at 4°C. The fibers were then exhaustively washed with deionized water in a Buchner funnel until the filtrate was free of color before being suspended in 1000 mL of deionized water for slide making.

An 18.5 cm diameter grade 415 qualitative filter paper (VWR, West Chester, PA, USA) was placed onto a wet screen in a TAPPI handsheet mold. Once closed, 5000 mL of deionized water and approximately 20 mL of the fiber suspension were top-filled into the mold. The sample was drained onto the filter paper and wet pressed onto four glass slides for two minutes at 0.34 MPa. The slides were allowed to dry and were kept at 23°C and 50% relative humidity before and during imaging.

Images of single fiber crossings were acquired with a Leica DM-IRM inverted polarized light microscope (Leica Microsystems Inc., Bannockburn, IL, USA). To allow imaging through a glass slide, a 40X objective with a correction collar was used. A mica sheet was brought

into optical contact with the bottom of a glass slide with microscopy immersion oil to increase image contrast. The specimen was then illuminated and viewed in polarized light to eliminate light reflected from the underside of the slide from the image. Other details of the optical setup and the implications to image quality have been described by Lowe *et al.* (Lowe, Page and Ragauskas 2005).

7.2.6 Handsheets

Handsheets were formed following TAPPI Standard T 205 sp-02 from the undyed remainder of each pulp sample. The handsheets were then analyzed for basis weight, caliper, light scattering coefficient, zero span tensile strength, and Z-direction tensile strength.

7.3 Results and Discussion

After charge substitution, total fiber charge and surface charge were measured along with the water retention value (SCAN-C 62:00). The results are presented in Table 38 and show increased WRV with increased charge. The methods described above were used to prepare and analyze micrographs of fiber crossings. Figure 51, Figure 52, and Figure 53 show several representative micrographs of fiber crossings.

Table 38 - Charge Analysis and WRV Results
Total and surface charge analysis along with water retention values for the bulk and surface treated unbleached softwood kraft fibers.

Description	Total Charge (μeq/g)	Surface Charge (μeq/g)	WRV (Ca^{2+} form) (g/g)
Surface – 0 mg CMC	73.6	2.8	1.48
Surface – 12 mg CMC	102.1	34.0	1.80
Surface – 40 mg CMC	147.9	72.1	1.99
Bulk – DS 0.027	164.7	6.3	1.22
Bulk – DS 0.087	487.7	20.2	1.44

Figure 51 - Surface Grafted 12 mg CMC/g
Unbleached softwood kraft fibers surface grafted with 12 mg of CMC per oven dry g of fiber.

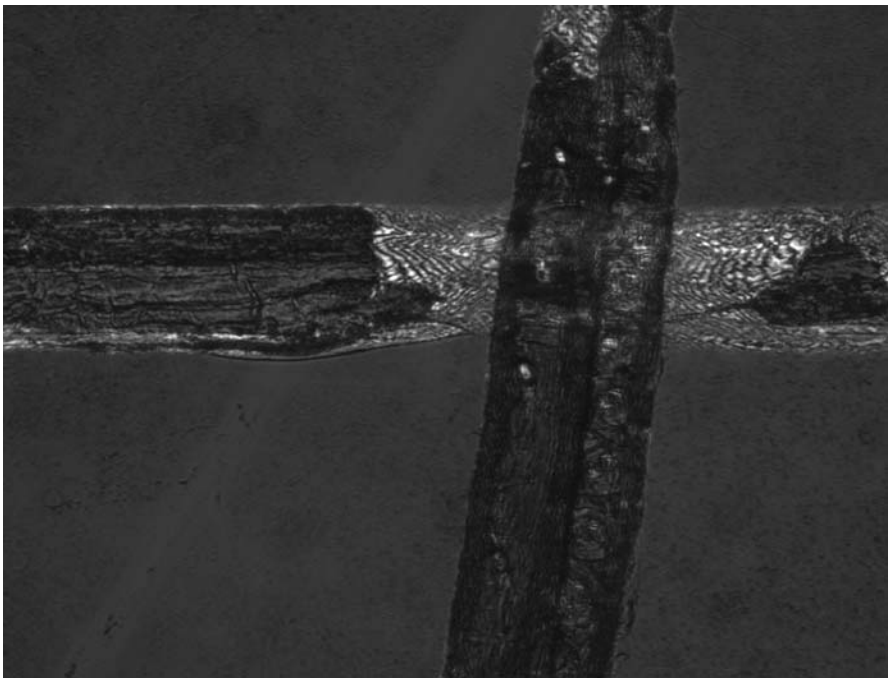

Figure 52 - Surface Grafted 40 mg CMC/g
Unbleached softwood kraft fibers surface grafted with 40 mg of CMC per oven dry g of fiber.

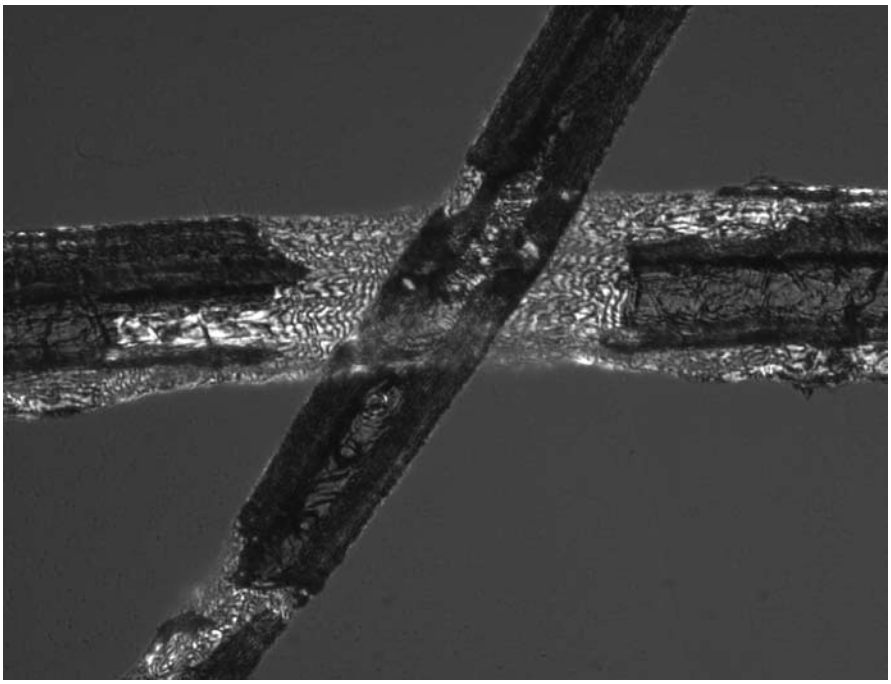

Figure 53 - Bulk Charge Degree of Substitution 0.087
Unbleached softwood kraft fibers with increased bulk charge. The degree of substitution was 0.087.

Freespans were generally measured along the central axis of each fiber and stepheights were determined by analyzing the interference fringe pattern. Average values of stepheight and freespan were calculated for each treatment level. Figure 54 demonstrates the effect of bulk carboxymethylation on the average stepheight and freespan of single fiber crossings. The bulk treatment appears to have an effect similar to refining; e. g. increased treatment level reduces both the stepheight and freespan. It should be noted that a 200% increase in total charge resulted only in a ~25% reduction is stepheight and freespan. Perhaps a greater benefit could be realized upon refining the bulk carboxymethylated samples.

Figure 55 shows the results for the surface grafted CMC fibers. While the stepheight remains essentially constant, the freespan increases by nearly 30%. With a high molecular weight CMC there should be little impact to the bulk of the cell wall; therefore, it is not surprising that the stepheights remain constant. Since the CMC is almost exclusively on the surface of the fiber, the swollen layer that results could conceivably alter the deformation behavior by changing either the modulus or moment of area resulting in stiffer fibers and longer freespans.

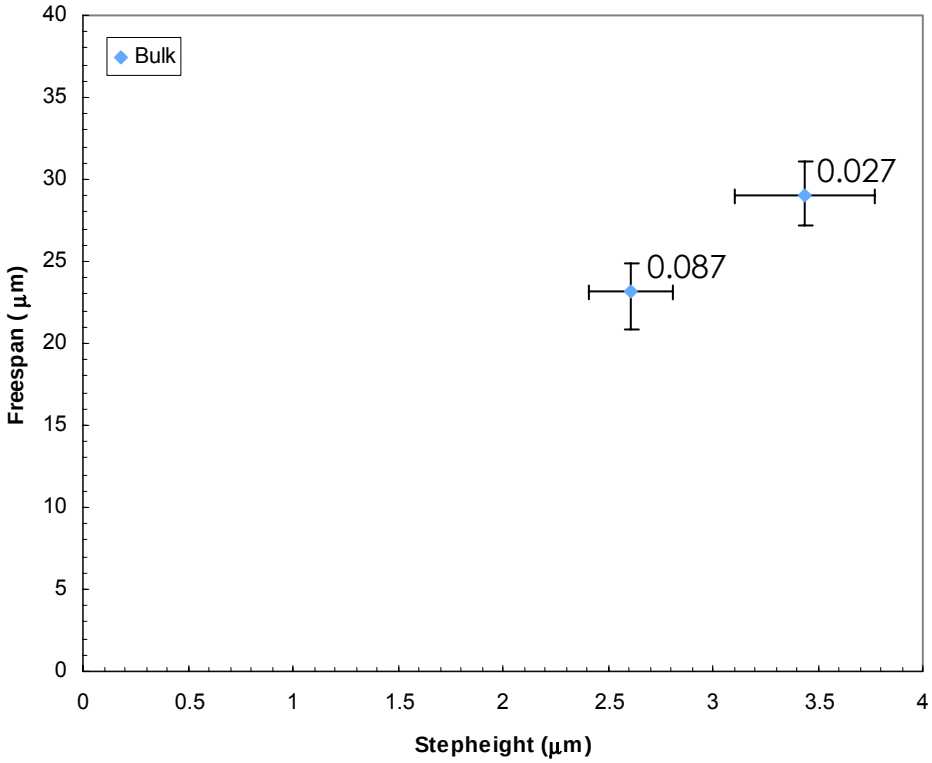

Figure 54 - Stepheight and Freespan for Bulk Carboxymethylation of Unbleached Softwood Kraft Fibers
A graph of stepheight versus freespan for bulk carboxymethylated pulps is shown. The degree of substitution and the standard error for stepheight and freespan is also indicated for each point.

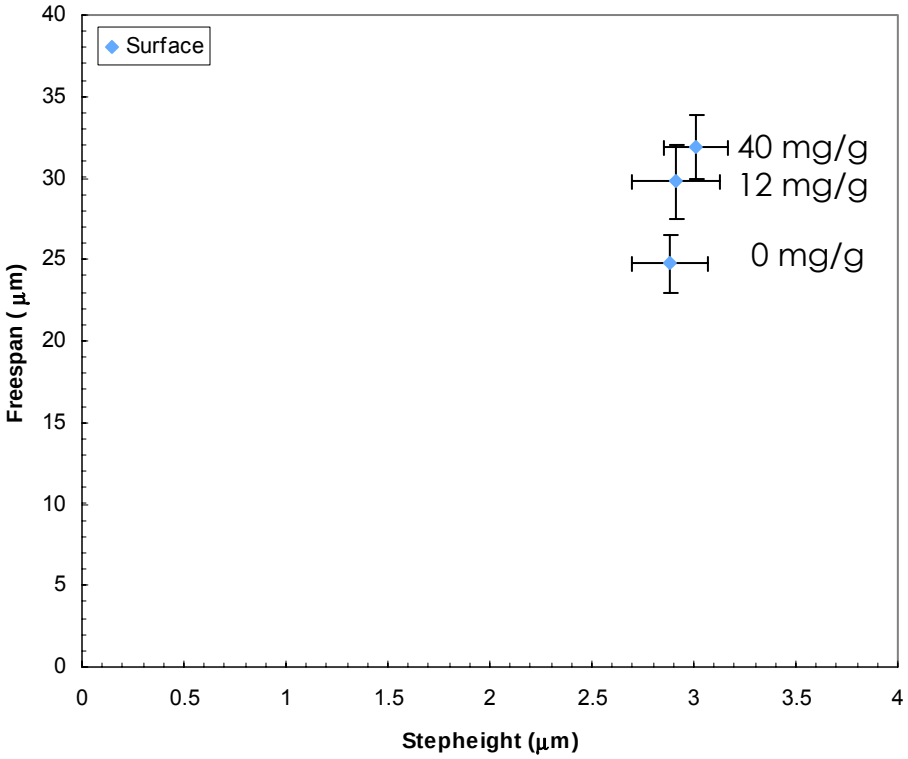

Figure 55 - Stepheight and Freespan for Surface CMC Grafting onto Unbleached Softwood Kraft Fibers
A graph of stepheight versus freespan for CMC surface grafted pulps is shown. The amount of CMC per gram of fiber is also indicated for each point.

Table 39 shows the physical and optical properties for handsheets made from the bulk and surface treated pulps. For the bulk treatment, an increase in fiber charge results in higher sheet density, tensile index, and z-direction tensile with a corresponding decrease in light scattering coefficient. Increased CMC on the surface resulted in a relatively constant density and light scattering coefficient with marked increases in tensile index and z-directional tensile. These results are similar to those reported by Laine *et al.* (Laine, Lindstrom, Nordmark *et al.* 2002; Laine, Lindstrom, Bremberg *et al.* 2003b). Since there was little impact on sheet density and light scattering coefficient, Laine concluded that the principal effect of surface CMC is to increase the specific bond strength. Figure 55 suggests that the effect of surface grafted CMC may be more complicated. Either the consolidation effect of CMC is masked by an increase in fiber stiffness or changes in the average fiber freespan have little relevance to sheet density.

Table 39 - Handsheet Physical and Optical Properties

	Density (g/cm^3)	Tensile Index (Nm/g)	Zero Span Index (N/cm)	ZDT (kPa)	Scattering Coefficient (m^2/kg)
Bulk – DS 0.027	0.412	30.8	90.1	179.3	37.66
Bulk – DS 0.087	0.541	74.1	101.8	360.3	26.69
Surface – 0 mg CMC	0.485	46.0	104.6	228.7	31.49
Surface – 12 mg CMC	0.518	73.2	113.2	434.0	29.77
Surface – 40 mg CMC	0.524	83.5	113.3	511.6	29.28

7.4 Conclusions

The role of surface and bulk charge modification on the deformation behavior of an unbleached softwood kraft pulp has been investigated. The surface charge was modified by grafting carboxymethyl cellulose onto the fiber surface, while the bulk charge was modified by a carboxymethylation of the pulp with a monochloroacetic acid treatment. Standard handsheets were made and compared against the fiber

deformation behavior. It was found that increased bulk charge resulted in reduced stepheights with an increased sheet density and decreased scattering coefficient. The surface CMC treatment increased fiber freespans without corresponding changes in stepheights, sheet density or scattering coefficient. The results suggest that the surface charge of CMC grafted fibers may play a more complicated role in the development of the physical and optical properties of paper sheet than previously thought.

CHAPTER 8: EXPLORING FIBER INTERFACES VIA FRET

A new method employing fluorescence microscopy and fluorescence resonance energy transfer (FRET) has been developed to image the surfaces involved in fiber-fiber bonding *in situ*. Image analysis of fluorescence micrographs indicates that FRET is occurring at the interface of single cellulose fiber crossings. Since FRET occurs over distances of 1-10 nanometers, this technique is capable of investigating fiber-fiber interfaces at the length scale relevant to molecular interactions. The FRET response to wet pressing was examined for single fiber crossings of both never dried white spruce (*Picea glauca*) and regenerated viscose fibers. Increased wet pressing results in an increased FRET signal for white spruce fibers. The FRET signal for viscose fiber crossings was comparatively low and remained unchanged with increased wet pressing, indicating that low FRET values may not be relevant to bonding.

8.1 Introduction

The local deformation behavior of pulp fibers plays a large role in the formation of fiber-fiber bonds. Fiber-fiber bonding is widely regarded as one of the most important properties for the papermaker because it is principally responsible for the internal cohesion of a paper sheet (Retulainen and Ebeling 1993). Bonding is traditionally defined using two

independent factors: bonded area and specific bond strength (bond strength per unit bond area) (Nordman 1957). There is significant industrial importance in decoupling these two factors because bonded area is directly related to both optical and strength properties, while specific bond strength has little impact on the optical properties.

Refining and wet pressing are traditional papermaking tools that effect fiber deformation behavior; hence, they can have a direct impact on bonded area (Ingmanson and Thode 1959; Nordman, Aaltonen and Makkonen 1965; Alexander and Marton 1968), and thus they manipulate both strength and optical properties. This trade-off can be overcome by directing research efforts toward enhancing specific bond strength leading to significant benefits for many paper grades. The determination of specific bond strength requires that a true bonded area between fibers be measured. Current methods may not accurately deconvolute the contributions of molecular interactions between fibers from the surface area over which they operate.

8.1.1 Inter-fiber Bonding

The strength of paper is inherently linked to the ability of pulp fibers to form inter-fiber bonds. An inter-fiber bond can be defined as the area between two fibers sufficiently close such that molecular interactions can

occur between the surfaces of the fibers. Several mechanisms for inter-fiber bond formation have been proposed: hydrogen bonding (Nissan 1961), diffusion (McKenzie 1984), van der Waals forces (Notley, Petterson and Wagberg 2004; Notley and Wagberg 2005), and electrostatic interactions (Wagberg and Annergren 1997). Lindstrom *et al.* have offered the most recent review (Lindstrom, Wagberg and Larsson 2005). While these mechanisms may operate under different constraints, they each must be accompanied by two fiber surfaces that are in close proximity, on the order of one nanometer, to each other. As the fiber surfaces approach one another, various molecular interactions begin to occur resulting in the formation of a fiber-fiber joint. Ultimately, the number of bonding interactions and the nature of those interactions determine the efficacy of the bonded area to transfer load between fibers. This dictates end product quality in terms of paper optical and strength properties.

8.1.2 Measuring Bonded Area

In order to measure the efficiency of the interfacial fiber-fiber area to transfer load, the total bonded area needs to be defined. Many researchers have offered methods (Parsons 1942; Haselton 1955; Ingmanson and Thode 1959; Caulfield 1973; Yang, Eusufzai, Sankar et al. 1978). According to Uesaka *et al.* relative bonded area (RBA) can be

measured either directly or indirectly (Uesaka, Retulainen, Paavilainen et al. 2002). Direct methods, such as Yang *et al.* (Yang, Eusufzai, Sankar et al. 1978), depend on the sectioning of sheets followed by an examination of micrographs and computer analysis. However, the accuracy of such methods is directly linked to the quality of sample preparation and the micrograph data collection methodology.

The more commonly used indirect methods were developed to measure the relative bonded area in paper sheets. They generally utilize gas adsorption or light scattering techniques. The scattering coefficient is related to the free specific surface area from which an approximation of the bonded area of a paper sheet can be derived. The most widely used method for measuring relative bonded area, developed by Ingmanson and Thode (Ingmanson and Thode 1959), relies on the use of light scattering coefficient and extrapolation to zero tensile strength.

Haselton's work utilized nitrogen gas adsorption and the Brunauer-Emmett-Teller (BET) method to calculate specific surface area (Haselton 1955). Since this method does not depend on the use of light scattering, it has been extensively used by scientists for pulp fibers. Graphs of BET area versus scattering coefficient go through the origin suggesting that the separation between bonded surfaces can not be more that 0.4 nm (the

radius of a nitrogen molecule); therefore, areas that are not available to scatter light must be in close enough contact for molecular interactions to occur. Since this method does not depend on the use of light scattering, it has been extensively used by scientists for pulp fibers.

Other work also supports the use of light scattering as an indication of bonded area. Barkas has shown that tremendous pressures can form from the Cambell's forces which would deform the malleable fiber surfaces and bring them into intimate contact (Barkas 1950). Asunmaa and Steenberg have directly observed the close contact between bonded fibers down to the limit of their micrographs of 20 Å (Asunmaa and Steenberg 1958) suggesting that the fiber surfaces are within the distance necessary for molecular interactions to occur.

Despite the evidence describe above, there is still debate surrounding the use of optical techniques such as light scattering to describe the bonded area (Page and Wagberg 1997). Currently, there is no definitive method to measure the areas in a fiber bond that are interacting on a molecular level. A new, preferably *in situ*, method that does not depend on the scattering of light is needed. Combining the technique of fluorescence microscopy with the principle of fluorescence resonance energy transfer could provide such an opportunity.

8.1.3 Fluorescence Resonance Energy Transfer

Further understanding of fiber-fiber interfaces and improved definitions of specific bond strength and relative bonded area clearly demand the application of novel experimental techniques. The photophysical phenomenon known as fluorescence resonance energy transfer (FRET) provides an opportunity for the modern paper physicist to study the fiber-fiber interaction on a molecular level.

A proper description of FRET requires a full understanding of electronic spectroscopy. For an extensive review of the basic principles of fluorescence spectroscopy and resonance energy transfer, see Lakowicz (Lakowicz 1983) and van der Meer *et al.* (Van Der Meer, Coker and Chen 1994). FRET is a long range dipole-dipole interaction between two fluorescing dye molecules resulting in a non-radiative transfer of excitation energy from a donor to an acceptor dye. FRET can only occur if there is sufficient spectral overlap and the two dye molecules are within 100 Å of one another. The interaction is electrostatic in nature and shows a characteristic inverse sixth power relationship between the energy transfer efficiency and the donor-acceptor distance.

Figure 14 illustrates the relevant spectra and a characteristic FRET response. The unique signature of FRET is the observation of long

wavelength emission attributed to the acceptor molecule with donor molecule excitation at a much shorter wavelength. Since the acceptor molecule has low absorbance (and correspondingly low fluorescence quantum efficiency) at the excitation wavelength of the donor, emission from the acceptor must be due to non-radiative energy transfer. Furthermore, if the nature of the donor and acceptor dye molecules and the index of refraction of the surrounding media are known quantities then the energy transfer efficiency can be used to determine the separation distance between the two molecules.

FRET has been widely used in medical and biochemical research as a tool to determine distances and global structural alterations in proteins and DNA (Somogyi, Matko, Papp et al. 1984; Hoppe, Christensen and Swanson 2002; Yapoudjian, Ivanova, Douchet et al. 2002). FRET gains new applications daily in a variety of fields, particularly material science. The technique is powerful because it can be used in imaging applications when a fluorescence microscope is employed (Jares-Erijman and Jovin 2003). Currently, FRET is not being utilized in the study of pulp and paper and more specifically it has not been used to probe the nature of the fiber-fiber bond.

An illustrative example of how FRET could operate in a paper system is shown in Figure 15. Two fibers, independently dyed with the donor and acceptor dyes, are brought into close proximity via capillary forces and wet pressing. When illuminated with the appropriate wavelength of light to excite the donor dye molecule, acceptor fluorescence can be detected if the two molecules are within 100 Å. Variations in the intensity of acceptor and donor fluorescence allow the FRET response to be used as a "spectroscopic ruler" to provide spatial information about the fiber-fiber interface.

8.2 Methods and Materials

8.2.1 Fiber and Sample Preparation

Both natural and regenerated cellulose fibers were prepared for this study. A never dried white spruce (*Picea glauca*) pulp, provided by Alberta Pacific (Canada), was bleached with chlorine dioxide and exhaustively washed with a final ISO brightness of 90. The bleached white spruce fibers were PFI refined to 3000 revolutions and then fractionated in a Bauer-McNett classifier. The long fiber fraction with an average fiber length of 3.1 mm was reserved for dyeing. Viscose staple fiber (39mm length, 1.2 denier) was supplied by Lenzing AG (Austria). The fiber was manually cut to an average fiber length of 1.9 mm, washed and then air dried before use.

Two fluorescent dyes were purchased from Molecular Probes (Eugene, OR, USA). The donor, 7-diethylaminocoumarin-3-carboxylic acid hydrazide (DCCH), and acceptor, fluorescein-5-thiosemicarbazide (FTSC), were chosen because they are an extensively used and well characterized FRET pair (Czworkowski, Odom and Hardesty 1991; Mitsui, Nanko and Yamana 2000).

The hydrazide dyes were applied to the fibers using a method adapted from Anderson (Anderson 1986). A 2% suspension of cellulose fiber (oven dry basis) in the appropriate solvent (FTSC: N,N,-dimethylformamide, DCCH: methanol), containing 1.6 mmol/L of dye, and 1.8 mmol/L of HCL was magnetically stirred in the dark overnight at room temperature. The resultant dyed fibers were briefly washed with their respective solvents and then subjected to a mild sodium borohydride reduction. Finally, to assure that only covalently linked dye remained on the fibers, they were Soxhlet extracted with acetonitrile overnight.

The most elemental structure in a paper sheet is a single fiber crossing. A method adapted from Lowe *et al.* (Lowe, Page and Ragauskas 2005) has been utilized to prepare glass slides with single fiber crossings. It was found that better fluorescence micrographs were acquired by imaging the top

surface of the fiber crossing with a black background placed on the opposite side of the glass slide. The FTSC dye has a pH dependence, therefore, a sodium tetraborate buffer solution was used to maintain pH 9 during the slide making process. A 50/50 mixture of DCCH and FTSC dyed fibers was diluted to volume in a standard handsheet mold and drained onto a filter paper. The fibers were couched onto glass slides and then wet pressed as described in Table 28. Slides were allowed to dry and condition at 50% relative humidity and 23°C before being imaged.

8.2.2 Fluorescence Microscopy and Image Analysis

A Leica inverted reflected light microscope, a 50 watt metal halide lamp, and a Hamamatsu ORCA-ER digital camera were used to acquire 1.0 megapixel images. The microscope was equipped with a fluorescence disc allowing a quick change of the filter sets without disturbing the sample. Exposure time was held constant between filter set changes and varied from 0.15 – 0.5 seconds depending on the initial sample intensity. During image acquisition, fiber crossings were minimally exposed to excitation light to prevent photobleaching. Intensity data was analyzed using a MATLAB program coupled with the MATLAB Image Analysis Toolpack to calculate a normalized FRET (FRETN) value at each image pixel in the fiber-fiber interface (see Appendix B for program).

Each fiber crossing was analyzed by collecting three fluorescence micrographs using three different custom filter sets manufactured by Chroma Technology Corp. (Brattleboro, VT). Each custom filter set was designed to capture a distinct signal from the fiber crossing: the donor emission (D), the directly excited acceptor emission (A), and the acceptor emission due to FRET (F). A detailed description of the image analysis technique can be found in Section 4.9.

8.3 Results and Discussion

One major consideration for the application of FRET to this system is minimization of dye migration. Covalent hydrazone linkages were selected because the hydrazide derivatives allow for the manipulation of the natural carbonyl groups on the cellulosic fibers. This is one of the least invasive methods to achieve covalent bonding of the dye without detrimental effects on the bulk mechanical or topochemical properties of the fiber (Meunier and Wilkinson 2002).

The main region of interest is the fiber crossing area in which FRET can occur. However, use of the FRETN correction algorithm proposed by Gordon *et al.* (Gordon, Berry, Liang *et al.* 1998) to normalize the FRET signal requires the collection of data from several other regions in the

image as described in Figure 25. Grayscale images using each of the filter sets were acquired and saved for image analysis (see Figure 24).

Slides with fiber crossings of white spruce or viscose were prepared as described for image analysis. The wet pressing pressure was varied for the white spruce and viscose fiber samples. Figure 56 - Figure 60 show representative FRETN surfaces from the fiber-fiber interfaces of viscose and white spruce fibers with various levels of wet pressing. The X and Y axes indicate the pixel location while the magnitude of the FRETN value is specified by the color. Red, orange, and yellow indicate areas with a higher FRETN value and hence a shorter distance between the fiber surfaces.

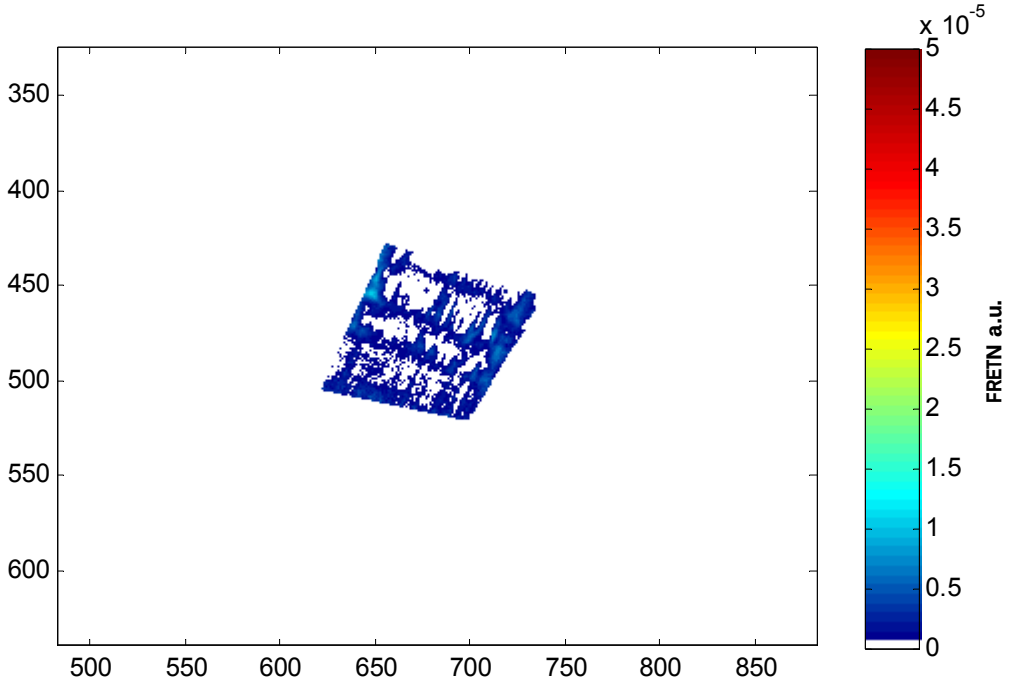

Figure 56 - FRET Surface for Couched Viscose
FRETN surface of a viscose fiber crossing couched onto a glass slide.

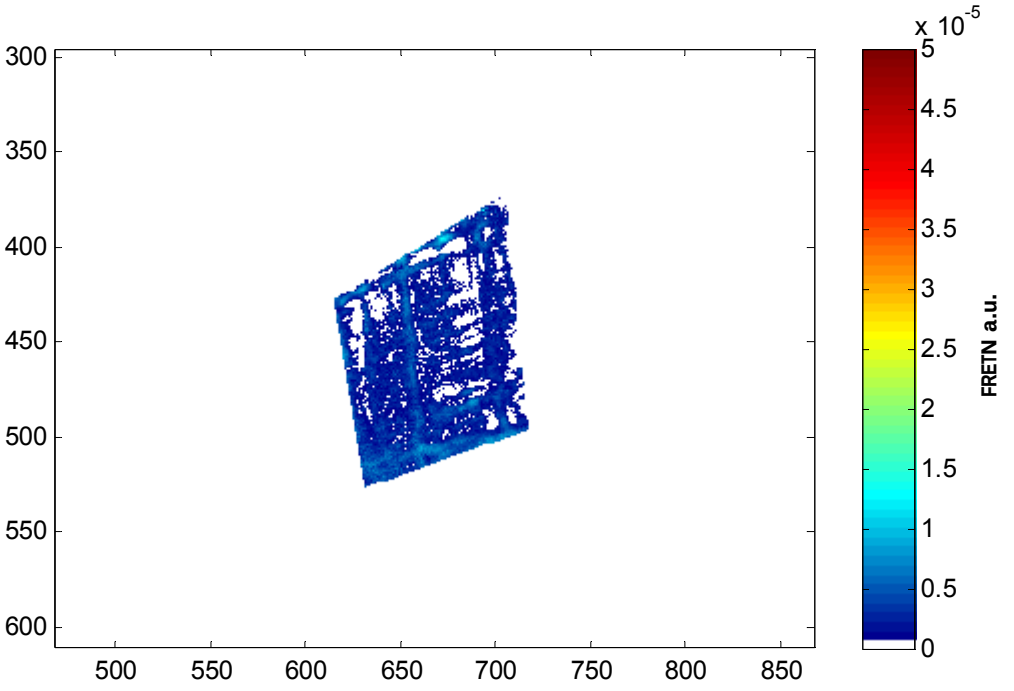

Figure 57 - FRET Surface for Pressed Viscose
FRETN surface of a viscose fiber crossing couched onto a glass slide and then wet pressed at 3.4 MPa for 5 minutes.

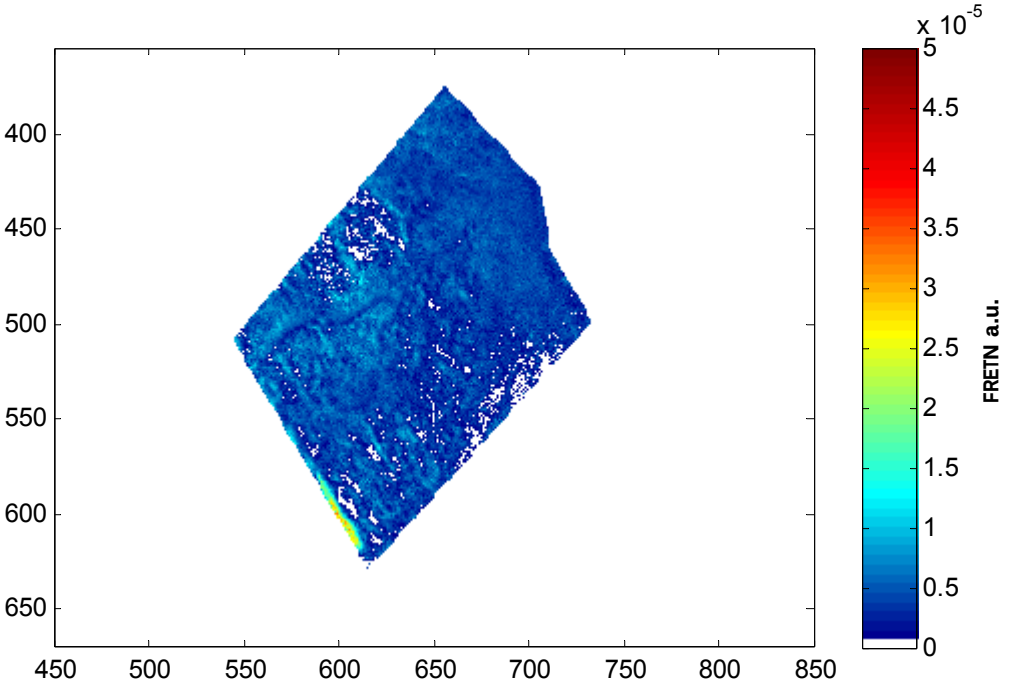

Figure 58 - FRET Surface for Couched White Spruce
FRETN surface of a white spruce fiber crossing couched onto a glass slide.

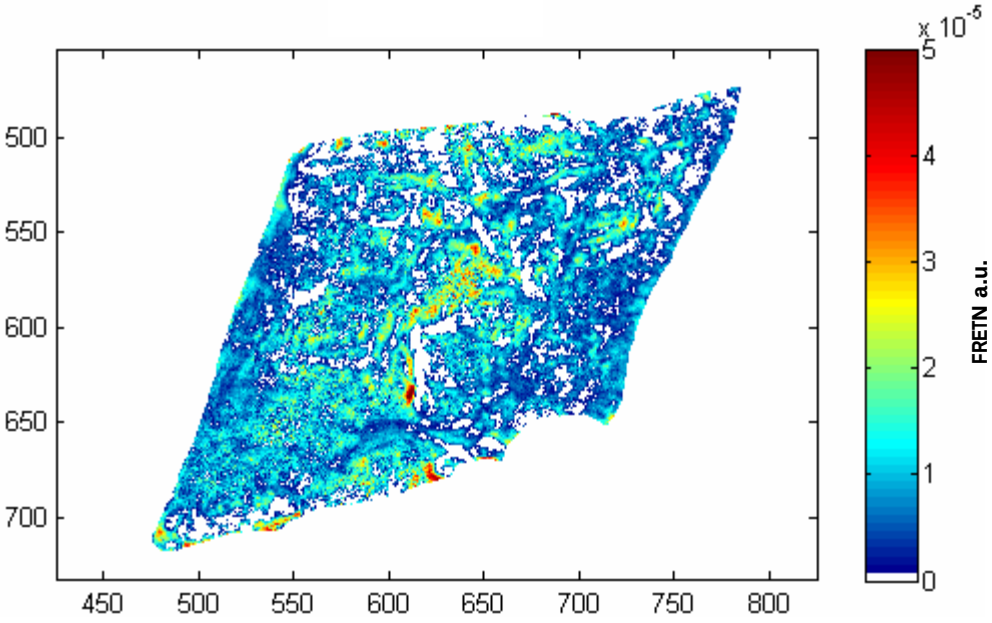

Figure 59 - FRETN Surface for Pressed White Spruce (0.35 MPa)
FRETN surface of a white spruce fiber crossing couched onto a glass slide and then wet pressed at 0.35 MPa for 5 minutes.

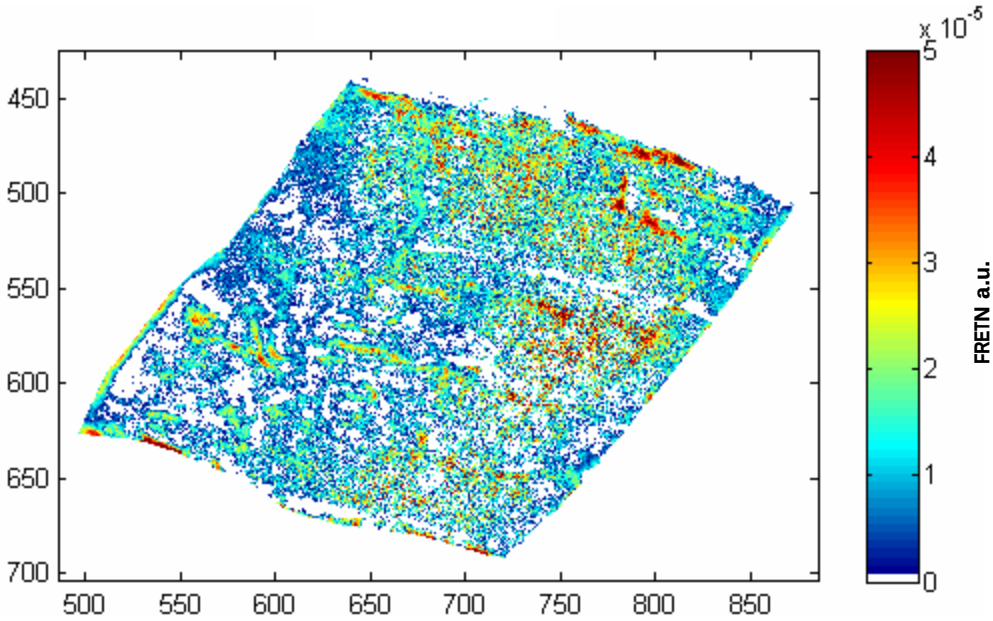

Figure 60 - FRETN Surface for Pressed White Spruce (2.1 MPa)
FRETN surface of a white spruce fiber crossing couched onto a glass slide and then wet pressed at 2.1 MPa for 5 minutes.

With increased pressing, the two fiber sources behave quite differently. There is virtually no change in the viscose fibers as shown in Figure 56 and Figure 57. The waffle like pattern visible in the viscose samples arises from ridges on the fiber surface created by the manufacturing process. Conversely, in Figure 58 - Figure 60, the white spruce fibers exhibit an increased number of pixels with large FRETN values. Higher wet pressing of white spruce fibers results in an increased number of pixels with high FRETN values as well as a decrease in the number of low FRETN pixels.

Morphological and topochemical differences most likely account for the different responses. Even at high wet pressing pressures, the rigid structure of the viscose prevents fiber surfaces from coming into close enough contact to allow molecular interactions. The viscose fibers employed here are rod like and have neither a fibrillar surface nor a collapsible lumen like the white spruce fibers. Also, natural fibers will have some amount of residual lignin and hemicelluloses that can contribute to deformability and bonding while the viscose is almost pure cellulose.

Ultrastructure and topochemical differences are critical to the consideration of fiber-fiber bonds as polyelectrolyte gel layers formed by the diffusion controlled adhesion of polymers (McKenzie 1984; Lindstrom 1992b; Pelton 1993; Pelton, Zhang, Wagberg *et al.* 2000). These theories are partially supported by the observation of compliant fibrillar layers at the surface of fibers by atomic force microscopy (Furuta and Gray 1998; Chhabra, Spelt, Yip *et al.* 2005) and would favour the spruce fiber with respect to forming a bonded region. Furthermore, Voyutskii's diffusion theory of adhesion postulates a direct relationship between pressing pressure and the resultant strength of the bond (McKenzie 1984).

Figure 61 is a representation of what could be occurring in the fiber-fiber bond. As the wet pressing pressure is increased, the two dyed fiber surfaces more interdiffusion occurs such that the average distance between the donor and acceptor dyes is reduced. Although the data presented does not consider the ultimate joint strength of these interfaces, our results are in agreement with increased diffusion of surface polymers in a gel-like surface layer.

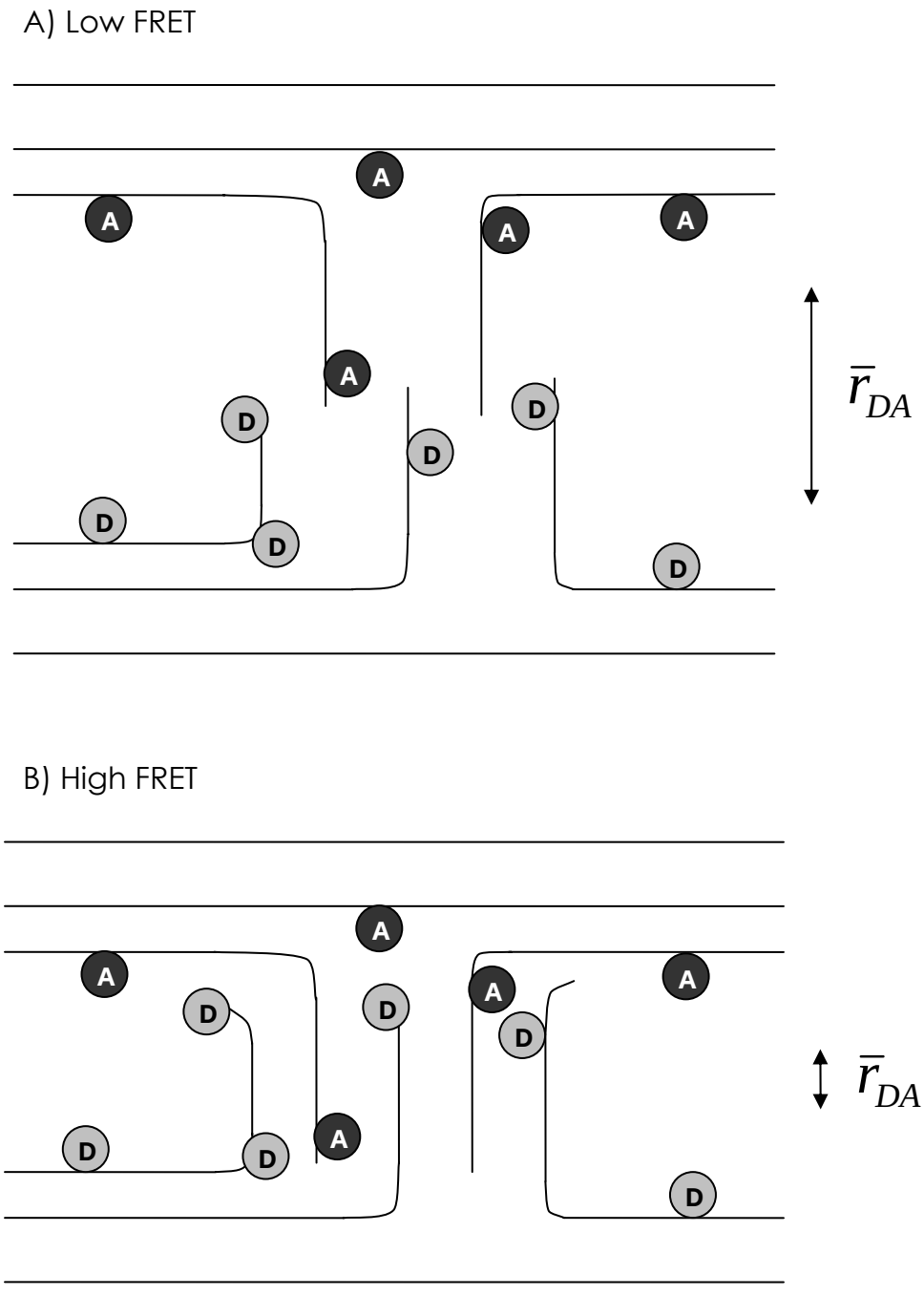

Figure 61 - FRET and Interdiffusion in a Fiber Bond
Interdiffusion between a donor (D) and acceptor (A) dyed fibers is shown. Low FRET corresponds to a large average donor-acceptor distance, r_{DA}, while high FRET has a short average donor-acceptor distance.

While images are useful tools for demonstrating how individual fiber interfaces appear, the variation in natural pulp fibers makes it difficult to get very much quantitative information by comparing single images. A more useful data analysis incorporates the FRETN data from many fiber-fiber crossings into histograms. The FRETN values from every pixel in all fiber crossings for a given condition are divided into bins and then normalized for the crossing area. The crossing area is calculated planimetrically and is necessary in order to help account for the variation of pulp fiber dimensions.

The response to wet pressing is shown as a histogram for the viscose fibers in Figure 62 and for the white spruce fibers in Figure 63. The viscose histogram shows almost no difference between low and high wet pressing values. Increased wet pressing for the white spruce fibers shifts the FRETN pixel distribution towards higher FRETN values suggesting that the fiber surfaces have areas that are in closer proximity.

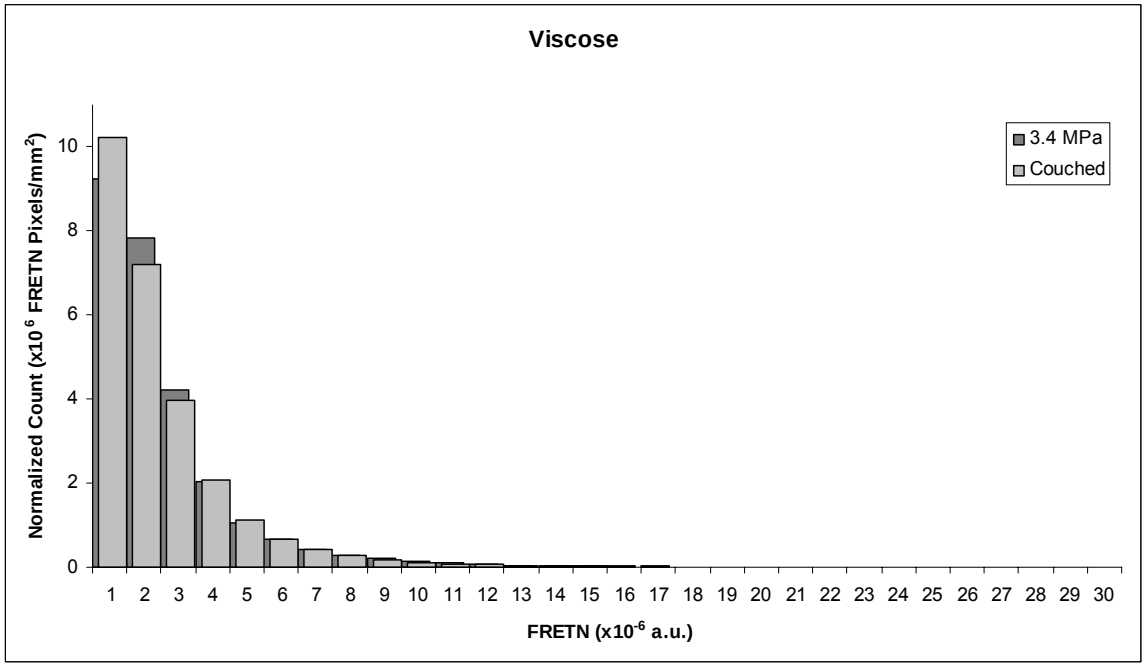

Figure 62 - Viscose Histogram
FRETN Histogram showing the response to wet pressing for viscose fibers.

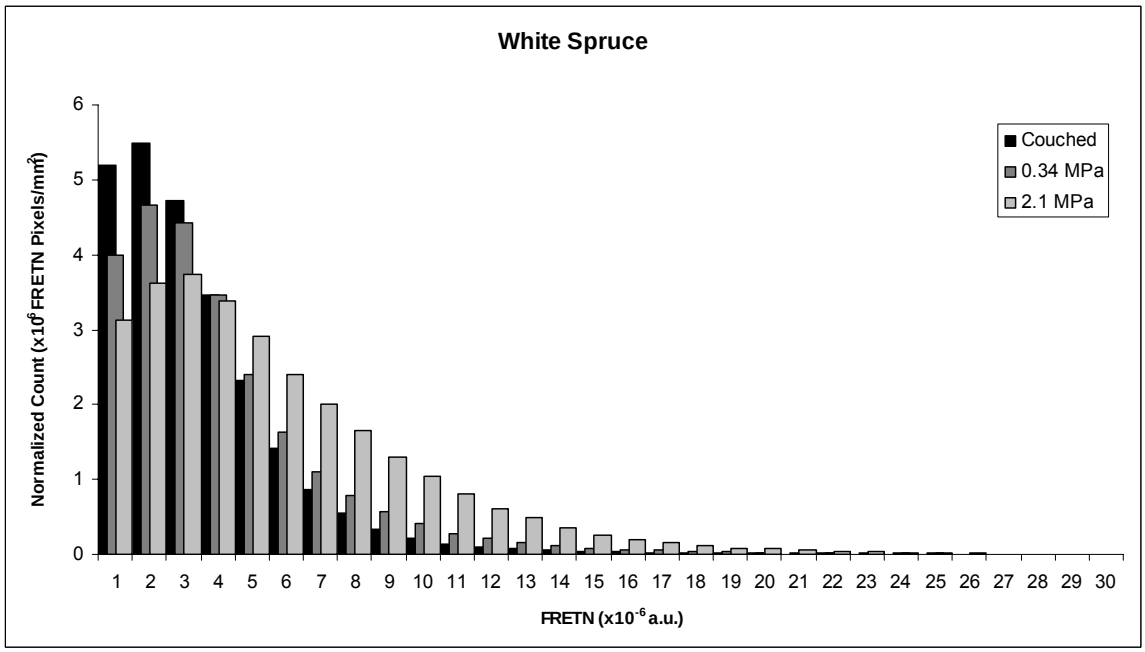

Figure 63 - White Spruce Histogram
FRETN histogram showing the response to wet pressing for white spruce fibers refined 3000 revolutions in a PFI mill.

Viscose images generally had large areas of very low FRETN values even at high pressing levels. However, sheets formed of viscose had almost no structural coherence indicating that low FRETN values are not relevant to inter-fiber bonding. This corroborates with other studies showing little bonding between unmodified regenerated cellulose fibers (Mohlin 1975a; Torgnysdotter and Wagberg 2003). The large FRETN values from those areas of the fiber-fiber interface are most likely within distances where molecular interactions can occur. In this study, all values greater than $1x10^{-5}$ FRETN arbitrary units were considered to be close enough for significant amounts of molecular interaction.

8.4 Conclusions

A new technique utilizing fluorescence microscopy and fluorescence resonance energy transfer to image the areas of a fiber-fiber interface which are within the realm of molecular interaction has been presented. Image analysis of fluorescence micrographs of both natural and regenerated cellulose indicates a FRET signal is being produced at fiber crossings. The distribution of image pixels shifts towards larger FRETN values with increased wet pressing for bleached white spruce fibers which is consistent with interdiffusion occurring in the fiber bond. The pressing response and viscose behavior indicate that low FRETN values may not be relevant to bonding.

CHAPTER 9: OVERALL CONCLUSIONS

This dissertation reviewed many methods that have previously been used to investigate the impact of chemistry, ultrastructure, and industrial processing on the fundamental behavior of fibers. Taking into consideration the current state of the art and recent works in the literature, two new techniques to investigate the deformation behavior and fiber-fiber bond formation of lignocellulosic fibers were developed.

Fiber deformation behavior was studied by draining a dilute suspension of dyed pulp fibers onto a filter paper and then wet pressing them onto glass slides. It was found that refining reduces the stepheight in the fiber crossing for both hardwood and softwood kraft pulps by increasing the tendency of the fibers to collapse, deform, and assume a lens like shape.

The effect of pulp type, bleaching, drying, wet pressing, and fiber charge were also investigated. Graphs of stepheight versus freespan were linear through the origin suggesting that the freespan (flexibility) of the crossing fiber is largely unimportant to the formation of fiber crossings. Quite surprisingly, the ratio of stepheight to freespan remained relatively constant no matter the treatment. Only bleaching and the addition of surface charge via CMC had any independent impact on freespan.

Theoretical attempts at an explanation have been lacking. The data do not fit bending or shear mechanisms that have been developed in the literature suggesting that another mechanism may be responsible for the deformation behavior of single fiber crossings.

Finally, fluorescence microscopy and fluorescence resonance energy transfer were used to image the areas of a fiber-fiber interface while they were bonded. Analysis of the FRET signal from fiber crossings indicate that wet pressing increased the FRET occurring between the two dyed fiber surfaces. The results are consistent with the increased amount of interdiffusion expected with higher levels of wet pressing.

Overall, two novel techniques have been developed to investigate fundamental aspects of fiber deformation behavior and fiber-fiber bond formation. As these methods are further refined and utilized they will provide new avenues for researchers to explore and expand the property space of fibers and paper sheets.

CHAPTER 10: RECOMMENDATIONS FOR FUTURE WORK

The main objective of this thesis was to develop new ways to investigate fundamental properties of cellulose pulp fibers. As with any work where new methods are utilized, there is still a tremendous opportunity to explore fiber and paper properties such as:

- An investigation into the constancy of the stepheight to freespan ratio by imaging the fiber crossing during compression, release and drying.
- The impact of the fiber-glass bond could exert some influence on formation of fiber crossings and should be investigated.
- Further linking changes in stepheight and freespan to changes in the physical and optical properties of a paper sheet.
- Exploring the effect of other dry strength aids on fiber deformation behavior.
- Empirical investigation into the distances between fiber surfaces on the FRET response.
- Dying hemicelluloses or CMC with the donor and acceptor dyes and applying them to the surface of fibers to study the effect of hemicellulose deposition and dry strength agents on specific bond strength.

APPENDIX A: TANGENTIAL RESEARCH

The following manuscript includes work that is tangential to this dissertation but was completed as part of the author's research program. It is published in the Nordic Pulp and Paper Research Journal, Volume 21, Number 3, pages 297-302, 2006 and is reproduced with the kind permission of NPPRJ [iii].

[iii] See Appendix C for copyright permission.

DIRECT OBSERVATIONS OF BONDING INFLUENCE ON THE TENSILE CREEP BEHAVIOR OF PAPER

Andrew DeMaio, Robert Lowe, Timothy Patterson & Art Ragauskas
Institute of Paper Science and Technology
Georgia Institute of Technology, Atlanta, USA

KEYWORDS

Creep, Tension, Bonding, Microscopy, Efficiency

SUMMARY

It has been shown, as sheet loading efficiency is improved through increased bonding (by increasing relative bonded area or specific bond strength), a fully efficient loaded structure can be achieved where further improvements in bonding become redundant and have no effect on creep behavior; deformation is dictated only by the characteristics of the fibers. In this study, fully efficient sheets were made at differing levels of specific bond strength by treating the sheets with a debonder or a bonder. Untreated control sheets were also prepared. Microscopic analysis of the bonded areas before and after creep testing was conducted. It was found that, although creep behavior was the same, the amount of bonded area loss was greater in the debonder treated sheets versus the bonder treated sheets. In addition, bonded area loss for all cases was skewed towards small bonded area losses with few bonds showing significant bonded area loss. Furthermore, observed bonded

area losses were shown to originate from the edges (or perimeters) of the bonds. The overall conclusion from this study, as with previous studies of stress-strain behavior, is bonded area loss is a strain-induced phenomenon caused by deformation and is not connected with or the inherent cause of creep behavior. Although, creep behavior can be shown to be affected by the initial level of bonding in an inefficient loaded structure, previous studies have shown subsequent bonded area loss during straining does not further influence (degrade) behavior.

INTRODUCTION

Creep is a characteristic behavior of a viscoelastic material which is undesirable in most paper applications. When paper is placed under a constant load, it will exhibit a time dependent increasing deformation otherwise known as creep. Fundamental work by Brezinski (1955, 1956), Schulz (1961a, 1961b), Sanborn (1962), Parker (1962) and Hill (1967a, 1967b) laid the groundwork in constant humidity tensile creep behavior. Recent work by DeMaio and Patterson (2004, 2005) studied the influence of bonding on constant humidity tensile creep behavior. Up until that point, there was a limited base of available research regarding bonding and creep behavior in paper (Brezinski, 1955, 1956, Byrd, 1971, Parker, 1962, Sanborn, 1962). DeMaio and Patterson (2004, 2005) showed that either decreasing specific bond strength with a debonder or increasing

specific bond strength with a bonder had no effect on creep behavior. As long as there was an adequate level of bonding to maintain an efficiently loaded structure, load was effectively distributed throughout the sheet. The only difference in the overall behavior was that creep failure times were increased as specific bond strength was improved. DeMaio and Patterson (2005) concluded once paper reaches a fully efficient loaded state, redundancies in bonding exist and no longer influence creep deformation. These findings are in agreement with the conclusions of Coffin (2005) and concur with what was found and concluded by Seth and Page (1981) with short-time deformation behavior (elastic modulus and stress-strain behavior).

With regard to bonded area loss, Sanborn (1962) showed that light scattering increased as the strain during creep increased. As a result, he showed that there is bonded area loss during creep deformation. It does not, however, imply that creep deformation is caused by bonded area loss, only that bonded area loss occurs concurrently. In later work, Byrd (1971) showed that light scatter decreased during creep, implying an increase in bonded area. However, in this case the decrease in light scatter may have occurred because bonded area loss was so small, it could not overcome error in measurement or the effect of fibers being drawn into optical contact from lateral contraction due to longitudinal

straining. This contradictory data was resolved by DeMaio and Patterson (2004, 2005) when they measured the change in light scatter before and after creep deformation. They found, that at a given strain, sheets treated with debonder had a higher change in light scatter versus sheets treated with bonder. Bonded area was not only decreasing with creep, but decreasing at a faster rate when sheets were treated with debonder versus a bonder. While not an extraordinary result by itself, it becomes significant, because creep behavior remained unaffected. The work of Seth and Page (1981) reported the same result with stress-strain curves.

Unfortunately, light scatter data does not definitively indicate how bonded area is changing during creep deformation. In order to determine this, direct observation of bonded area changes must be conducted to validate the findings of light scatter data with optical evidence. This would also offer insight into the bond failure mechanism as it relates to tensile creep behavior. No such study has been conducted prior to this with regard to creep behavior in paper. However, Page et al. (1961a) examined stress-strain behavior and found that a vast majority of the bonds they analyzed showed little or no loss in bonded area and few exhibited full failure. Furthermore, they observed that bonded area loss, when it did occur, propagated from the perimeter (or edge) of the bond. In more recent publications, Page (2002a, 2002b) determined that the

reason this occurred was because bonds are under the highest level of shear stress on their perimeters. He concluded that bonded area loss is a strain-induced phenomenon and there is no connection between bond breakage and stress-strain behavior. Since creep behavior is a highly time-dependant viscoelastic phenomenon, it is uncertain whether the conclusions of Page can be directly applied towards creep behavior. This paper presents a method whereby bonded area behavior as a result of creep can be directly observed. It also presents results obtained using that method.

MATERIALS AND METHODS

Pulp & Preparation

NIST standard reference material 8495 Northern Softwood Bleached Kraft Pulp was used in this study. The pulp arrived in dry lap sheets in a hermitically sealed package and had remained sealed for approximately 15 years. It was refined in a valley beater at a charge of 300 O.D. grams per batch for 30 minutes. The final pulp Canadian Standard Freeness was measured at 407 ml. FQA results from the refined pulp show a length weighted average curl of 0.047 and a coarseness of 0.143 mg/g. The results indicate that the pulp was prepared in such a manner to create straight, conformable fibers that should easily bond.

Chlorazol Black, from Sigma-Aldrich, was added to the pulp slurry at a 0.20% by weight dosage and allowed to soak for 24 hours. Once soaking was complete, the pulp slurry was washed exhaustively with deionized water until wash water was free of color. Prior to making handsheets, the pulp slurry was treated with either a debonder or a bonder or received no treatment. The debonder used was a cationic surfactant (Incrosoft AS-55), from Croda, while the bonder used was locust bean gum, from Sigma-Aldrich. Bonder and debonder were added to the pulp slurry and mixed for 1 minute at dosages of 0.45% and 0.11% by weight respectively.

Handsheets

Handsheets were made using a 210 mm x 210 mm Williams handsheet mold. A 100 mesh screen was used as the forming wire. The handsheets made from the treated pulp slurries were targeted to have an oven dry basis weight of 90 g/m^2. Sheets were wet pressed at 1.03 MPa and dried under full restraint on a drum dryer at 0.14 MPa steam pressure for 5 minutes. Sheets were pressed for five minutes, followed by a blotter change and pressed again at the same level for two minutes. Gloss plates were not used. All sheets were immediately bagged and placed in a 23°C and 50% RH room for conditioning prior to testing.

Physical & Creep Testing

Extensive physical testing was conducted including, handsheet grammage using Tappi Standard T 410 om-02, hard caliper using Tappi Standard T 411 om-05, ultrasonic velocities with reference to Baum et al. (1981), formation, zero-span tensile strength using Tappi Standard T 231 cm-96, z-directional tensile strength using Tappi Standard T 541 om-05 and in-plane tensile strength using Tappi Standard T 494 om-01. In-plane tensile measurements were made using an Instron tester with jaw spacing of 140 mm to be consistent with creep testing spans. The Instron also made stress-strain curves measurements as well as tensile strengths. Although no direct measurement of specific bond strength is made in this study, a difference in z-directional tensile strength indicates a change in specific bond strength when relative bonded area remains constant. Within each set of handsheets, density was held constant and thereby relative bonded area, by careful control of refining, pressing and drying. Creep testing was conducted using the IPST tensile creep tester under a constant 23 °C and 50% RH condition. Samples were cut into 170mm x 25 mm wide strips, mounted and conditioned for 24 hours at 23 °C and 50% RH condition prior to application of load. The effective test length of the samples after mounting was 140 mm. Two different magnitude dead loads (initial applied stress levels) were evaluated. These load levels were 2.50 N/mm and 4.09 N/mm respectively. Displacements and failure times were

recorded using linear variable displacement transducers (LVDT sensors) with the output signals sent to a computer based data acquisition system.

Microscopy

Images of bonded areas were captured using a method similar to one developed by Page et al. (1961b). Prior to creep testing, each strip was examined with a Leica DM-IRM inverted, reflected light microscope equipped with a Hamamatsu ORCA-ER digital camera and a 50 watt metal halide lamp. Pre-creep images were collected by illuminating each strip with polarized monochromatic light (λ=547±10 nm) to increase contrast between dyed and un-dyed fibers. After creep testing, the same techniques were utilized to capture images of the same areas. The orientation of the fibers and the shape of the bonds were used to verify the images were of the same area. *Figure 1* shows a representative image of fiber crossings and bonded areas at 600X magnification.

Changes in fiber orientation and bond area were measured using Simple PCI, an image analysis software package. Orientation was determined by drawing a line down the central axis of each fiber forming the intersection and measuring the angle relative to the direction of the applied stress. Simple PCI can be calibrated to measure image areas. Bond areas were traced on each pre-creep and post-creep image and a percent bond area change was calculated.

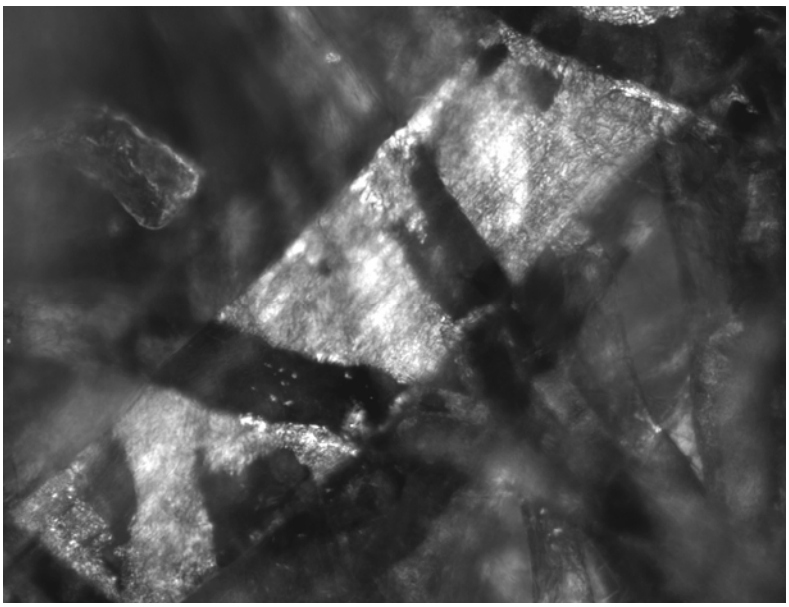

Figure 1 - A representative image of an un-dyed pulp fiber bonded to several Chlorazol black dyed fibers (600X).

RESULTS

Physical & Creep Testing

The results presented are for debonder, control, and bonder sheets that were wet pressed at high load (1.03 MPa) resulting in high density, highly bonded sheets. The intent of the high press load is to make sheets that are fully efficient loaded structures, where the initial level of bonding does not influence deformation behavior and bonded area loss can be isolated for analysis. *Table 1* shows the physical testing results from these sheets.

Table 1 - Physical testing results of debonder, control, and bonder treated sheets.

Sheet Treatment	Grammage (g/m^2)	Hard Caliper (mm)	Density (g/cm^3)	Ultrasonic Modulus (km^2/s^2)
Debonder	97.6	0.144	0.678	10.7
Control	96.6	0.141	0.685	10.9
Bonder	96.5	0.139	0.694	11.0
Variation	1.1%	3.6%	2.4%	2.8%

Sheet Treatment	Z-Tensile (N/mm^2)	Tensile (N/mm)	Failure Strain (%)	Zero-Span (N/mm)
Debonder	0.473	7.97	2.93	16.0
Control	0.584	8.80	3.26	16.3
Bonder	0.852	10.3	4.22	16.7
Variation	80.1%	29.2%	44.0%	4.4%

The data from physical testing presented in *Table 1* shows that sheets treated with debonder and bonder did not show significant differences from the control with regard to grammage, hard caliper, density, formation and zero-span tensile strength. Deformation behavior, as indicated by the ultrasonic elastic modulus data in *Table 1* and stress-strain curves shown in *Figure 2* were similar for all three sets. The differences in the sheets were in z-directional tensile strength, tensile strength and strain to failure, caused predominantly by differences in specific bond strength. *Figure 2* shows that sheets treated with debonder

were the weakest, while the sheets treated with bonder were the strongest.

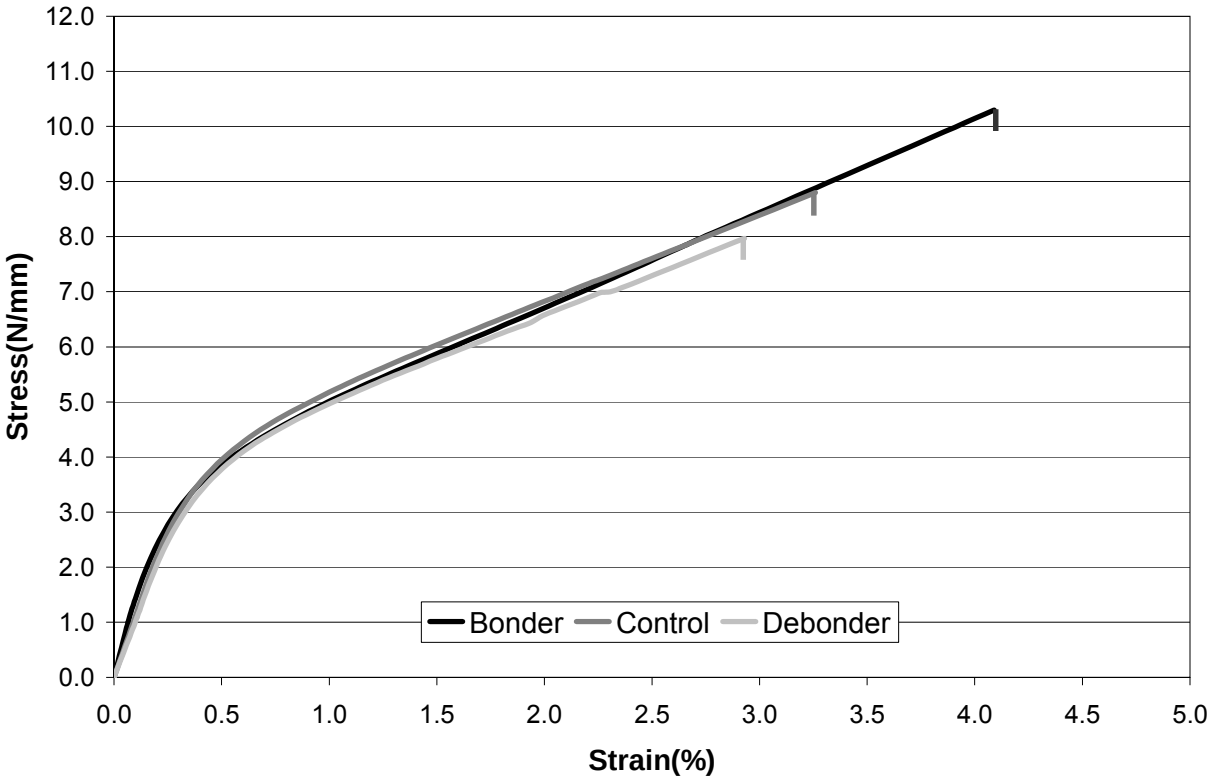

Figure 2 - Stress-strain curves from in-plane Instron tensile testing for debonder, control, and bonder treated sheets.

These results are consistent with the past work of Seth and Page (1981), and DeMaio and Patterson (2004, 2005). The data in *Table 1* and *Figure 2* confirm that high levels of bonding create a fully efficient loaded paper structure where elastic modulus has reached a plateau. Differences in specific bond strength do not affect deformation behavior, but do

influence failure behavior. Overall, the physical testing results confirm that all sheet sets are fully efficient loaded structures.

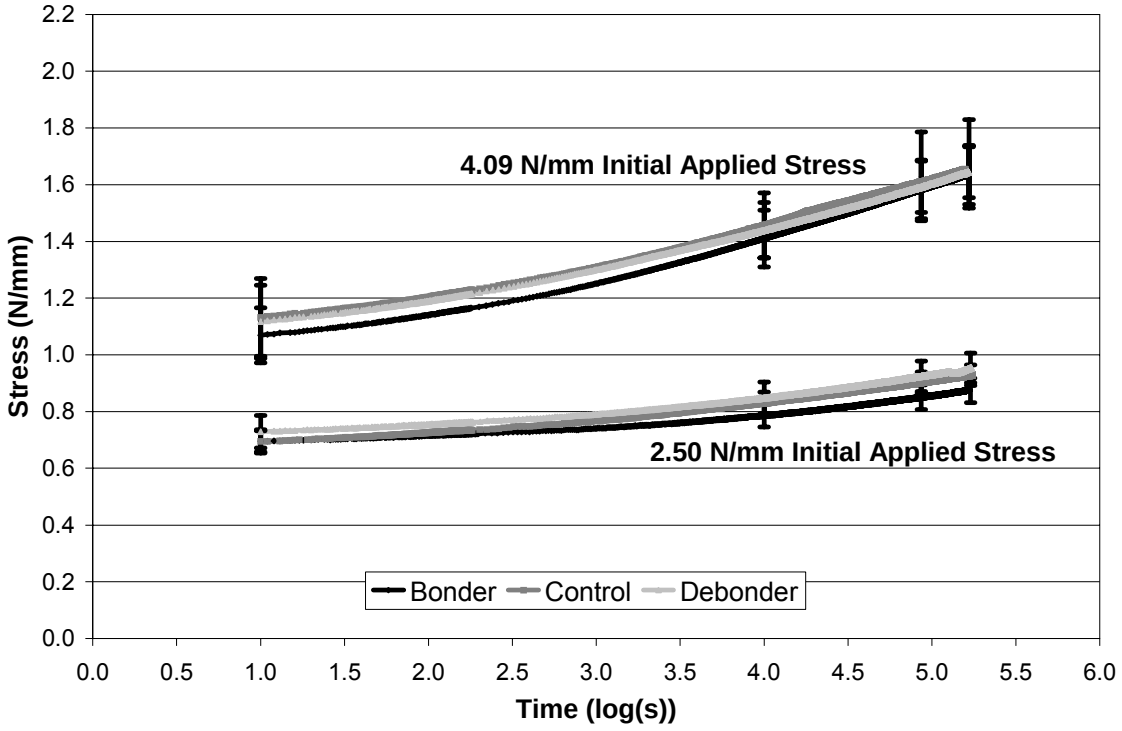

Figure 3 - Creep curves at high and low load initial applied stress levels for debonder, control, and bonder treated sheets.

The creep behavior results shown in *Figure 3*, follow the same trend as the physical testing data in *Table 1* and *Figure 2*. The results show that the creep curves generated at both initial applied stress levels show good overlap and fall within the standard error bars, indicating they have creep behaviors that cannot be differentiated from each other. Again, this was

expected as the results of DeMaio and Patterson (2004, 2005) have shown similar results with fully efficient loaded sheets.

Microscopy Results

Before and after creep testing of the sheets at both initial applied stress levels, images of bonded areas were taken and analyzed for the debonder treated, control and bonder treated sheets. *Table 2* shows the results from the image analysis of the 2.50 N/mm initial applied stress (low creep) and 4.09 N/mm initial applied stress (high creep) testing levels.

Table 2 - Bonded area results from microscopy image analysis for debonder, control, and bonder treated sheets.

Sheet Treatment	Bonds Analyzed	Average Initial Bonded Area (μm^2)	Low Creep Average Bonded Area Decrease	High Creep Average Bonded Area Decrease
Debonder	94	933	8.8 %	14.5 %
Control	62	880	4.5 %	8.7 %
Bonder	89	998	1.5 %	5.1 %
Variation		13.4%	> 100%	>100%

The sheets treated with debonder and bonder did not show significant differences from the control with regard to the average initial bonded areas. Furthermore, these average bonded areas are consistent with the work of Page et al. (1961a) who found an average bonded area of 932 μm^2 for a similar pulp type and refining level. More importantly, the data

shows that at the low and high creep testing levels, the average bonded area decreased by different amounts. The debonder treated sheets had the highest loss in bonded area and the bonder treated sheets had the lowest. The amount of bonded area loss was also relatively small. Even the debonder treated sheets at the high creep testing level showed less than a 15% average bonded area loss.

Based on these results and that the creep behaviors of the debonder, control and bonder treated sheets are all the same, it is apparent that the deformation behavior is not influenced by the rate of bonded area loss. *Figure 4* shows the average bonded area loss versus strain for the debonder, control and bonder treated sheets. The data points do not overlap or fall within standard error bars. Lines were fit through the data points as a means to better illustrate differences in rate of bonded area loss.

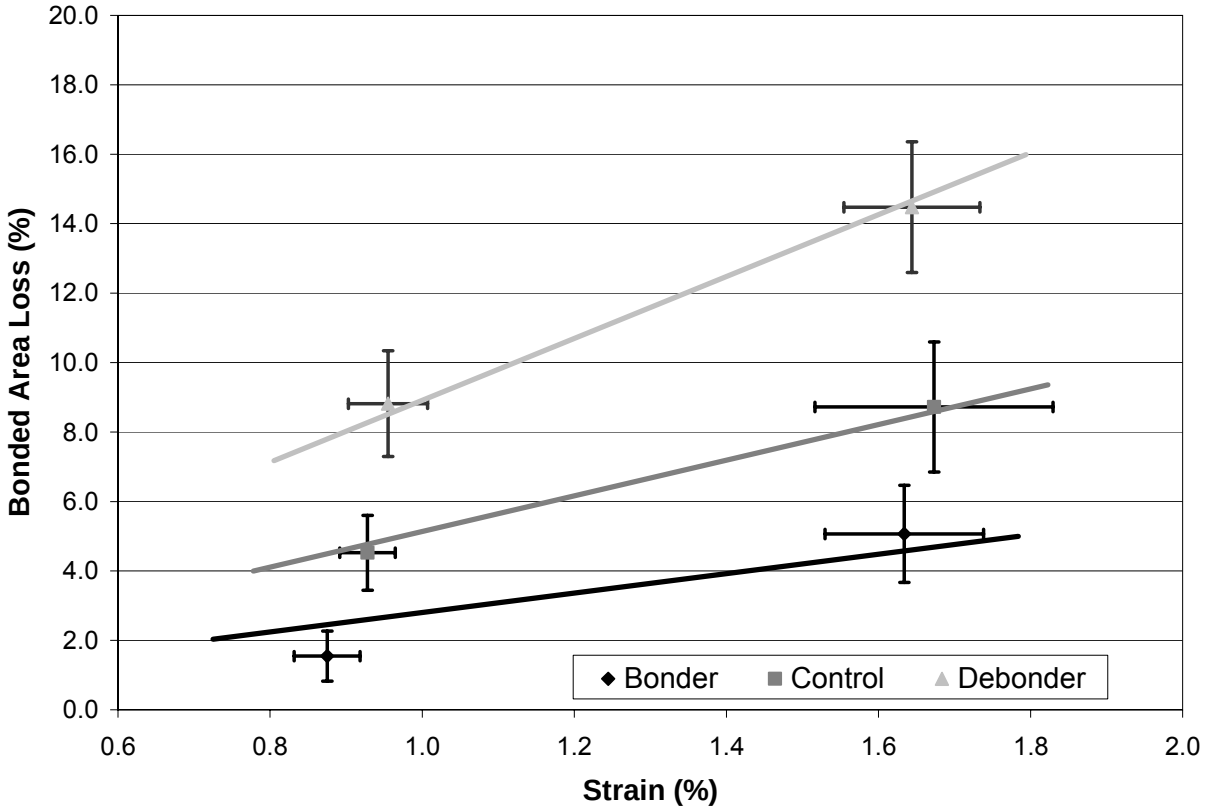

Figure 4 - Average bonded area loss versus strain from creep testing for debonder, control, and bonder treated sheets.

Other than the observation of bonded area loss at different rates, several other observations were made from the microscopy analysis. First, the orientation of the fibers which were bonded did not show a measurable change as a result of creep testing. This indicates that the fibers did not move significantly in the direction of the applied stress. Secondly, the overall level of bonded area loss was small and bond failure originated from the perimeters (or edges) of the bonded area. This is consistent with what Page et al. (1961a) observed. *Figures 5-7* show representative

examples of what was observed at differing levels of bonded area loss. Dashed lines of the before creep bonded areas are superimposed onto the after creep images to better illustrate bonded area loss.

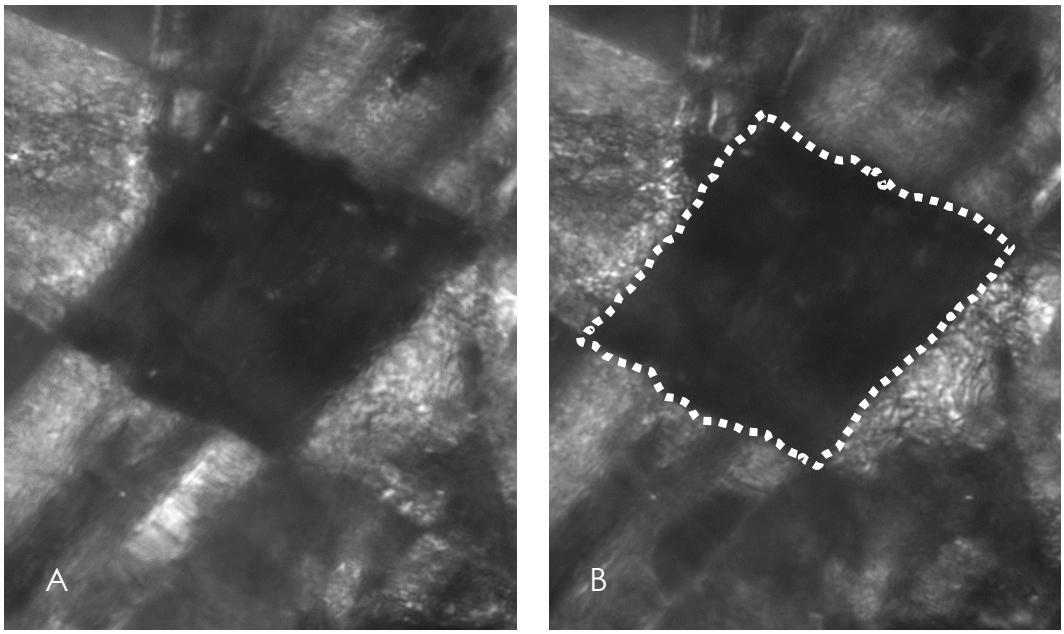

Figure 5 - Before creep (A) and after creep (B) images of a bond showing approximately no loss in bonded area (600X). Dashed lines of the before creep bonded areas are superimposed onto the after creep images to better illustrate bonded area loss.

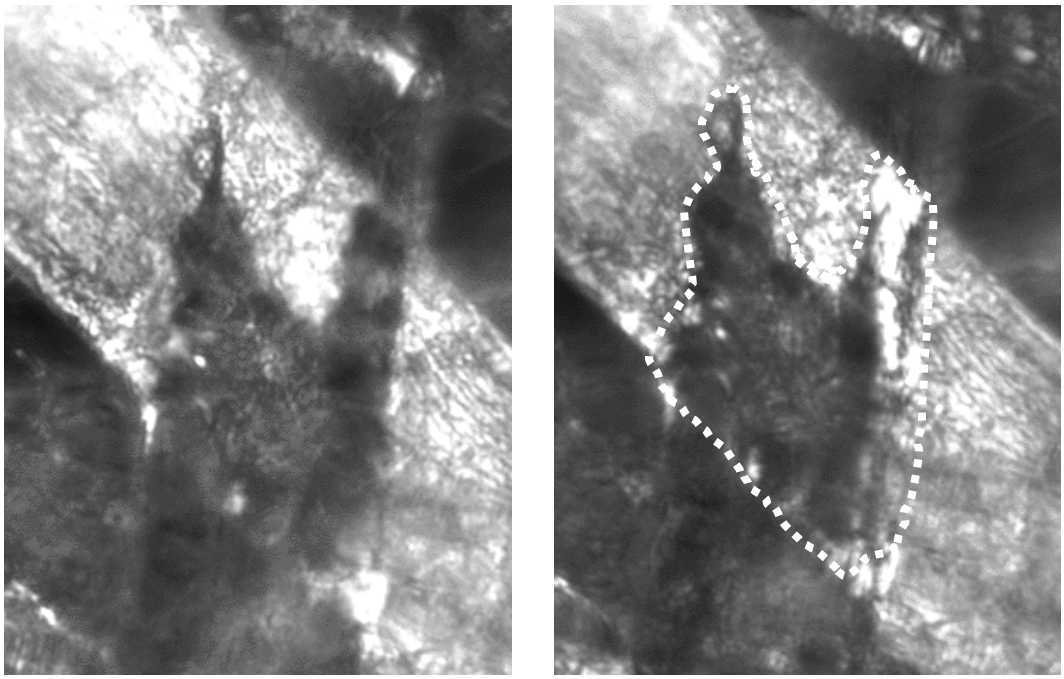

Figure 6 - Before creep (A) and after creep (B) images of a bond showing an approximate 20% loss in bonded area (600X). Dashed lines of the before creep bonded areas are superimposed onto the after creep images to better illustrate bonded area loss.

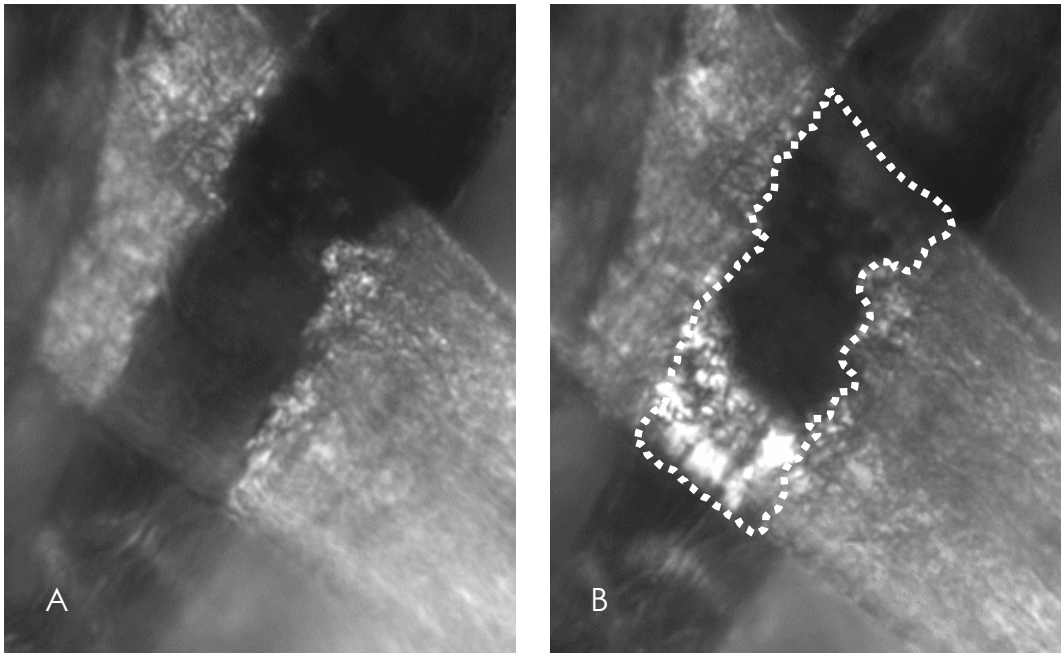

Figure 7 - Before creep (A) and after creep (B) images of a bond showing an approximate 30% loss in bonded area (600X). Dashed lines of the before creep bonded areas are superimposed onto the after creep images to better illustrate bonded area loss.

Figure 5 shows approximately no loss in bonded area during creep. *Figures 6* and *7* show bonded area losses of approximately 20% and 30% respectively. In addition, the bonded area losses are seen from the edges of the bonds. This is typical of what was observed in this study. Overall, the amounts of bonded area losses were predominantly observed between the extremes of *Figure 5* and *Figure 6*. Bonded area losses greater than 20%, as seen with the 30% loss of *Figure 7*, were far less common. *Figure 8* shows a histogram of measured bonded area loss for sheets tested at high creeps loads.

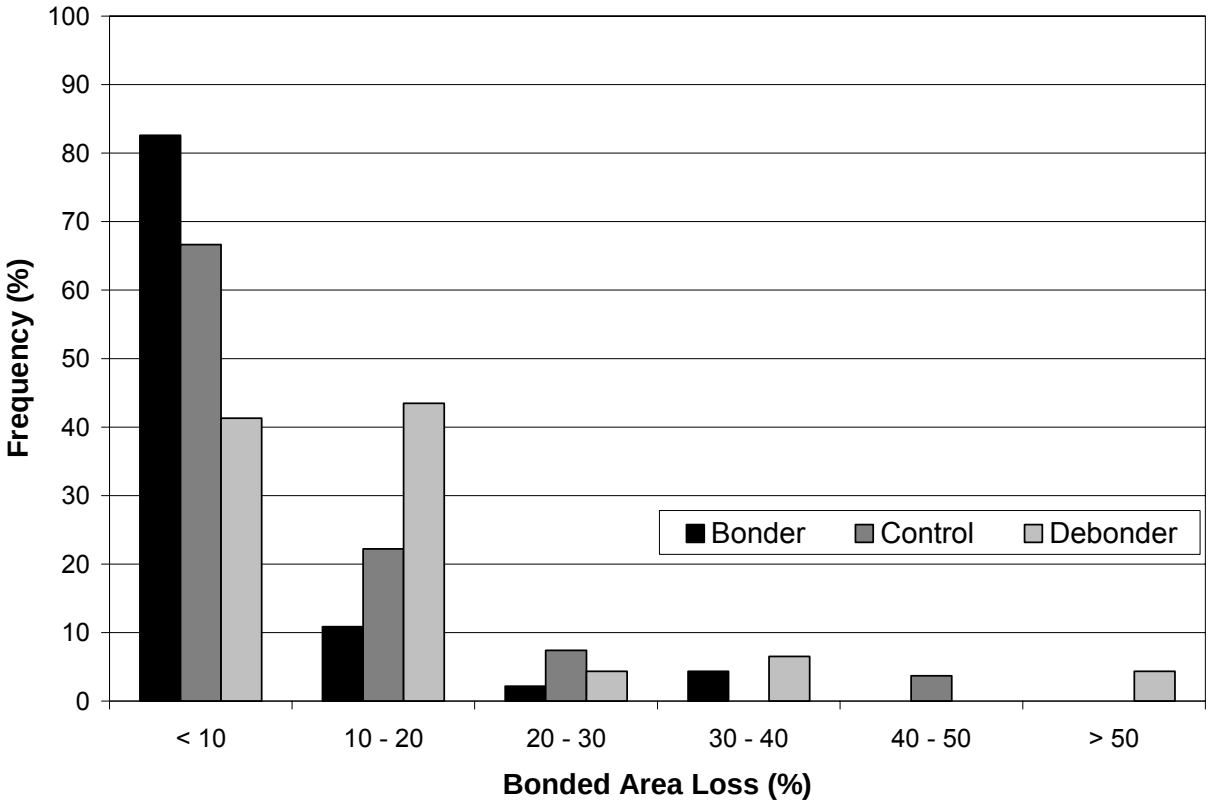

Figure 8 - Histogram of bonded area loss in high creep load testing for debonder, control, and bonder treated sheets.

As *Figure 8* shows, the amount of bonded area loss is not significant, even at the high creep load used in these tests. The data shows a histogram with a skewed distribution towards many small bonded area losses. The skewness increases with specific bond strength; the sheets with bonder had the least amount of large bonded area loss and the debonder sheets had the greatest. Still, even the debonder treated sheets show greater than 80% of measured bonds have less than 20% bonded area loss. The

results for the low creep load testing show an even more skewed distribution towards less bonded area loss. This type of bonded area loss distribution is the same behavior Page et al. (1961a) observed with stress-strain behavior.

DISCUSSION

Based on the results from this study, the data confirms that the initial level of bonding (both in relative bonded area and specific bond strength) and subsequent bonded area loss does not influence the creep behavior of paper when it is a fully efficient loaded structure. Although, the specific bond strength's of the debonder, control and bonder treated sheets are different and the rate at which bonded area loss is occurring is different (based on microscopy), the deformation behavior is not influenced. This confirms what was reported by DeMaio and Patterson (2004, 2005) and correlates with what was seen with light scatter data.

The results strengthen the case that bonding is not the main controlling factor that determines creep behavior in paper. Rather, that distinction belongs to the fibers. In some cases, when paper is less than fully efficient, bonding will influence creep behavior due to lack of an effective stress distribution through the sheet. That said, DeMaio and Patterson (2004, 2005) conducted additional studies on inefficiently loaded sheets and

found that even though the deformation was influenced by the initial level of bonding within the sheet, the subsequent loss in bonded area during creep testing did not further degrade behavior. Seth and Page (1981) found this to be true in stress-strain behavior as well, and found that only when bonding is significantly low will loss in bonded area be significant enough to further influence deformation during straining. This led Page (2002a, 2002b) to the overall conclusion that bonded area loss does not necessarily influence deformation, but rather bonded area loss is a strain-induced phenomenon (i.e., not a cause, but rather an effect of deformation). The results from this study and DeMaio and Patterson (2004, 2005) confirm this result for creep behavior.

The level and type of bonded area loss in the sheets further substantiate this strain-induced conclusion. In this study, the level of bonded area loss was small, even at the highest creep load with the debonder treated sheets. Furthermore, this loss originated from the edges of the bonded areas, where as Page (2002b) points out, the shear stresses are the highest. This is where the bonds would be first affected when fibers are strained. As a result, the level and type of bonded area loss does not lend itself towards a reduction in the overall ability of the bonds being able to distribute load effectively throughout the sheet.

CONCLUSIONS

A novel application of a known method was utilized to directly examine bonded area change as a result of creep. Prior to this study, it was known that creep behavior in a fully efficient loaded structure is not influenced by the initial level of bonding and subsequent loss of bonded area. It is now known why, as the average level of bonded area loss is small and skewed towards many bonds failing partially and very few failing significantly. As a result, the stress distribution in paper during creep should not be significantly disrupted and behavior will remain unaffected. Based on Page (2002a, 2002b), bonded area loss is a strain-induced phenomenon that is a caused by deformation and there is no connection between bonded area loss and stress-strain behavior. In this study, the same conclusion is made with regard to creep behavior. The deformation behavior in paper during creep is dictated solely by the fibers. Although, creep behavior can be shown to be affected by the level of bonding in an inefficient loaded structure, DeMaio and Patterson (2004, 2005) have shown subsequent bonded area loss during straining does not further influence (degrade) behavior. This will hold true until an extreme case is achieved, where the initial level of bonding is so small any loss in bonded area would significantly disrupt the stress distribution within the sheet.

ACKNOWLEDGMENTS

The authors wish to thank the IPST at Georgia Tech Endowment for its gracious support of this research. Portions of the work were used by Mr. Andrew DeMaio and Mr. Robert Lowe as partial fulfillment of the requirements for the PhD program at the Georgia Institute of Technology.

LITERATURE

Baum, G., Brennan, D. and Habeger, C. (1981). Orthotropic Elastic Constants of Paper. Tappi J. 64(8), 97-101.

Brezinski, J. (1955) A Study of the Viscoelasticity of Paper by Means of Tensile Creep Tests. Appleton, Wisconsin, USA, Institute of Paper Chemistry.

Brezinski, J. (1956) The Creep Properties of Paper. Tappi J. 39(2), 116-128.

Byrd, V. (1971) An Investigation of Handsheet Structural and Property Changes During and After Creep Under Constant and Cyclic Relative Humidity Environments. Raleigh, North Carolina, USA, North Carolina State University.

Coffin, D. (2005) The Creep Response of Paper. Advances in Paper Science and Technology, Transactions of the 13th Fundamental Research Symposium. Cambridge, UK, FRC. 651-747.

DeMaio, A. and Patterson, T. (2004) The Role of Fiber-Fiber Bonding on the Tensile Creep Compliance of Paper. The 2004 Progress in Paper Physics Seminar. Trondheim, Norway. 41-42.

DeMaio, A. and Patterson, T. (2005) Influence of Fiber-Fiber Bonding on the Tensile Creep Compliance of Paper. Advances in Paper Science and Technology, Transactions of the 13th Fundamental Research Symposium. Cambridge, UK, FRC. 749-775.

Hill, R. (1967a) The Creep Behavior of Individual Pulp Fibers Under Tensile Stress. Appleton, Wisconsin, USA, Institute of Paper Chemistry.

Hill, R. (1967b) The Creep Behavior of Individual Pulp Fibers Under Tensile Stress. Tappi J. 50(8), 432-440.

Page, D. (2002a) The Meaning of Nordman Bond Strength. The 2002 Progess in Paper Physics Seminar. Finger Lakes/ Syracuse, New York, USA. 2.

Page, D. (2002b) The Meaning of Nordman Bond Strength. Nord. Pulp Pap. Res. J. 17(1), 39-44.

Page, D., Tydeman, P. and Hunt, M. (1961a) The Behavior of Fiber-to-Fiber Bonds In Sheets Under Dynamic Conditions. The Formation and Structure of Paper, Transactions of the 2nd Fundamental Research Symposium. Oxford, UK, FRC. 249-276.

Page, D., Tydeman, P. and Hunt, M. (1961b) A Study of Fiber-Fiber Bonding by Direct Observation. The Formation and Structure of Paper, Transactions of the 2nd Fundamental Research Symposium. Oxford, UK, FRC. 171-203.

Parker, J. (1962) The Effects of Ethylamine Decrystallization of Cellulose Fibers on the Viscoelastic Properties of Paper. Tappi J. 45(12), 936-943.

Sanborn, I. (1962) A Study of Irreversible, Stress-Induced Changes in the Macrostructure of Paper. 45(6), 465-474.

Schulz, J. (1961a) The Effect of Strain Applied During Drying on the Mechanical Behavior of Paper. Appleton, Wisconsin, USA, Institute of Paper Chemistry.

Schulz, J. (1961b) Effect of Straining During Drying on the Mechanical and Viscoelastic Behavior of Paper. Tappi J. 44(10), 736-744.

Seth, R. and Page, D. (1981) The Stress Strain Curve of Paper. The Role of Fundamental Research in Papermaking, Transactions of the 7th Fundamental Research Symposium. Cambridge, UK, FRC. 421-452.

APPENDIX B: MATLAB PROGRAM FOR FRET ANALYSIS

The following code was used with MATLAB 7.1 along with the MATLAB Image Processing Toolbox to analyze the fluorescence images captured for the FRET portion of this work. The basic program was prepared by Ms. Delphine Nain and modified for use in this research by the author.

The script tells the program where to find the files:

```
%%%%%%%%%%%%%%%%%%%%%%%%%%%%%%%%%%%%%%%%%%%%%%%%%%%%%%%%%%%%
path='C:\Documents and Settings\rlowe\Desktop\Images\';

Afile = [path '2006-08-01_CF1_A-1.tif'];
Dfile = [path '2006-08-01_CF1_D-1.tif'];
Ffile = [path '2006-08-01_CF1_F-1.tif'];

fiberCrossing_rob_background_subtracted_images(Afile,
Dfile, Ffile);
%%%%%%%%%%%%%%%%%%%%%%%%%%%%%%%%%%%%%%%%%%%%%%%%%%%%%%%%%%%%
```

The program determines the FRETN value at each pixel in the fiber crossing:

```
%%%%%%%%%%%%%%%%%%%%%%%%%%%%%%%%%%%%%%%%%%%%%%%%%%%%%%%%%%%%%%%%%%%%%%
function fiberCrossing(Afile, Dfile, Ffile) % author
Delphine Nain, copyright 2006, delfin@alum.mit.edu
%
%

Aimg = imread(Afile); %read the Afile
A_img = double(Aimg(:,:,1));
Dimg = imread(Dfile);
```

```
D_img = double(Dimg(:,:,1));
Fimg_orig = imread(Ffile);
F_img = double(Fimg_orig(:,:,1));

% show the F image, prompt for the rectangle
% defined by str returns a mask

%%%%%%%%%%%%% MASK 1 %%%%%%%%%%%%%%%%%%%%%%%%%%%%%
str = sprintf('rectangle of fibers crossing');
figure(1);imagesc(Fimg_orig);
axis equal;
%tell the user what to do in title
title_str = sprintf('Draw polygon to delineate  %s by
clicking with the mouse. Double click to end.',str);
title(title_str,'FontSize',11,'Color','b');
[mask_cross_F,xcoords,ycoords] = roipoly;
line(xcoords,ycoords);
xcoords_cross_F(1) = (min(xcoords));
xcoords_cross_F(2) = (max(xcoords));
ycoords_cross_F(1) = (min(ycoords));
ycoords_cross_F(2) = (max(ycoords));

%%%%%%%%%%%%% MASK 2 %%%%%%%%%%%%%%%%%%%%%%%%%%%%%

str = sprintf('bottom rectangle of A fiber');
figure(1);imagesc(Fimg_orig);
axis equal;
%tell the user what to do in title
title_str = sprintf('Draw polygon to delineate  %s by
clicking with the mouse. Double click to end.',str);
title(title_str,'FontSize',11,'Color','b');
[mask_bottom_A,xcoords,ycoords] = roipoly;
xcoords_bottom_A(1) = floor(min(xcoords));
xcoords_bottom_A(2) = ceil(max(xcoords));
ycoords_bottom_A(1) = floor(min(ycoords));
ycoords_bottom_A(2) = ceil(max(ycoords));

%%%%%%%%%%%%% MASK 3 %%%%%%%%%%%%%%%%%%%%%%%%%%%%%

str = sprintf('top rectangle of A fiber');
figure(1);imagesc(Fimg_orig);
axis equal;
%tell the user what to do in title
title_str = sprintf('Draw polygon to delineate  %s by
clicking with the mouse. Double click to end.',str);
title(title_str,'FontSize',11,'Color','b');
[mask_top_A,xcoords,ycoords] = roipoly;
```

```
xcoords_top_A(1) = floor(min(xcoords));
xcoords_top_A(2) = ceil(max(xcoords));
ycoords_top_A(1) = floor(min(ycoords));
ycoords_top_A(2) = ceil(max(ycoords));

%%%%%%%%%%%%% MASK 4 %%%%%%%%%%%%%%%%%%%%%%%%%%%%%%

str = sprintf('bottom rectangle of D fiber');
figure(1);imagesc(Fimg_orig);
axis equal;
%tell the user what to do in title
title_str = sprintf('Draw polygon to delineate  %s by
clicking with the mouse. Double click to end.',str);
title(title_str,'FontSize',11,'Color','b');
[mask_bottom_D,xcoords,ycoords] = roipoly;
xcoords_bottom_D(1) = floor(min(xcoords));
xcoords_bottom_D(2) = ceil(max(xcoords));
ycoords_bottom_D(1) = floor(min(ycoords));
ycoords_bottom_D(2) = ceil(max(ycoords));


%%%%%%%%%%%%% MASK 5 %%%%%%%%%%%%%%%%%%%%%%%%%%%%%%

str = sprintf('top rectangle of D fiber');
figure(1);imagesc(Fimg_orig);
axis equal;
%tell the user what to do in title
title_str = sprintf('Draw polygon to delineate  %s by
clicking with the mouse. Double click to end.',str);
title(title_str,'FontSize',11,'Color','b');
[mask_top_D,xcoords,ycoords] = roipoly;
xcoords_top_D(1) = floor(min(xcoords));
xcoords_top_D(2) = ceil(max(xcoords));
ycoords_top_D(1) = floor(min(ycoords));
ycoords_top_D(2) = ceil(max(ycoords));


%%%%%%%%%%%%% MASK 6 %%%%%%%%%%%%%%%%%%%%%%%%%%%%%%

str = sprintf('Background');
figure(1);imagesc(Fimg_orig);
axis equal;
%tell the user what to do in title
title_str = sprintf('Draw polygon to delineate  %s by
clicking with the mouse. Double click to end.',str);
title(title_str,'FontSize',11,'Color','b');
[mask_top_B,xcoords,ycoords] = roipoly;
```

```
xcoords_top_B(1) = floor(min(xcoords));
xcoords_top_B(2) = ceil(max(xcoords));
ycoords_top_B(1) = floor(min(ycoords));
ycoords_top_B(2) = ceil(max(ycoords));

%%%%%%%%%%%%%%%%%%%%%%%%% COMPUTATIONS
%%%%%%%%%%%%%%%%%%%%%%%%%%%%%%%%%%%%



Z=ones(size(mask_cross_F,1),size(mask_cross_F,2)); %Z is
size of bounding box of crossing

%fret image, D fiber, average int for both rectangles
[Fd_top_value] =
findAverage(F_img,mask_top_D,xcoords_top_D,ycoords_top_D);
[Fd_bottom_value] =
findAverage(F_img,mask_bottom_D,xcoords_bottom_D,ycoords_bo
ttom_D);
Fd_value = (Fd_top_value + Fd_bottom_value) / 2.0;
Fd=Fd_value*Z; %fret image, D fiber, average int for both
rectangles

% fret image, A fiber, average int for both rectangles
[Fa_top_value] =
findAverage(F_img,mask_top_A,xcoords_top_A,ycoords_top_A);
[Fa_bottom_value] =
findAverage(F_img,mask_bottom_A,xcoords_bottom_A,ycoords_bo
ttom_A);
Fa_value = (Fa_top_value + Fa_bottom_value) / 2.0;
Fa=Fa_value*Z; % fret image, A fiber, average int for both
rectangles

% fret image, crossing average
[F_cross_average] =
findAverage(F_img,mask_cross_F,xcoords_cross_F,ycoords_cros
s_F);
F_cross_average_value = F_cross_average;

% fret image, background
[F_background] =
findAverage(F_img,mask_top_B,xcoords_top_B,ycoords_top_B);

Fb = 1.0*F_background*Z; % fret image, background

%D image, D fiber, average int for both rectangles
```

```
[Dd_top_value] =
findAverage(D_img,mask_top_D,xcoords_top_D,ycoords_top_D);
[Dd_bottom_value] =
findAverage(D_img,mask_bottom_D,xcoords_bottom_D,ycoords_bo
ttom_D);
Dd_value = (Dd_top_value + Dd_bottom_value) / 2.0;
Dd=Dd_value*Z; %D image, D fiber, average int for both
rectangles

%D image, A fiber, average int for both rectangles
[Da_top_value] =
findAverage(D_img,mask_top_A,xcoords_top_A,ycoords_top_A);
[Da_bottom_value] =
findAverage(D_img,mask_bottom_A,xcoords_bottom_A,ycoords_bo
ttom_A);
Da_value = (Da_top_value + Da_bottom_value) / 2.0;
Da=Da_value*Z;  %D image, A fiber, average int for both
rectangles

% D image, crossing average
[D_cross_average] =
findAverage(D_img,mask_cross_F,xcoords_cross_F,ycoords_cros
s_F);
D_cross_average_value = D_cross_average;

% D image, background
[D_background] =
findAverage(D_img,mask_top_B,xcoords_top_B,ycoords_top_B);
D_background_value = D_background;
Db=D_background_value*Z; % D image, background

%A image, D fiber, average int for both rectangles
[Ad_top_value] =
findAverage(A_img,mask_top_D,xcoords_top_D,ycoords_top_D);
[Ad_bottom_value] =
findAverage(A_img,mask_bottom_D,xcoords_bottom_D,ycoords_bo
ttom_D);
Ad_value = (Ad_top_value + Ad_bottom_value) / 2.0;
Ad=Ad_value*Z; %A image, D fiber, average int for both
rectangles

%A image, A fiber, average int for both rectangles
[Aa_top_value] =
findAverage(A_img,mask_top_A,xcoords_top_A,ycoords_top_A);
[Aa_bottom_value] =
findAverage(A_img,mask_bottom_A,xcoords_bottom_A,ycoords_bo
ttom_A);
```

```
Aa_value = (Aa_top_value + Aa_bottom_value) / 2.0;
Aa=Aa_value*Z; %A image, A fiber, average int for both
rectangles

% A image, crossing average
[A_cross_average] =
findAverage(A_img,mask_cross_F,xcoords_cross_F,ycoords_cros
s_F);
A_cross_average_value = A_cross_average;

% A image, background
[A_background] =
findAverage(A_img,mask_top_B,xcoords_top_B,ycoords_top_B);
A_background_value = A_background;
Ab=A_background_value*Z; % fret image, background

G=1.519*Z;  %correction

Ax = mask_cross_F .* A_img;
Dx = mask_cross_F .* D_img;
Fx = mask_cross_F .* F_img;


%%%%%%%%%%%%%%%%% background corrected
values%%%%%%%%%%%%%%%%%%%%%%
Ax_c = Ax-(Ab.*mask_cross_F);
Dx_c = Dx-(Db.*mask_cross_F);
Fx_c = Fx-(Fb.*mask_cross_F);

Aa_c = Aa-(Ab.*mask_cross_F);
Da_c = Da-(Db.*mask_cross_F);
Fa_c = Fa-(Fb.*mask_cross_F);

Ad_c = Ad-(Ab.*mask_cross_F);
Dd_c = Dd-(Db.*mask_cross_F);
Fd_c = Fd-(Fb.*mask_cross_F);

Afa=(Ax_c-(Fx_c.*Ad_c./Fd_c))./(Z-
(Fa_c./Aa_c).*(Ad_c./Fd_c));
FRET1=(Fx_c-Dx_c.*Fd_c./Dd_c-Afa.*((Fa_c./Aa_c)-
(Fd_c.*Da_c./Dd_c./Aa_c))./(G.*(Z-
Da_c.*Fd_c./Fa_c./Dd_c));
Dfd=Dx_c+FRET1.*(Z-G.*Da_c./Aa_c)-Afa.*Da_c./Aa_c;
FRETN=FRET1./(Dfd.*Afa);

load('MyColormaps_warm','mycmap_warm')
```

```
FRETN_graph=FRETN.*mask_cross_F;
FRETN_graph(find(FRETN_graph<0)) = 0;
FRETN_image = imagesc(FRETN_graph);
set(gcf,'Colormap',mycmap_warm);
%axis ([xcoords_cross_F(1) xcoords_cross_F(2)
ycoords_cross_F(1) ycoords_cross_F(2)]);
axis ([450 850 450 700]);
axis equal;
caxis ([0 5e-5]); colorbar




%i=find(FRETN>0.0);A=FRETN(i);
%count = numel(A)
%crossing_average = sum(A)/numel(A)
%A_log10_corrected=-1.0./log10(A);

%B =
[F_cross_average_value;D_cross_average_value;A_cross_averag
e_value;Fd_value;Dd_value;Ad_value;Fa_value;Da_value;Aa_val
ue;F_background;D_background_value;A_background_value];
Background_corrected = [F_cross_average_value-F_background
D_cross_average_value-D_background A_cross_average_value-
A_background Fd_value-F_background Dd_value-D_background
Ad_value-A_background Fa_value-F_background Da_value-
D_background Aa_value-A_background F_background
D_background_value A_background_value]
%dlmwrite('hist.txt', A, ' ' )
dlmwrite('averages.txt', Background_corrected, ';' )
%%%%%%%%%%%%%%%%%%%%%%%%%%%%%%%%%%%%%%%%%%%%%%%%%%%%%%%%%%%%%%%%%%%%%%%
```

APPENDIX C: COPYRIGHT PERMISSIONS

Permission from the Fundamental Research Committee:

Dear Rob
We seem to have fallen foul of the vagaries of the electronic world with your recent copyright request. I did in fact reply to your original request but on checking back it seems that our server rejected the frc sending address, hence I am now sending this reply from one of the PITA addresses.

The original reply used the following words in response to your request which I have pasted in as well.: -

Rob
I have no problem with this request. Same conditions apply regarding due credit etc.
John

----- Original Message -----
From: Rob Lowe
To: FRC@PITA
Sent: Tuesday, November 28, 2006 4:32 PM
Subject: RE: Copyright Permission

John, I have one more request for copyright permission. I would like to reproduce a portion of Figure 14 from "Structure of Paper in Cross-Section" by Page, Sargent, and Nelson. It was published in the Transactions of the Third Fundamental Research Symposium, p. 329, 1965.

I would like to reproduce this in my dissertation and in a journal manuscript that I am preparing. Please let me know if there are any issues with this request.

Many thanks,

Rob Lowe

Hope this enables you to proceed. Apologies for not having picked this problem up sooner.

Best Regards
John Clewley
Chief Executive

Paper Industry Technical Association
5 Frecheville Court
Bury, Lancs
BL9 0UF

Tel: 0161 764 5858
Fax: 0161 764 5353
Email: info@pita.co.uk

From: FRC@PITA [frc@pita.co.uk]
Sent: Friday, August 04, 2006 12:34 PM
To: Rob Lowe
Cc: Steve I'Anson
Subject: Re: Copyright Permission
Dear Rob
Further to your request below we are happy to grant you permission to reproduce the text, tables and figures from the manuscript described in your Ph D dissertation as long as credit is quite clearly given to the event at which the presentation was made and the publication in which the manuscript was first published.

Best of luck with the Ph D dissertation.

Best regards

John Clewley
Administrator to the FRC.

----- Original Message -----
From: Rob Lowe
To: frc@pita.co.uk
Sent: Thursday, August 03, 2006 7:32 PM
Subject: Copyright Permission

Sir/Madame, I would like to request permission to reproduce the text, tables and figures from the manuscript entitled "Imaging Fiber Deformations" by Rob Lowe, Art Ragauskas, and Derek Page. It was published in the Transactions of the 13th Fundamental Research Symposium, Vol 2, p. 921-941.

As first author, I would like to include this paper as part of my PhD dissertation which will be published by the Georgia Institute of Technology in Atlanta, Georgia, USA. If you are not the copyright holder or do not have authority to grant this request, I would appreciate any information you can provide concerning the current copyright holder. Also, please specify any additional source from whom permission must be obtained. Thank you for your prompt consideration of this request.

Sincerely,

Rob Lowe

****
Rob Lowe
rob.lowe@ipst.gatech.edu

Institute of Paper Science and Technology
500 10th Street NW
Atlanta, GA 30332-0620

Office: +1.404.894.9713
Fax: +1.404.894.4778
****

Permission from Nordic Pulp and Paper Research Journal.

From: Diana Aminoff [diana.aminoff@spci.se]
Sent: Tuesday, August 08, 2006 3:40 AM
To: Rob Lowe

Subject: Re: Copyright Permission
Dear Rob Lowe,
You are free to include the paper in your dissertation, referring to that it was first published in NPPRJ. NPPRJ will be published in the end of September. I will send you a final proof soon and if everything is alright you can use the PDF in your dissertation.
With best regards
Diana Aminoff Sandström

Diana Aminoff Sandström
Editor-in-Chief/Chefredaktör
Nordic Pulp and Paper Research Journal
Box 5515, S-114 85 Stockholm, Sweden
Tel/Phone +46 8 783 84 81
E-mail: diana.aminoff@spci.se
www.npprj.se
---

3 aug 2006 kl. 20.24 skrev Rob Lowe:

Ms. Aminoff, I would like to request permission to reproduce the text, tables and figures from the manuscript entitled "Direct observations of bonding influence on the tensile creep behavior of paper" by Andrew DeMaio, Robert Lowe, et al. It will be appearing in Vol 21, No. 3, p. 297-302.

As a co-author, I would like to include this paper as part of my PhD dissertation which will be published by the Georgia Institute of Technology in Atlanta, Georgia, USA. If you are not the copyright holder or do not have authority to grant this request, I would appreciate any information you can provide concerning the current copyright holder. Also, please specify any additional source from whom permission must be obtained. Thank you for your prompt consideration of this request.

Sincerely,

Rob Lowe

****

Rob Lowe
rob.lowe@ipst.gatech.edu

Institute of Paper Science and Technology
500 10th Street NW
Atlanta, GA 30332-0620

Office: +1.404.894.9713
Fax: +1.404.894.4778

APPENDIX D: DATA

Unbleached Hardwood, Never Dried 300 Revs, 50 psi

Stepheight	Freespan	(microns)	Stepheight	Freespan
6.2905	37.91		4.6495	56.84
5.1965	42.82		2.4615	20.29
2.735	33.16		3.5555	29.47
4.1025	30.9		4.1025	48.94
4.376	49.45		2.735	17.05
4.923	53.96		5.7435	38.64
4.923	53.65		2.4615	25.25
1.641	17.08		3.5555	44.35
4.376	21.17		2.188	21.68
3.282	45.64		1.3675	16.43
3.0085	27.24		2.188	20.36
5.7435	51.11		2.4615	27.13
3.0085	23.85		2.188	24.6
5.7435	39.26		3.282	41.4
4.376	48.31		2.735	32.36
4.1025	25.54		2.188	26.22
1.9145	18.8		3.829	19.81
2.735	28.96		3.5555	39.82
2.188	30.44		1.641	12.95
5.7435	46.4		2.4615	33.4
4.923	36.75		3.5555	40.18
3.829	47.9		2.188	22.98
4.6495	45.7		2.735	27.27
1.094	16.91		1.641	27.41
4.376	37.43		3.829	33.67
2.188	25.91		1.3675	18.97
4.6495	42.65		1.3675	16.6
3.282	34.21		1.9145	23.99
4.376	26.05		4.6495	58.06
			3.5555	27.05
			1.641	26.9
			4.376	50.47
			5.1965	41.32
			1.9145	29.01
			2.735	20.53
			1.3675	16.43
		average	3.42895522	33.2367164
		st dev	1.43490053	12.5248434
		count	67	67
		95% CI	0.34358365	2.99904507
		std error	0.175301	1.53015315

Unbleached Hardwood, Never Dried 1000 Revs, 50 psi

Stepheight	Freespan	(microns)	Stepheight	Freespan
3.5555	22.06		2.4615	20.32
3.0085	44.51		5.1965	50.07
6.017	42.38		1.641	11.69
1.641	9.99		2.735	24.22
1.641	33.81		1.3675	19.31
1.641	15.24		3.282	40.98
2.4615	23.82		0.547	12.7
2.735	25.51		1.641	18.29
2.188	20.66		1.3675	17.15
3.829	39.26		1.9145	22.5
2.735	34.21		2.735	18.6
2.735	23.37		1.9145	14.56
1.3675	13.55		1.9145	26.76
3.0085	16.93		3.829	36.69
2.4615	22.23		1.9145	19.86
3.0085	45.86		1.641	10.84
1.641	12.7		2.735	25.85
5.7435	52.1		4.376	34.59
2.735	30.96		2.735	33.71
2.735	40.55		3.282	34.25
0.547	2.88		2.188	17.9
2.735	37.97		2.4615	23.37
4.376	44.75		3.5555	35.9
1.9145	14.1		1.9145	25.74
2.735	32.18		2.4615	31.64
2.188	11.85		1.641	13.18
1.9145	23.68		3.5555	36.38
2.188	32.68		1.641	17.9
4.6495	36.11		2.4615	45.94
2.188	17.1		1.3675	20.99
3.829	34.72		2.188	12.19
1.3675	17.56		1.3675	17.87
3.0085	32.68		1.641	13.52
			1.9145	31.51
			1.641	15.92
			2.4615	30.65
			1.641	32.01
			4.1025	42.11
			3.0085	23.34
			2.4615	21.99
			4.376	49.49
		average	2.63289333	27.0537333
		st dev	1.23282073	12.3197204
		count	75	75
		95% CI	0.27900847	2.78816397
		std error	0.14235388	1.42255878

Unbleached Hardwood, Never Dried 2000 Revs, 50 psi

Stepheight	Freespan	(microns)	Stepheight	Freespan
0.547	6.44		5.1965	56.12
3.829	29.97		3.0085	30.82
1.9145	18.77		2.188	21
4.1025	50.51		3.0085	24.53
3.282	19.81		1.094	9.96
1.641	12.02		3.282	47.02
3.829	42.48		1.9145	25.19
4.1025	31.13		1.094	8.51
1.9145	16.77		1.094	6.1
3.282	38.44		5.7435	59.41
2.735	22.35		0.547	3.87
0.8205	7.96		1.094	19.01
2.188	13.38		2.4615	30.82
0.547	4.74		1.094	22.83
2.735	17.25		1.9145	21.34
3.282	36.58		2.188	17.75
3.829	31.3		2.735	18.46
3.0085	20.32		1.9145	11.51
0.8205	6.77		0.8205	4.06
1.3675	9.82		2.4615	22.02
2.188	21.85		1.9145	13.38
1.3675	11.99		0.547	4.74
2.188	29.13		1.094	6.77
3.282	24.43		4.376	48.48
1.3675	14.78		4.376	51.35
1.094	7.28		3.5555	28.27
3.5555	34.35		5.1965	55.83
1.9145	19.48		0.8205	11.52
3.5555	30.52		2.735	19.14
0.547	6.6		1.3675	12
1.3675	7.96		1.9145	17.24
1.9145	11.69		2.735	36.96
2.735	24.77		1.641	9.14
2.4615	19.48		2.4615	16.88
3.0085	21.85		0.8205	7.59
1.9145	8.95		0.547	7.45
1.3675	12.19		1.3675	13.01
1.641	12.19		1.3675	16.74
			3.0085	31.67
			1.3675	16.6
			1.094	13.04
		average	2.22560625	21.282375
		st dev	1.21047928	13.7826426
		count	80	80
		95% CI	0.26525309	3.02019922
		std error	0.1353357	1.54094628

Unbleached Hardwood, Never Dried 4000 Revs, 50 psi

Stepheight	Freespan	(microns)	Stepheight	Freespan
2.188	21.14		2.188	26.71
4.376	52.2		0.8205	11.09
3.282	40.11		1.3675	19.96
2.188	27.27		1.641	9.46
1.094	8.44		1.641	17.82
3.5555	27.77		1.641	17.95
2.4615	15.41		2.735	19.31
2.4615	25.74		2.188	20.15
1.641	13.72		1.094	12.84
2.735	21.64		1.3675	12.7
2.188	18.32		1.094	10.33
1.094	17.27		3.829	27.1
1.9145	11.85		0.8205	6.48
1.9145	25.11		1.094	11.53
2.4615	14.7		0.8205	3.9
0.547	3.7		1.094	11.12
1.3675	8.44		1.3675	7.79
2.188	27.1		1.3675	19.93
4.1025	38.1		1.094	18.63
4.6495	52.84		0.547	4.91
1.9145	14.56		0.8205	6.94
3.282	23.37		1.3675	6.77
1.641	15.58		0.547	4.23
0.8205	5.42		1.094	11.68
1.3675	14.23		2.188	14.37
3.282	37.6		1.3675	14.06
0.8205	5.85		1.3675	12.53
1.3675	9.31		0.547	3.95
1.641	16.6		2.735	24.39
1.9145	18.36		0.547	6.44
2.4615	15.86		1.9145	11.69
0.8205	10.5		2.188	11.52
0	0		0	0
0.547	13.47		2.188	13.21
4.6495	25.06		1.094	11.05
1.641	19.32		1.641	21.38
			1.9145	19.86
			0.547	4.21
			1.094	9.14
			0.547	5.63

average	1.73816447	16.0357895
st dev	1.03468724	10.3624255
count	76	76
95% CI	0.23262179	2.32971457
std error	0.11868677	1.18865172

Unbleached Softwood, Never Dried 300 Revs, 50 psi

Stepheight	Freespan	(microns)	Stepheight	Freespan
4.1025	32.85		2.4615	35.77
4.376	30.82		4.1025	32.26
3.5555	30.31		2.4615	20.43
3.5555	26.25		1.641	24.05
6.2905	63.51		2.4615	30.45
1.641	15.41		3.282	32.01
4.376	48.43		4.6495	33.47
2.735	19.64		2.188	20.66
6.8375	63.98		2.735	24.26
5.7435	73.64		3.0085	26.19
3.829	40.02		2.4615	21.14
1.641	13.35		5.7435	47.29
5.47	47.12		4.923	38.92
3.5555	33.02		5.47	38.45
2.188	12.7		2.188	20.2
3.0085	33.87		2.4615	50.44
3.5555	52.33		2.4615	31.47
1.094	7.79		2.188	26.63
4.376	40.64		1.094	14.54
3.829	40.64		4.1025	36.32
6.017	63.04		1.3675	19.66
1.641	13.72		2.4615	35.84
3.5555	37.93		3.282	45.77
4.923	55.52		2.735	16.26
4.376	58.26		2.735	24.72
5.1965	52.3		3.0085	23.24
6.8375	70.08		3.282	21.85
2.188	21.17		1.9145	29.51
3.282	31.88		2.735	33.3
3.5555	16.23		2.735	19.86
2.188	30.4		6.017	64.49
3.5555	38.31		2.188	25.88
2.188	38.44		2.188	14.36
2.188	27.98		4.376	30.11
5.47	37.17		3.5555	21.99
3.829	32.32		3.282	28.28
			1.9145	46.39
		average	3.40563699	33.6647945
		st dev	1.40204219	14.8196861
		count	73	73
		95% CI	0.32162348	3.39958312
		std error	0.16409663	1.73451306

Unbleached Softwood, Never Dried 1000 Revs, 50 psi

Stepheight	Freespan		Stepheight	Freespan
1.9145	20.15		3.282	18.63
4.1025	26.42		1.641	14.39
1.9145	14.54		1.9145	18.86
2.188	10.84		4.6495	49.18
3.829	23.88		4.1025	41.02
1.9145	27.1		0.8205	8.02
2.735	15.58		3.282	39.74
3.282	38.44		5.47	27.74
2.4615	31.33		1.3675	12.31
1.094	9.11		3.0085	26.63
2.4615	32.15		1.9145	19.74
1.641	13.35		4.923	35.51
2.735	22.86		4.6495	36.55
3.282	19.79		2.4615	20.66
2.188	13.04		2.188	24.27
3.0085	30.12		2.188	33.39
1.9145	10.84		4.923	28.2
0	0		4.376	54.7
3.282	25.23		4.376	31.37
4.1025	25.37		4.923	44.82
5.47	39.29		2.735	25.78
1.9145	14.39		1.9145	11.83
3.282	20.66		4.923	55.99
3.829	35.51		1.9145	26.31
3.282	29.1		2.735	23.68
3.5555	34.86		7.111	45.5
3.829	42.51		5.47	35.27
2.188	17.44		1.9145	22.24
1.094	10.5		2.735	26.87
3.282	23.37		2.4615	25.06
3.829	38.24		3.0085	16.93
2.188	14.73		2.188	21.99
3.282	27.6		1.3675	9.51
2.188	22.86		5.47	37.71
1.641	15.07		1.3675	10.84
1.3675	19.49			
		average	3.00068571	25.6714286
		st dev	1.3161743	11.2705487
		count	70	70
		95% CI	0.30832765	2.6402444
		std error	0.15731292	1.34708822

Unbleached Softwood, Never Dried 2000 Revs, 50 psi

Stepheight	Freespan
3.829	33.36
1.641	13.86
2.188	17.25
2.735	25.23
2.4615	20.46
3.0085	25.91
1.3675	10.64
1.641	17.95
3.829	28.62
3.0085	45.38
3.0085	24.02
2.188	16.74
0.547	7.62
1.3675	20.12
2.735	19.79
1.9145	10.84
1.094	9.82
0.8205	7.96
1.3675	13.04
2.188	32.32
0	0
1.9145	15.58
2.188	13.21
0.8205	9.14
1.094	17.61
1.3675	10.67
2.735	26.76
2.188	29.95
5.47	33.33
1.094	8.3
1.641	14.23
1.9145	18.29
1.3675	13.21
1.641	11.01
1.094	7.45
2.188	29.95
0.547	4.06
2.188	13.89

Stepheight	Freespan
0.8205	6.77
0.8205	8.98
1.9145	18.63
0.8205	7.76
0.8205	8.3
2.188	19.14
0.8205	9.31
2.188	11.49
1.3675	19.79
2.4615	23.84
3.282	27.28
3.282	30.12
2.188	37
1.3675	17.75
3.282	21.99
1.3675	15.12
1.9145	11.46
0.8205	8.84
1.9145	16.23
1.641	9.7
1.094	11.05
1.3675	15.13
6.2905	41.46
1.3675	14.58
1.641	15.85
0.2735	4.55
2.4615	19.19
5.47	37.95
1.3675	18.33
3.282	28.06
1.641	23.98
1.641	24.05
2.735	19.35
0.8205	8.94
1.641	16.74
1.3675	13.1
1.3675	20.49
2.735	31.32
1.3675	21.93
1.9145	27.75
0.8205	6.6

average	1.9283481	18.0692405
st dev	1.12161401	9.31572709
count	79	79
95% CI	0.24733067	2.05424057
std error	0.12619143	1.04810118

Unbleached Softwood, Never Dried 4000 Revs, 50 psi

Stepheight	Freespan		Stepheight	Freespan
0	0		1.094	11.52
3.0085	21.51		0.8205	8.04
0.8205	6.44		2.188	14.56
2.188	18.8		3.0085	13.83
0.8205	6.41		1.3675	10.3
2.4615	13.88		1.641	23.22
1.9145	13.21		1.641	13.15
0.2735	4.04		0.8205	7.93
2.4615	17.95		2.735	27.18
2.4615	25.04		2.735	14.73
2.4615	16.23		2.4615	15.33
2.735	22.18		2.735	22.9
1.641	12.7		0.547	6.24
1.3675	17.61		2.4615	17.25
2.188	19.14		1.9145	14.51
1.641	10.33		0	0
0	0		1.9145	14.54
3.5555	29.47		1.3675	10.81
1.094	7.11		0.2735	4.06
2.188	26.08		2.188	20.97
1.9145	17.95		1.094	10.28
0	0		1.3675	9.33
2.735	27.94		1.9145	16.81
1.094	7.11		2.188	15.21
0.2735	4.91		2.735	41.08
1.9145	11.85		1.641	21.85
2.188	21.85		0.547	4.91
2.188	18.8		0.8205	9.12
1.094	8.64		2.188	19.39
2.735	20.8		2.188	21.32
2.735	24.05		1.094	7.93
0.8205	5.64		1.9145	23.68
2.735	16.26		2.735	30.74
1.3675	9.99		1.3675	9.19
2.188	24.39		0.8205	5.59
3.829	29.81		2.4615	17.08
2.188	13.89		0.8205	6.41
1.641	14.39		2.4615	22.41
3.5555	35.22			
1.9145	16.26			
0	0			
1.641	14.9	average	1.76327059	15.0367059
2.188	16.6	st dev	0.88775312	8.38228921
1.641	12.19	count	85	85
2.188	15.92	95% CI	0.18872561	1.78197361
1.3675	10.81	std error	0.09629035	0.90918692
2.188	26.42			

Bleached Hardwood, Never Dried 300 Revs, 50 psi

Stepheight	Freespan
1.641	16.59
5.7435	47.84
3.5555	33.53
3.282	32.05
2.735	27.72
1.094	16.3
2.735	46.1
5.7435	47.42
4.1025	39.94
3.829	27.31
3.5555	32.73
4.1025	25.85
3.0085	28.42
5.1965	68.43
3.282	20.8
2.4615	27.58
1.3675	13.21
4.923	35.51
3.5555	24.19
3.5555	26.59
2.4615	21.82
2.188	19.31
3.5555	25.83
6.2905	61.02
1.9145	19.48
1.3675	12.53
2.735	29.61
2.735	14.37
5.47	39.43
2.735	26.39
5.7435	58.09
6.8375	50.97
3.282	20.83
1.094	9.46
2.735	32.51
3.0085	25.06
2.4615	17.1
4.1025	35.37
3.829	26.09

average	3.43628205	30.3430769
st dev	1.44830673	13.7869561
count	39	39
95% CI	0.45454443	4.32697295
std error	0.23191468	2.20767983

Bleached Hardwood, Never Dried 1000 Revs, 50 psi

Stepheight	Freespan
2.4615	19.11
3.282	18.84
1.9145	24.37
3.282	19.03
3.282	19.96
1.641	15.24
1.9145	22.52
4.923	33.02
3.829	42.14
3.282	37.12
3.0085	30.96
4.1025	33.87
1.641	23.71
1.094	10.64
3.0085	30.6
1.3675	10.69
1.641	19.64
3.0085	36.92
4.376	22.52
3.0085	21.85
2.735	26.25
3.0085	19.79
1.641	25.42
2.188	16.09
2.188	18.12
2.188	20.29
2.4615	21.55
1.9145	20.66
2.188	23.41
3.0085	39.5
3.829	35.03
3.282	22.69
0.8205	4.91
1.3675	21.04
3.282	32.33
3.829	32.66
2.188	15.96
1.9145	16.13
2.188	16.43

average	2.62279487	23.615641
st dev	0.9489223	8.43491422
count	39	39
95% CI	0.29781491	2.64725915
std error	0.15194918	1.35066724

Bleached Hardwood, Never Dried 2000 Revs, 50 psi

Stepheight	Freespan
3.282	23.85
2.188	14.85
3.5555	23.37
1.094	9.12
2.188	14.06
2.4615	21.55
0.547	5.25
0.8205	9.96
3.829	32.02
1.641	12.7
1.094	5.25
1.3675	10.16
3.282	18.5
1.641	9.63
4.1025	34.76
2.188	20.99
3.829	28.96
1.641	23.37
0	0
2.188	10.81
1.9145	13.72
3.5555	36.79
1.9145	21.35
2.4615	25.74
1.641	8
4.376	37.81
3.282	22.06
1.641	20.44
1.641	21.11
0.547	5.23
2.188	14.56
4.1025	31.16
2.188	18.43
2.4615	19.45
3.0085	18.29
3.282	27.07
4.376	33.91
1.9145	23.54

average	2.35353947	19.1531579
st dev	1.13666824	9.54890544
count	38	38
95% CI	0.36140156	3.03605675
std error	0.18439194	1.54903701

Bleached Hardwood, Never Dried 4000 Revs, 50 psi

Stepheight	Freespan
0.8205	3.89
2.4615	19.48
0.8205	7.62
1.3675	11.83
0	0
2.4615	22.49
2.188	13.93
1.9145	15.24
3.282	38.75
1.3675	8.47
1.094	7.43
3.5555	35.41
1.641	13.86
1.3675	12.02
3.5555	31.2
0.8205	5.23
2.188	17.78
2.4615	20.29
0.8205	7.62
3.282	26.56
1.094	7.96
1.641	14.54
2.4615	22.5
1.094	9.82
1.641	12.87
1.641	19.14
1.3675	10.5
2.735	25.91
3.0085	23.58
1.3675	13.52
3.282	21.68
1.3675	11.83
1.094	10.13
0.2735	4.04
1.3675	15.12
1.641	18.29
1.9145	17.9
3.282	20.12
2.4615	19.64
0.2735	2.54
1.9145	15.35

average	1.81443902	15.5141463
st dev	0.93502626	8.57676133
count	41	41
95% CI	0.28620681	2.62530332
std error	0.14602657	1.33946508

Bleached Hardwood, Dried 300 Revs, 50 psi

	Stepheight	Freespan
	3.0085	23.2
	3.282	29.47
	4.1025	44.17
	2.735	29.94
	4.6495	43.8
	1.3675	13.86
	4.1025	45.06
	1.9145	11.32
	1.9145	15.75
	3.282	30.12
	4.1025	29.13
	2.735	14.39
	3.829	26.02
	0.8205	12.7
	3.5555	32.68
	2.735	20.86
	3.0085	17.27
	3.829	24.54
	1.3675	15.07
	1.9145	18.63
	4.1025	33.16
	3.5555	26.74
	4.1025	30.79
	5.47	59.26
	2.735	22.86
	4.6495	49.03
	3.0085	34.69
	3.5555	25.57
	2.188	19.31
	3.282	25.04
	2.188	13.21
	2.735	23.71
	4.376	41.8
	3.5555	39.31
	1.094	7.79
	4.1025	34.05
	5.1965	41.69
average	3.1932973	27.7294595
st dev	1.12960992	11.955225
count	37	37
95% CI	0.3639785	3.85216591
std error	0.18570673	1.96542689

Bleached Hardwood, Dried 1000 Revs, 50 psi

Stepheight	Freespan
2.188	19.35
2.4615	14.44
4.923	25.44
3.829	29.27
3.0085	29.64
1.9145	23.81
3.0085	28.28
1.9145	9.79
1.9145	9.99
3.5555	27.91
1.3675	9.8
2.188	16.77
4.1025	28.79
2.735	25.4
4.6495	47.59
0.547	3.56
1.9145	26.76
1.9145	8.64
1.641	7.11
1.3675	10.64
4.376	34.89
1.9145	15.24
2.188	17.42
3.829	34.56
4.1025	37.91
0.8205	4.57
2.188	19
3.0085	27.24
1.3675	15.07
1.641	11.66
1.3675	17.32
2.4615	19.44
4.6495	37.78
0.547	3.73
1.641	11.35

average	2.49275714	20.2902857
st dev	1.20641538	10.9814387
count	35	35
95% CI	0.39967863	3.63808894
std error	0.20392142	1.85620194

Bleached Hardwood, Dried 2000 Revs, 50 psi

Stepheight	Freespan
1.094	12.87
1.094	13.38
1.641	17.95
1.9145	11.01
1.641	16.47
0.8205	6.6
2.735	19.64
1.641	12.17
3.282	23.88
2.735	19.11
1.9145	12.91
3.0085	21.48
1.3675	9.82
1.094	21.17
1.9145	9.65
1.9145	19.64
0.8205	4.91
1.9145	15.82
3.829	23.37
2.188	12.87
1.641	16.6
0.8205	4.91
1.641	12.36
1.3675	7.45
3.5555	29.3
1.641	9.99
2.188	16.6
2.188	18.29
1.3675	9.6
3.829	32.18
2.4615	20.49
1.3675	8.47
2.735	27.77
1.3675	7.62
2.4615	20.49

average	1.97701429	15.624
st dev	0.82873265	6.88291371
count	35	35
95% CI	0.27455447	2.28027063
std error	0.14008138	1.16342476

Bleached Hardwood, Dried 4000 Revs, 50 psi

Stepheight	Freespan
1.3675	8.1
0.547	3.73
3.0085	25.2
2.735	14.53
1.9145	8.47
0.2735	3.72
1.3675	8.13
2.735	14.54
1.9145	17.08
1.9145	20.15
2.188	20.32
1.3675	10.3
0.8205	6.1
0.8205	5.93
2.188	21.51
2.735	16.09
1.094	7.62
0.547	3.43
1.3675	5.59
2.188	15.62
0.2735	2.03
1.3675	19.18
1.641	13.69
1.3675	12.7
1.3675	11.01
1.3675	11.35
2.188	16.93
2.735	24.05
1.9145	11.49
3.0085	21.89
1.094	8.47
0	0
0.547	6.1
1.9145	12.19
1.094	5.59
0.547	4.28
0.8205	4.23
1.9145	13.72

average	1.53303947	11.4489474
st dev	0.81317265	6.62457578
count	38	38
95% CI	0.25854673	2.10627157
std error	0.13191402	1.0746481

Surface CMC – 0 mg

	Stepheight	Freespan
	2.735	19.45
	3.282	47.22
	4.1025	25.06
	4.6495	38.61
	2.4615	15.24
	3.0085	24.38
	4.923	47.08
	2.188	23.2
	2.735	19.64
	1.3675	8.81
	3.282	19.64
	2.188	16.6
	2.188	21.17
	3.829	34.38
	2.4615	20.49
	4.376	39.46
	6.017	38.44
	1.3675	11.18
	3.0085	31.16
	3.0085	22.13
	2.735	22.16
	2.4615	22.86
	1.9145	19.14
	3.0085	34.55
	3.5555	18.63
	2.4615	23.58
	1.641	12.84
	0.8205	5.59
	2.735	27.77
	3.5555	31.5
	1.641	13.86
	3.5555	35.22
	2.188	19.81
	2.4615	31.16
average	2.87979412	24.765
st dev	1.09033745	10.2736395
count	34	34
95% CI	0.36649627	3.45328923
std error	0.18699133	1.76191464

Surface CMC – 12 mg

Stepheight	Freespan
6.017	49.79
4.376	51.52
5.1965	44.2
4.376	34.52
2.735	27.77
4.1025	34.01
2.188	28.08
5.1965	45.72
2.188	27.27
2.735	22.07
1.641	25.04
2.188	23.17
2.4615	21.34
3.282	19.81
3.5555	35.56
4.1025	34.55
1.641	19.81
4.1025	47.9
3.282	21.82
2.735	45.43
1.9145	48.65
1.3675	17.95
2.188	19.11
1.3675	15.04
5.47	55.88
2.188	22.86
2.735	28.45
2.188	25.54
1.9145	18.29
1.641	11.49
3.282	55.52
2.188	19.47
2.188	19.31
1.9145	13.86
1.3675	11.52

average	2.91472857	29.7805714
st dev	1.27757492	13.2675249
count	35	35
95% CI	0.42325339	4.39545644
std error	0.21594958	2.24262103

Surface CMC – 40 mg

	Stepheight	Freespan
	4.1025	32.68
	4.923	35.56
	3.282	25.06
	1.9145	18.12
	2.4615	28.42
	3.5555	22.66
	3.5555	25.72
	3.5555	19.48
	3.0085	31.33
	4.376	57.55
	3.5555	30.31
	2.4615	36.38
	4.376	36.38
	2.188	20.97
	1.9145	23.88
	5.47	62.23
	1.3675	16.09
	1.9145	24.89
	1.9145	21.85
	2.4615	27.27
	3.282	34.18
	2.735	21.68
	2.4615	29.13
	3.5555	34.72
	2.188	29
	3.282	25.23
	1.9145	25.71
	3.282	51.28
	3.282	67.71
	2.735	37.93
	4.1025	36.92
	3.5555	35.9
	3.0085	45.22
	3.829	29.61
	1.9145	26.93
	1.9145	39.6
	1.9145	13.35
average	3.0085	31.917027
st dev	0.96696852	12.1672363
count	37	37
95% CI	0.31157282	3.92047934
std error	0.15896865	2.00028132

Bulk Carboxymethylation – DS 0.027

	Stepheight	Freespan
	1.3675	18.29
	1.3675	9.14
	3.829	30.96
	1.3675	14.39
	2.4615	15.24
	3.829	44.71
	1.3675	14.56
	1.641	18.67
	3.0085	37.46
	4.923	33.53
	3.282	51.99
	2.735	33.36
	3.829	20.83
	6.564	38.24
	7.9315	41.99
	3.5555	28.59
	2.4615	28.78
	2.735	30.99
	2.188	16.26
	4.923	38.27
	0.547	6.44
	3.5555	34.67
	4.1025	38.75
	2.4615	21.85
	2.188	23.54
	6.017	48.4
	4.6495	34.55
	3.5555	27.77
	3.282	24.56
	7.3845	42.38
average	3.43698333	28.972
st dev	1.80947204	11.7666924
count	30	30
95% CI	0.64749936	4.21057944
std error	0.33036288	2.14829429

Bulk Carboxymethylation – DS 0.087

Stepheight	Freespan
5.7435	38.41
4.1025	43.18
1.9145	15.75
3.829	32.83
3.0085	30.82
2.188	21
2.4615	26.08
3.0085	30.99
1.3675	11.35
2.4615	32.85
3.0085	15.92
2.735	22.16
1.641	8.13
1.3675	14.06
2.735	20.63
4.376	45.86
1.9145	28.25
2.188	17.25
2.735	25.06
4.923	36.96
3.0085	25.74
2.4615	17.78
2.4615	25.61
2.188	20.97
2.188	19.67
0.8205	11.18
2.188	18.29
2.188	14.06
1.3675	9.48
1.641	13.04

average	2.60736667	23.112
st dev	1.09100942	9.97436141
count	30	30
95% CI	0.39040553	3.5692138
std error	0.19919016	1.82106091

CMC – Surface – Physical Properties

0 mg CMC

Sample ID	Basis Weight g/m2	Soft Caliper µm	T410 Density g/cm3	T411 Zero Span psi	T220 Zero Span kg/15mm	Zero Span Index N/cm	ZDT kPa
1	60.21	121	0.497603	49.1	17.082	108.9989	250.8
2	61.83	130	0.475615	48.1	16.717	106.6699	224.5
3	64.035	134	0.477873	48.6	16.8995	107.8344	258.6
4	60.93	123	0.495366	45.6	15.8045	100.8473	229.3
5	62.37	130	0.479769	47.6	16.5345	105.5054	249.1
6	59.76	121	0.493884	46.1	15.987	102.0118	217.2
7	61.065	127	0.480827	46.1	15.987	102.0118	201.7
8	60.885	128	0.475664	49.1	17.082	108.9989	208.1
9	61.065	126	0.484643	46.6	16.1695	103.1763	231
10	62.595	128	0.489023	45.1	15.622	99.68277	216.3
Average	61.4745	126.8	0.485027	47.43333	16.47367	104.5737	228.66
St. Dev.	1.258651	4.184628	0.008382	1.369306	0.499797	3.189165	19.03571
Count	10	10	10	10	10	10	10
St. Error	0.39802	1.323296	0.002651	0.433013	0.15805	1.008502	6.01962

12 mg CMC

Sample ID	T410 Basis Weight g/m2	T411 Soft Caliper µm	T220 Density g/cm3	Zero Span psi	Zero Span kg/15mm	Zero Span Index N/cm	ZDT kPa
1	62.1	118	0.526271	52	18.1405	116.7506	460.2
2				49.6	17.2645	111.1127	489.1
3	61.65	124	0.497177	45.6	15.8045	101.7163	418.4
4	60.795	118	0.515212	51	17.7755	114.4015	427.1
5	61.11	116	0.52681	55.5	19.418	124.9725	395.6
6	59.58	118	0.504915	51	17.7755	114.4015	394.3
7	60.525	113	0.535619	50.6	17.6295	113.4618	408.1
8	60.885	117	0.520385	49.1	17.082	109.9382	459.6
9				47.6	16.5345	106.4145	392.2
10				53	18.5055	119.0997	495.1
Average	60.94929	117.7143	0.518056	50.22222	17.49161	113.2269	433.97
St. Dev.	0.808689	3.302236	0.013384	2.789614	1.018209	6.553099	39.25795
Count	7	7	7	10	10	10	10
St. Error	0.305656	1.248128	0.005058	0.882153	0.321986	2.072272	12.41445

40 mg CMC

Sample ID	T410 Basis Weight g/m2	T411 Soft Caliper µm	T220 Density g/cm3	Zero Span kg	Zero Span kg/15mm	Zero Span Index N/cm	ZDT kPa
1	58.095	110	0.528136	49.6	17.2645	113.6173	517.1
2	59.535	113	0.526858	49.1	17.082	112.4163	573.1
3				46.1	15.987	105.2101	568.4
4				48.6	16.8995	111.2153	484.8
5	59.895	115	0.520826	48.1	16.717	110.0142	519.3
6	59.85	114	0.525	51	17.7755	116.9802	462.4
7	60.345	115	0.524739	52.5	18.323	120.5833	404.2
8	61.02	116	0.526034	52	18.1405	119.3823	532.6
9				49.6	17.2645	113.6173	483.9
10	58.5	113	0.517699	48.1	16.717	110.0142	570.6
Average	59.60571	113.7143	0.524185	49.62222	17.27261	113.3051	511.64
St. Dev.	1.016528	1.976047	0.003663	1.996107	0.728579	4.794765	54.22273

CMC – Surface – Optical Properties

0 mg CMC

	Basis Wt. g/m2	R(0)	R(inf)	a	b	X	Scattering Power	Scattering Coefficient m2/kg	Absorption Power	Absorption Coefficient m2/kg
1	60.21	0.46	0.48	1.28	0.80	1.10	1.89	31.41	0.53	8.85
2	61.83	0.47	0.48	1.28	0.79	1.09	1.99	32.11	0.55	8.89
3	64.04	0.47	0.48	1.28	0.79	1.07	2.17	33.81	0.60	9.36
4	60.93	0.46	0.47	1.29	0.82	1.10	1.85	30.38	0.54	8.87
5	62.37	0.46	0.47	1.29	0.82	1.10	1.84	29.57	0.54	8.68
6	59.76	0.46	0.48	1.28	0.80	1.11	1.82	30.45	0.52	8.63
7	61.07	0.47	0.49	1.27	0.78	1.10	1.94	31.77	0.52	8.58
8	60.89	0.46	0.48	1.29	0.81	1.08	1.98	32.56	0.57	9.34
9	61.07	0.46	0.48	1.29	0.81	1.09	1.95	31.93	0.56	9.10
10	62.60	0.46	0.48	1.29	0.81	1.09	1.94	30.93	0.56	8.92
Average	62.59	0.46	0.48	1.28	0.80	1.09	1.94	31.49	0.55	8.92
St. Dev.	1.61	0.01	0.00	0.01	0.01	0.01	0.10	1.23	0.02	0.27
10	10.00	10.00	10.00	10.00	10.00	10.00	10.00	10.00	10.00	10.00
St error	0.51	0.00	0.00	0.00	0.00	0.00	0.03	0.39	0.01	0.09

12 mg CMC

	Basis Wt. g/m2	R(0)	R(inf)	a	b	X	Scattering Power	Scattering Coefficient m2/kg	Absorption Power	Absorption Coefficient m2/kg
1	62.10	0.43	0.45	1.33	0.87	1.12	1.66	26.73	0.55	8.78
2										
3	61.65	0.46	0.48	1.29	0.81	1.10	1.91	30.92	0.55	8.86
4	60.80	0.45	0.47	1.30	0.84	1.10	1.84	30.23	0.56	9.20
5	61.11	0.45	0.47	1.30	0.84	1.11	1.77	29.00	0.54	8.82
6	59.58	0.45	0.47	1.30	0.83	1.12	1.73	28.96	0.52	8.71
7	60.53	0.45	0.47	1.30	0.83	1.08	1.93	31.82	0.58	9.56
8	60.89	0.46	0.47	1.30	0.82	1.10	1.87	30.74	0.55	9.08
9										
10										
Average	62.59	0.45	0.47	1.30	0.83	1.10	1.81	29.77	0.55	9.00
St. Dev.	1.61	0.01	0.01	0.01	0.02	0.01	0.10	1.69	0.02	0.30
10	7.00	7.00	7.00	7.00	7.00	7.00	7.00	7.00	7.00	7.00
St error	0.61	0.00	0.00	0.00	0.01	0.00	0.04	0.64	0.01	0.11

	Basis Wt. g/m2	R(0)	R(inf)	a	b	X	Scattering Power	Scattering Coefficient m2/kg	Absorption Power	Absorption Coefficient m2/kg
1	58.10	0.45	0.47	1.29	0.82	1.13	1.70	29.31	0.50	8.55
2	59.54	0.45	0.47	1.30	0.83	1.13	1.68	28.18	0.50	8.42
3										
4										
5	59.90	0.46	0.48	1.28	0.80	1.11	1.85	30.91	0.52	8.76
6	59.85	0.44	0.47	1.31	0.84	1.12	1.70	28.41	0.52	8.74
7	60.35	0.44	0.46	1.31	0.85	1.12	1.68	27.87	0.53	8.73
8	61.02	0.45	0.47	1.30	0.83	1.11	1.77	28.97	0.53	8.61
9										
10	58.50	0.46	0.48	1.29	0.81	1.11	1.83	31.31	0.53	9.03
Average	62.59	0.45	0.47	1.30	0.83	1.12	1.74	29.28	0.52	8.69
St. Dev.	1.61	0.01	0.01	0.01	0.02	0.01	0.07	1.34	0.01	0.19

CMC – Bulk – Physical Properties

DS .027

Sample ID	T410 Basis Weight g/m2	T411 Soft Caliper µm	T220 Density g/cm3	Zero Span psi	Zero Span kg/15mm	Zero Span Index N/cm
1	59.67	138.3333	0.431349	43.2	14.9285	94.3323
2	59.895	139.3333	0.429868	42.2	14.5635	92.02588
3	61.335	144.6667	0.423975	39.2	13.4685	85.10664
4	64.08	148	0.432973	41.2	14.1985	89.71947
5	61.425	144	0.426563	40.7	14.016	88.56626
6	63.855	152.3333	0.419179	43.2	14.9285	94.3323
7	63.54	164.3333	0.386653	41.7	14.381	90.87268
8	62.46	161.6667	0.386351	40.7	14.016	88.56626
9	63.72	164.6667	0.386964	39.7	13.651	86.25985
10	60.795	154	0.394773	41.7	14.381	90.87268
Average	62.0775	151.1333	0.411865	41.35	14.23906	90.06543
St. Dev.	1.677755	9.90847	0.020451	1.334375	0.514393	3.077619
Count	10	10	10	10	10	10
St. Error	0.530553	3.133333	0.006467	0.421966	0.162665	0.973229

DS .087

Sample ID	T410 Basis Weight g/m2	T411 Soft Caliper µm	T220 Density g/cm3	Zero Span psi	Zero Span kg/15mm	Zero Span Index Nm/g
1	58.95	107.3333	0.549224	45.6	15.8045	100.5162
2	62.325	116.6667	0.534214	45.1	15.622	99.35548
3	62.415	120	0.520125	46.6	16.1695	102.8376
4	61.92	114.6667	0.54	47.6	16.5345	105.159
5	61.425	113.3333	0.541985	47.6	16.5345	105.159
6	62.19	115.6667	0.537666	45.1	15.622	99.35548
7	60.48	112.6667	0.536805	47.6	16.5345	105.159
8	62.28	114.3333	0.544723	48.1	16.717	106.3197
9	62.01	111.3333	0.556976	47.1	16.352	103.9983
10	62.775	114.6667	0.547456	41.2	14.1985	90.30206
Average	61.677	114.0667	0.540917	46.16	16.21006	101.8162
St. Dev.	1.149865	3.343688	0.009949	2.060852	0.425833	4.784041
Count	10	10	10	10	10	10
St. Error	0.363619	1.057367	0.003146	0.651699	0.13466	1.512847

CMC – Bulk – Optical Properties

DS .027

	Basis Wt. g/m2	R(0)	R(inf)	a	b	X	Scattering Power	Scattering Coefficient m2/kg	Absorption Power	Absorption Coefficient m2/kg
1	59.67	0.55	0.58	1.15	0.58	1.15	2.30	38.47	0.35	5.93
2	59.895	0.55	0.58	1.15	0.57	1.16	2.25	37.61	0.34	5.72
3	61.335	0.55	0.58	1.15	0.57	1.15	2.33	37.95	0.35	5.70
4	64.08	0.56	0.58	1.15	0.57	1.14	2.39	37.32	0.36	5.60
5	61.425	0.54	0.57	1.16	0.59	1.15	2.22	36.21	0.36	5.91
6	63.855	0.55	0.58	1.15	0.57	1.15	2.33	36.56	0.36	5.60
7	63.54	0.55	0.58	1.16	0.58	1.12	2.45	38.62	0.38	5.99
8	62.46	0.55	0.58	1.15	0.57	1.15	2.34	37.51	0.36	5.70
9	63.72	0.55	0.58	1.15	0.57	1.14	2.40	37.67	0.37	5.77
10	60.795	0.55	0.58	1.15	0.57	1.15	2.35	38.67	0.36	5.84
Average	62.59444	0.55	0.58	1.15	0.57	1.15	2.34	37.66	0.36	5.78
St. Dev.	1.610793	0.00	0.00	0.00	0.01	0.01	0.07	0.83	0.01	0.14

DS .087

	Basis Wt. g/m2	R(0)	R(inf)	a	b	X	Scattering Power	Scattering Coefficient m2/kg	Absorption Power	Absorption Coefficient m2/kg
1	58.95	0.50	0.55	1.19	0.64	1.29	1.61	27.28	0.31	5.18
2	62.325	0.49	0.54	1.19	0.65	1.27	1.63	26.17	0.32	5.10
3	62.415	0.50	0.55	1.19	0.64	1.26	1.68	26.86	0.32	5.07
4	61.92	0.50	0.54	1.19	0.65	1.27	1.65	26.62	0.32	5.09
5	61.425	0.50	0.55	1.19	0.64	1.27	1.66	27.03	0.31	5.10
6	62.19	0.49	0.54	1.20	0.66	1.28	1.60	25.79	0.32	5.08
7	60.48	0.49	0.54	1.19	0.65	1.28	1.61	26.55	0.31	5.14
8	62.28	0.50	0.54	1.19	0.65	1.26	1.67	26.89	0.32	5.17
9	62.01	0.50	0.54	1.19	0.65	1.27	1.64	26.40	0.32	5.11
10	62.775	0.50	0.54	1.19	0.65	1.24	1.71	27.32	0.33	5.22
Average	62.59444	0.50	0.54	1.19	0.65	1.27	1.65	26.69	0.32	5.13
St. Dev.	1.610793	0.00	0.00	0.00	0.00	0.01	0.04	0.49	0.01	0.05

Viscose Crossing Micrographs

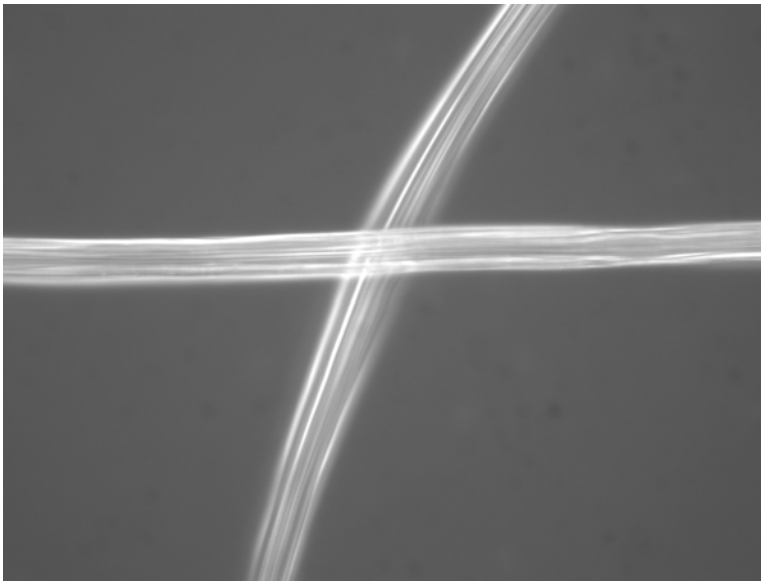

Couched viscose

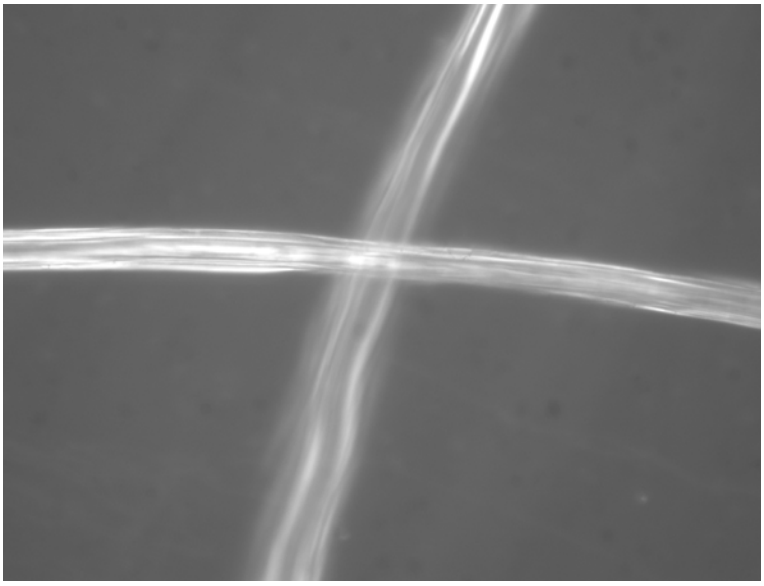

Viscose pressed at 50 psi

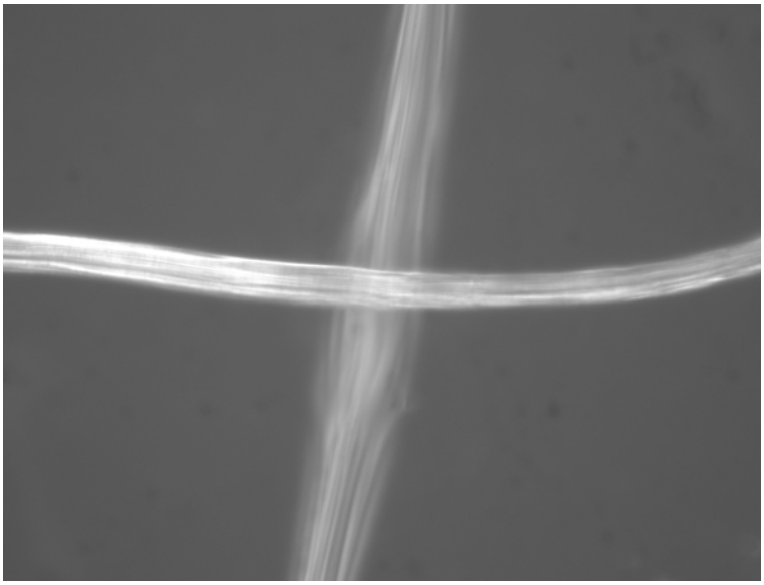

Viscose pressed at 300 psi.

REFERENCES

Abitz, P. and P. Luner (1991). The Relationships of Wet Fiber Flexibility (WFF) to Piber and Pulp Properties. ESPRI Research Report No. 94. Syracuse, NY, Empire State Paper Research Institute**:** 67-87.

Alexander, S. and R. Marton (1968). "Effect of Beating and Wet Pressing on Fiber and Sheet Properties." Tappi Journal **51**(6): 283-288.

Ampulski, R. (1985). The Influence of Fiber Surface Charge on Tensile Strength. TAPPI Papermakers Conference.

Anderson, J. M. (1986). "Fluorescent Hydrazides for the High-Performance Liquid Chromatiographic Determination of Biological Carbonyls." Analytical Biochemistry **152**(1): 146-153.

Asunmaa, S. and B. Steenberg (1958). "Beaten Pulps and the Fibre-to-fibre Bond in Paper." Svensk Papperstiding **61**(18): 686-695.

Barkas, W. (1950). Proceedings of the Technical Section of the British Paper and Board Makers' Association **31**(3): 463.

Barzyk, D. (1996). "Topochemical and Performance Aspects of Fiber Oxidation." Institute of Paper Science and Technology: Atlanta, GA.

Barzyk, D., D. H. Page and A. Ragauskas (1997a). "Acidic Group Topochemistry and Fibre-to-Fibre Specific Bond Strength." Journal of Pulp and Paper Science **23**(2): J59-J61.

Barzyk, D., D. H. Page and A. Ragauskas (1997b). Carboxylic Acid Groups and Fibre Bonding. The Fundamentals of Papermaking Materials: Transactions of the 11th Fundamental Research Symposium. C. F. Baker. Cambridge, FRC**:** 893-907.

Biermann, C. J. (1996). Handbook of Pulping and Papermaking. New York, Academic Press.

Brodeur, P. H. and T. M. Runge (1995). "Compactibility of a Wet Fiber Mat Using Acoustic Radiation Pressure." Journal of Pulp and Paper Science **22**(8): 278-282.

Busker, L. H. and D. C. Cronin (1982). The Relative Importance of Wet Press Variables in Water Removal. International Water Removal Symposium, Vancouver, BC.

Caulfield, D. (1973). "Small-Angle X-Ray Scattering by Paper: A new Method for investigating Inter-fiber Bonding." Tappi Journal **56**(3): 102-106.

Chai, X.-S., Q. X. Hou and J. Y. Zhu (2003). "Carboxyl Groups in Wood Fibers 2. The Fate of Carboxyl Groups During Alkaline Delignification and Its Application for Fiber Yield and Prediction in Alkaline Pulping." Industrial and Engineering Chemical Research **42**(22): 5445-5449.

Chakar, F. and A. Ragauskas (2004). "Review of current and future softwood draft lignin process chemistry." Industrial Crops and Products **20**: 131-141.

Chhabra, N., J. K. Spelt, C. M. Yip and M. T. Kortschot (2005). "An Investigation of Pulp Fibre Surfaces by Atomic Force Microscopy." Journal of Pulp and Paper Science **31**(1): 52-56.

Clark, J. (1985). Pulp Technology and Treatment for Paper. San Francisco, Miller Freeman Publications.

Cote, W. (1967). Wood Ultrastructure. Seattle, University of Washington Press.

Czworkowski, J., O. Odom and B. Hardesty (1991). "Fluorescence Study of the Topology of Messenger RNA Bound to the 30S Ribosomal Subunit of *Escherichia coli*." Biochemistry **30**(19): 4821-4830.

Emerton, H. W. (1957). Fundamentals of the Beating Process. Kenley, The British Paper and Board Industry Research Association.

Engstrand, P., B. Sjogren, K. Olander and M. Htun (1991). The Significance of Carboxylic Groups for the Physical Properties of Mechanical Pulp Fibers. Sixth International Symposium on Wood and Pulping Chemistry.

Fengel, D. and G. Wegener (1989). Wood: Chemistry, Ultrastructure, Reactions. New York, Walter de Gruyter.

Forgacs, O. L. and S. G. Mason (1958). "The Flexibility of Wood-Pulp Fibers." Tappi Journal **41**(11): 695-704.

Frolander, U. and N. Hartler (1970). "Determination of the Bulk Fibre Stiffness from the Network Shear Modulus." Svensk Papperstiding **73**(2): 21-27.

Furuta, T. and D. G. Gray (1998). "Direct Force-Distance Measurements on Wood-Pulp Fibres in Aqueous Media." Journal of Pulp and Paper Science **24**(10): 320-324.

Gordon, G. W., G. Berry, X. H. Liang, B. Levine and B. Herman (1998). "Quantitative Fluorescence Resonance Energy Transfer Measurement Using Fluorescence Microscopy." Biophysical Journal **74**(5): 2702-2713.

Goring, D. (1963). "Therman Softening of Lignin, Hemicellulose, and Cellulose." Pulp and Paper Magazine of Canada **64**(12): T517-T527.

Gorres, J., R. Amiri, M. Grondin and J. R. Wood (1993). Fibre Collapse and Sheet Structure. Products of Papermaking: Transactions of the 10th Fundamental Research Symposium. C. F. Baker. Oxford, FRC**:** 285-310.

Gullichsen, J. (1999). Fiber Line Operations. Chemical Pulping 6A. J. Gullichsen and C.-J. Fogelholm. Helsinki, Fapet Oy**:** 19-244.

Halliday, D., R. Resnick and J. Walker (1993). Fundamentals of Physics. New York, John Wiley & Sons, Inc.

Hartler, N. and J. Nyren (1970). "Transverse Compressibility of Pulp Fibers II: Influence of Cooking, Yield, Beating, and Drying." Tappi Journal **53**(5): 820-823.

Haselton, W. (1955). "Gas Adsorption by Wood, Pulp, and Paper." Tappi Journal **38**(12): 716-723.

Herman, B. (1998). Fluorescence Microscopy.

Hietanen, S. and K. Ebeling (1990). "Fundamental Aspects of the Refining Process." Paperi Ja Puu-Paper and Timber **72**(2): 158-170.

Higgins, H. G. and J. deYong (1961). The Beating Process: Primary Effects and Their Influence on Pulp and Paper Properties. Formation and Structure of Paper, Tranactions of the Second Fundamental Research Symposium. F. Bolam. Oxford, FRC.

Hoppe, A., K. Christensen and J. Swanson (2002). "Fluorescence Resonance Energy Transfer-Based Stoichiometry in Living Cells." Biophysical Journal **83**(6): 3652-3664.

Horii, F. (2001). Structure of Cellulose: Recent Developments in Its Characterization. Wood and Cellulosic Chemistry. D. Hon and N. Shiraishi. New York, Marcel Dekker.

Ingmanson, W. and E. Thode (1959). "Factors Contributing to the Strength of a Sheet of Paper II: Relative Bonded Area." TAPPI Journal **42**(1): 83-93.

Jares-Erijman, E. and T. Jovin (2003). "FRET Imaging." Nature Biotechnology **21**(11): 1387-1395.

Jayme, G. (1958). "Properties of Wood Celluloses: II. Determination and Significance of Water Retention Value." Tappi Journal **41**(11): 180A-183A.

Jenkins, F. A. and H. E. White (1976). Fundamentals of Optics. New York, McGraw-Hill Book Company.

Jiang, Z-H., Van Lierop, B. and R. Berry (2000). "Hexenuronic Acid Groups in Pulping and Bleaching Chemistry. TAPPI Journal **83**(1):167-175.

Katz, S., R. Beatson and A. M. Scallan (1984). "The Determination of Strong and Weak Acidic Groups in Sulfite Pulps." Svensk Papperstiding **87**(6): 48-53.

Katz, S., N. Liebergott and A. M. Scallan (1981). "A mechanism for the alkali strengthening of mechanical pulps." TAPPI Journal **64**(7): 97-100.

Kerekes, R. J. (2005). "Characterizing Refining Action in PFI Mills." Tappi Journal **4**(3): 9-14.

Kibblewhite, R. (1973). "Effects of beating on wet web behaviour." APPITA Journal **26**(5): 341-347.

Kim, D. H., L. Allison, B. Carter, Q. Hou, C. Courchene, A. Ragauskas and J. Sealey (2005). "Profiling the Wood and Pulping Properties of Southern Pine Thinning Resources." Tappi Journal **4**(1): 21-25.

Kuhn, D. C. S., X. Lu, J. A. Olson and A. G. Robertson (1995). "A dynamic Wet Fibre Flexibility Measurement Device." Journal of Pulp and Paper Science **21**(10): 337-342.

Laine, J., T. Lindstrom, C. Bremberg and G. Nordmark (2003a). "Studies on Topochemical Modification of Cellulosic Fibres, Part 4: Toposelectivity of carboxymethylation and its effects on the swelling of fibres." Nordic Pulp and Paper Research Journal **18**(3): 316-324.

Laine, J., T. Lindstrom, C. Bremberg and G. Nordmark (2003b). "Studies on Topochemical Modification of Cellulosic Fibres, Part 5: Comparison of the effects of surface and bulk chemical modification and beating of pulp on paper properties." Nordic Pulp and Paper Research Journal **18**(3): 325-332.

Laine, J., T. Lindstrom, G. Nordmark and G. Risinger (2000). "Studies on Topochemical Modification of Cellulosic Fibres, Part 1: Chemical conditions for the attachment of carboxymethyl cellulose onto fibres " Nordic Pulp and Paper Research Journal **15**(5): 520-526.

Laine, J., T. Lindstrom, G. Nordmark and G. Risinger (2002). "Studies on Topochemical Modification of Cellulosic Fibres, Part 2: The effect of carboxymethyl cellulose attachment on fibre swelling and paper strength." Nordic Pulp and Paper Research Journal **17**(1): 50-56.

Laine, J. and P. Stenius (1997a). "Effect of charge on the fiber and paper properties of bleached industrial kraft pulps." Paperi Ja Puu-Paper and Timber **79**(4): 257-266.

Lainins, G. V. and A. M. Scallan (1993). The Mechanism of Hornification o0f Wood Pulps. Products of Papermaking.

Laivins, G. V. and A. M. Scallan (1993). The Mechanism of Hornification of Wood Pulps. Products of Papermaking: Transactions of the Tenth Fundamental Research Symposium. C. F. Baker. Oxford, FRC.

Lakowicz, J. (1983). Principles of Fluorescence Spectroscopy. New York, Plenum Press.

Liitia, T., S. L. Maunu, B. Hortling, T. Tamminen, O. Pekkala and A. Varhimo (2003). "Cellulose Crystallinity and ordering of Hemicelluloses in Pine and Birch Pulps as Revealed by Solid-State NMR Spectroscopic Methods." Cellulose **10**(4): 307-316.

Lindstrom, T. (1989). Some Fundamental Chemical Aspects on Paper Forming. Fundamentals of Papermaking. C. F. Baker and V. Punton. Cambridge, FRC**:** 311-412.

Lindstrom, T. (1992a). "Chemical Factors Affecting the Behaviour of Fibres During Papermaking." Nordic Pulp and Paper Research Journal **7**(4): 181-192.

Lindstrom, T. (1992b). "Chemical Factors affecting the behaviour of fibres during papermaking." Nordic Pulp and Paper Research Journal(4): 181-192.

Lindstrom, T., L. Wagberg and T. Larsson (2005). On the Nature of Joint Strength in Paper - A Review of Dry and Wet Strength Resins Used in Paper Manufacturing. 13th Fundamental Research Symposium, Cambridge, United Kingdom, The Pulp and Paper Fundamental Research Society.

Lowe, R., D. H. Page and A. Ragauskas (2005). Imaging Fibre Deformations. Advances in Paper Science and Technology: Transactions of the 13th Fundamental Research Symposium. S. J. l'Anson. Cambridge, FRC**:** 921-941.

McKenzie, A. (1984). "The Structure and Properties of Paper Part XXI: The Diffusion Theory of Adhesion Applied to Interfibre Bonding." APPITA Journal **37**(7): 580-583.

Meunier, F. and K. Wilkinson (2002). "Nonperturbing Fluorescent Labeling of Polysaccharides." Biomacromolecules **3**(4): 857-864.

Mitsui, T., H. Nanko and K. Yamana (2000). "Coumarin-fluorescein pair as a new donor-acceptor set for fluorescence energy transfer study of DNA." Tetrahedron Letters **41**: 2605-2608.

Mohlin, U.-B. (1975a). "Cellulose Fibre Bonding Part 4: Effect of Chemical Modification on Rayon Fibre Bonding Ability." Svensk Papperstiding **10**: 373-375.

Mohlin, U.-B. (1975b). "Cellulose Fibre Bonding Part 5: Conformability of Pulp Fibres." Svensk Papperstiding **78**(11): 412-416.

Nanko, H. and J. Ohsawa (1989). Mechanisms of Fibre Bond Formation. Fundamentals of Papermaking: Transactions of the Ninth Fundamental Research Symposium. C. F. Baker and V. Punton. Cambridge, FRC**:** 783-830.

Nilsson, B., L. Wagberg and D. G. Gray (2001). Conformability of Wet Pulp Fibres at Small Length Scales. The Science of Papermaking: Transactions of the 12th Fundamental Research Symposium. C. F. Baker. Oxford, FRC**:** 211-224.

Nissan, A. H. (1961). General Principles of Adhesion: With Particular Reference to the Hydrogen Bond. Formation and Structure of Paper: Transactions of the IInd Fundamental Research Symposium. F. Bolam. Oxford, FRC**:** 119-130.

Nissan, A. H. and S. Sternstein (1964). "Cellulose-Fiber Bonding." Tappi Journal **47**(1): 1-6.

Nordman, L. (1957). Bonding in Paper Sheets. Transactions of the Ist Fundamental Research Symposium. F. Bolam. Cambridge, FRC**:** 333-347.

Nordman, L., P. Aaltonen and T. Makkonen (1965). Relationships Between Mechanical and Optical Properties of Paper Affected by Web Consolidation. Transactions of the IIIrd Fundamental Research Symposium. F. Bolam. Cambridge, FRC**:** 909-927.

Notley, S., B. Petterson and L. Wagberg (2004). "Direct Measurement of Attractive van der Waals' Forces Between Regenerated Cellulose Surfaces in an Aqueous Environment." Journal of the American Chemical Society **126**(43): 13930-13931.

Notley, S. and L. Wagberg (2005). "Morphology of Modified Regenerated Model Cellulose II Surfaces Studied by Atomic Force Microscopy; Effect of Carboxymethylation and Heat Treatment." Biomacromolecules **6**(3): 1586-1591.

Nyren, J. (1971). "The Transverse Compressibility of Pulp Fibers." Pulp and Paper Magazine of Canada **72**(10): 81-83.

Paavilainen, L. (1993). "Conformability - Flexibility and Collapsibility - of Sulphate Pulp Fibres." Paperi Ja Puu-Paper and Timber **75**(9): 689-702.

Page, D. H. (1967). "The Collapse Behavior of Pulp Fibers." Tappi Journal **50**(9): 449-455.

Page, D. H. (1969). "A Theory for the Tensile Strength of Paper." Tappi Journal **52**(4): 674-681.

Page, D. H. (1989). The Beating of Chemcal Pulps - The Action and the Effects. Fundamentals of Papermaking: Transactions of the 9th Fundamental Research Symposium. C. F. Baker and V. Punton. Cambridge, FRC**:** 1-38.

Page, D. H., J. W. Sargent and R. Nelson (1965). Sturcture of Paper in Cross-Section. Consolidation of the Paper Web: Transactions of the Third Fundamental Research Symposium. F. Bolam. Cambridge, FRC**:** 313-349.

Page, D. H., R. S. Seth and F. El-Hosseiny (1985). Strength and Chemical Compostion of Wood Pulp Fibers. Papermaking Raw Materials. V. Punton. Oxford, FRC**:** 77-91.

Page, D. H. and L. Wagberg (1997). Discussion Contributions to the Transactions of the XIth Fundamental Research Symposium. C. F. Baker. Cambridge, FRC**:** 1521-1526.

Panshin, A. J. and C. deZeeuw (1980). Textbook of Wood Technology. New York, McGraw-Hill.

Parsons, S. (1942). "Optical Characteristics of Paper as a Function of Fiber Classification." Paper Trade Journal **115**(25): 34-42.

Pelton, R. (1993). "A model of the external surface of wood pulp fibers." Nordic Pulp and Paper Research Journal(1): 113-119.

Pelton, R., J. Zhang, L. Wagberg and M. Rundlof (2000). "The role of surface polymer compatibility in the formation of fiber/fiber bonds in paper." Nordic Pulp and Paper Research Journal **15**(5): 400-406.

Retulainen, E. and K. Ebeling (1993). "Fiber-Fiber Bonding and Ways of Characterizing Bond Strength." APPITA Journal **46**(4): 282-288.

Risen, J., A. H. Hulten and M. Paulsson (2004). "Influence of Fiber Properties on the Network Strength of Softwood and Hardwood Kraft Pulp Fibers from Different Stages of a Bleaching Sequence." Journal of Wood Chemistry and Technology **24**(4): 289-306.

Robertson, A. A., E. Meindersma and S. G. Mason (1961). "The Measurement of Fibre Flexibility." Pulp and Paper Magazine of Canada **62**(1): 3-10.

Rowell, R. M., R. Pettersen, J. S. Han, J. S. Rowell and M. A. Tshabalala (2005). Cell Wall Chemistry. Wood Chemistry and Wood Composites. R. M. Rowell. New York, Taylor & Francis**:** 35-74.

Saka, S. (2001). Chemical Composition and Distribution. Wood and Cellulosic Chemistry. D. Hon and N. Shiraishi. New York, Marcel Dekker.

Samuelsson, L.-G. (1963). "Measurement of the Stiffness of Fibres." Svensk Papperstidning **66**(15): 541-546.

Scallan, A. M. (1974). "The Structure of the Cell Wall of Wood - A Consequence of Anisotropic Inter-Microfibrillar Bonding?" Wood Science **6**(3): 266-271.

Scallan, A. M. (1983). "The effect of acidic groups on the swelling of pulps: a review." Tappi Journal **66**(11): 73-75.

Scallan, A. M. and J. Grignon (1978). "The effect of cations on pulp and paper properties." Svensk Papperstiding **82**(2): 40-47.

Scallan, A. M. and J. Grignon (1979). "The effect of cations on pulp and paper properties." Svensk Papperstiding **82**(2): 40-47.

Scallan, A. M. and A. C. Tigerstrom (1992). "Swelling and Elasticity of the Cell Walls of Pulp Fibres." Journal of Pulp and Paper Science **18**(5): 188-193.

Seborg, C. O. and F. A. Simmonds (1941). "Measurement of the Stiffness in Bending of Single Fibers." Paper Trade Journal **113**(17): 225-226.

Sjostrom, E. (1989). "The Origin of Charge on Cellulosic Fibers." Nordic Pulp and Paper Research Journal **4**(2): 90-93.

Sjostrom, E. (1993). Wood Chemistry Fundamentals and Applications. New York, Academic Press.

Sjostrom, E. and U. Westermark (1999). Chemical Composition of Wood Pulps: Basic Constituents and Their Distribution. Analytical Methods in Wood Chemistry, Pulping, and Papermaking. E. Sjostrom and R. Alen. New York, Springer.

Somogyi, B., J. Matko, S. Papp, J. Hevessy, G. R. Welsh and S. Damjanovich (1984). "Forster-Type Energy Transfer as a Probe for Changes in Local Fluctuations of the Protein Matrix." Biochemistry **23**(15): 3403-3411.

Steadman, R. and P. Luner (1985). The Effect of Wet Fibre Flexibility on Sheet Apparent Density. Papermaking Raw Materials: Transactions of the 8th Fundamental Research Symposium Held at Oxford. V. Punton, FRC. **Vol. 1:** 311-337.

Stone, J. E. and A. M. Scallan (1967). "The Effect of Component Removal Upon the Porous Structure of the Cell Wall of Wood. II. Swelling in Water and the Fiber Saturation Point." Tappi Journal **50**(10): 496-501.

Suckling, I. D., R. W. Allison, S. H. Campion, K. G. McGrouther and A. G. McDonald (2001). "Monitoring Cellulose Degradation During Convential and Modified Kraft Pulping." Journal of Pulp and Paper Science **27**(10): 336-341.

Sundrani, R. S., J. L. Hill and C. J. Biermann (1993). "Correction tables for Canadian standard freeness of chemical pulps at nonstandard temperature and consistency." TAPPI Journal **76**(5): 147-152.

Tam Doo, P. A. and R. J. Kerekes (1981). "A method to measure wet fiber flexibility." TAPPI Journal **63**(3): 113-116.

TamDoo, P. A. and R. J. Kerekes (1981). "A Method to Measure Wet Fiber Flexibility." Tappi Journal **64**(3): 113-116.

TAPPI Standard (2000) T 248 sp-00, Labortory Beating of Pulp (PFI Mill Method).

Torgnysdotter, A. and L. Wagberg (2003). "Study of the Joint Strength Between regenerated cellulose fibres and its Influence on the Sheet Strength." Nordic Pulp and Paper Research Journal **18**(4): 455-459.

Uesaka, T., E. Retulainen, L. Paavilainen, R. Mark and S. Keller (2002). Determination of Fiber-Fiber Bond Properties. Handbook of Physical Testing of Paper. R. Mark, C. Habeger, J. Borch and B. Lyne. New York, Marcel Dekker, Inc. **1:** 873-900.

Van Den Akker, J. (1959). "Structural Aspects of Bonding." TAPPIJournal **42**(12): 940-947.

Van Der Meer, B., C. Coker and S.-Y. S. Chen (1994). Resonance Energy Transfer: Theory and Data. New York, VCH Publishers.

Wagberg, L. and G. Annergren (1997). Physicochemical Characterization of Papermaking Fibres. The Fundamentals of Papermaking Materials, Transactions of the XIth Fundamental Research Symposium. C. F. Baker. Cambridge, FRC**:** 1-82.

Wagberg, L., L. Winter and T. Lindstrom (1985). Determination of Ion-Exchange Capacity of Carboxymethylated Cellulose Fibres Using Colloid and Conductometric Titrations. Papermaking Raw Materials: Transactions of the 8th Fundamental Research Symposium held in Oxford. Oxford, FRC**:** 914-923.

Walecka, J. (1956). "An Investigation of Low Degree of Substitution Carboxymethylcelluloses." Tappi Journal **39**(7): 458-463.

Waterhouse, J. F. and D. H. Page (2004). "The Contribution of Transverse Shear to Wet Fiber Deformation Behavior." Nordic Pulp and Paper Research Journal **19**(1): 89-92.

Wiedenhoeft, A. and R. Miller (2005). Structure and Function of Wood. Wood Chemistry and Wood Composites. R. M. Rowell. New York, Taylor & Francis**:** 9-33.

Wild, P., I. Omholt, D. Steinke and A. Schuetze (2005). "Experimental Characterization of the Behaviour of Wet Single Wood-Pulp fibres under Transverse Compression." Journal of Pulp and Paper Science **31**(3): 116-120.

Willfor, S., A. Sundberg, J. Hemming and B. Holmbom (2005a). "Polysaccharides in some industrially important hardwood species." Wood Science and Technology **39**(8): 601-617.

Willfor, S., A. Sundberg, J. Hemming and B. Holmbom (2005b). "Polysaccharides in some industrially important softwood species." Wood Science and Technology **39**(4): 245-258.

Yang, C.-F., A. R. K. Eusufzai, R. Sankar, R. E. Mark and R. W. Perkins (1978). "Measurements of Geometrical Parameters of Fiber Networks." Svensk Papperstiding **81**(13): 426-433.

Yapoudjian, S., M. Ivanova, I. Douchet, A. Zenatti, M. Sentis, W. Marine, A. Svendsen and R. Verger (2002). "Surface Fluorescence Resonance Transfer Studies on Interfacial Adsorption of *Thermomyees (Humicola) lanuginosa* Lipase, Using Monomolecular Films of *cic*-Paninaric Acid." Biopolymers **65**: 121-128.

Yiannos, P. N. (1965). "Swellability of Pulps Determined by Isopropanol Retention." Tappi Journal **48**(9): 494.

Zhand, D., X. Chi, Q. Hou, A. Ragauskas. (2005) "Characterization of Fiber Carboxylic Acid Groups during One-stage Oxygen Delignificaiton." Industrial and Engineering Chemistry Research **44**(24): 9279-9285.

VITA

Rob Lowe was born in Charlotte, North Carolina. In the fall of 2001 he graduated from North Carolina State University with Bachelor of Science degrees in Chemical Engineering and Pulp and Paper Science and Technology. After completing his undergraduate education, he moved to Atlanta, Georgia where he pursued a PhD at the Georgia Institute of Technology's Institute of Paper Science and Technology. As part of the School of Chemical and Biomolecular Engineering, his research focused on fiber and paper physics. During both his undergraduate and graduate education he completed several internships with Kimberly-Clark Corporation and Novo Nordisk NA in various locations across the United States. Upon completion of his PhD, he joined Nalco Company as a Senior Engineer with their Paper Research Group in Naperville, Illinois.